Raman Spectroscopy in Tandem with Chemometric Methods for the Characterization and Analysis of Quality and Shelf Life of Poultry Meat

Dissertation

zur

Erlangung des Doktorgrades (Dr. rer. nat.)

der

Mathematisch-Naturwissenschaftlichen Fakultät

der

Rheinischen Friedrich-Wilhelms-Universität Bonn

vorgelegt von

Sawsan Jaafreh

aus

Zarqa, Jordanien

Bonn, 2020

Angefertigt mit Genehmigung der Mathematisch-Naturwissenschaftlichen Fakultät der Rheinischen Friedrich-Wilhelms-Universität Bonn

1. Gutachter: Professor Dr. Klaus Günther
2. Gutachter: Professor Dr. Matthias Wüst

Tag der Promotion: 12.08.2020
Erscheinungsjahr: 2020

To My late Mother

To My Family and My Loved Ones

"Arise, awake, and stop not till the goal is reached."

-Swami Vivekananda (1863-1902)

Abstract

Discrimination and classification of eight strains related to meat spoilage microorganisms commonly found in poultry meat were successfully carried out using two dispersive Raman spectrometers (Microscope and Portable Fiber-Optic systems) in combination with chemometric methods. Principal Components Analysis (PCA) and Multi-Class Support Vector Machines (MC-SVM) were applied to develop discrimination and classification models. These models were certified using validation data sets which were successfully assigned to the correct bacterial genera and even to the right strain. The discrimination of bacteria down to the strain level was performed for the pre-processed spectral data using a 3-stage model based on PCA. The spectral features and differences among the species on which the discrimination was based were clarified through PCA loadings. In MC-SVM the pre-processed spectral data was subjected to PCA and utilized to build a classification model. When using the first two components, the accuracy of the MC-SVM model was 97.64% and 93.23% for the validation data collected by the Raman Microscope and the Portable Fiber-Optic Raman system, respectively. The accuracy reached 100% for the validation data by using the first eight and ten PC's from the data collected by Raman Microscope and by Portable Fiber-Optic Raman system, respectively. The results reflect the strong discriminative power and the high performance of the developed models, the suitability of the pre-processing method used in this study and that the low accuracy of the Portable Fiber-Optic Raman system does not adversely affect the discriminative power of the developed models.

Using the same portable fiber-optic Raman spectrometer (a QE Pro-Raman spectrometer with a laser excitation wavelength of 785 nm from Ocean Optics); the freshness changes in poultry fillets during storage were studied. Poultry fillets with the same storage life (9 days) and expiry date were purchased from a local store and stored at 4 °C. Their Raman spectra were measured on a daily basis up to day 21. The complex spectra were analysed using PCA, which resulted in a separation of the samples into three quality classes according to their freshness: fresh, semi-fresh, and spoiled. These classes were based on and similar to the information inferred from the product label on the packages of poultry fillets. The PCA loadings revealed a decrease in the protein content of the poultry meat during spoilage, an increase in the formation of free amino acids, an increase in oxidation of amino acid residues, and an increase in microbial growth on the surface of the poultry fillets, as well as revealing information about hydrophobic interaction around the aliphatic residues. Similar groupings

(fresh, semi-fresh, and spoiled) were also obtained from the results of an Agglomerative Hierarchical Cluster Analysis (AHCA) of the first five principal components. The results allow the conclusion that the portable fiber-optic Raman spectrometer can be used as a reliable and fast method for real-time freshness evaluation of poultry during storage.

Further, the characterization and discrimination of fillets samples from different poultry meat production lines (conventional and alternative) of a German poultry producer were successfully accomplished using portable fiber-optic Raman spectrometer in tandem with chemometric analysis (PCA, Canonical Discriminant Analysis (CDA) and AHCA). The investigations were conducted at five repeated investigation times during storage started 24 h after slaughter at 0, 72, 120, 168 and 240 h of the experiment. Raman measurements were conducted directly on fillets surfaces parallel with microbiological and nutrients analysis. A total of 80 fillets were investigated in two repeated storage trials under the same conditions. PCA model was constructed using the 1st storage trial (1st investigation time; 0 h). The model was able to group the poultry samples according to their production line into two classes: conventional and alternative. The testing data points from the 2nd storage trial (1st investigation time; 0 h) were used to validate the model and all have been successfully assigned to the correct cluster. Similar results were also obtained from CDA and AHCA models. The origin of the separation in PCA model was investigated by analysing the loading plots. The results show that the alternative production line has higher collagen, protein and carbohydrates content than the conventional. These results were consistent with the analysis of nutrients in both production lines. The alternative production line also shows a higher carotenoids content which may account for the color difference between both production lines, with the alternative production line displaying more yellowish fillets. Moreover, CDA models were constructed for each production line to classify poultry fillets according to their storage time (five investigation times) and their microbial load (three quality classes). The 1st storage trial (training set) was used to build the models and the 2nd storage trial (testing set) was used to validate these models. For both production lines, all constructed CDA models showed good ability to classify poultry fillets according to their storage time and to their microbial load with error rates less than 25.00%. However, the classification ability of the constructed CDA models showed different results when tested with the 2nd storage trial. For the classification according to the storage time, CDA models showed poor classification ability for both production lines (error rate: 42.06% and 62.99% for conventional and alternative, respectively). The high error rates could be correlated to the high variations of the bacterial load between the two storage trials for each production line. For the classification

according to the microbial load, CDA models classification ability was good for the conventional production line (error rate: 24.60%) and poor for the alternative production line (error rate: 54.33%). The low error rate for the conventional production line indicates that the variations between the two storage trials were low. While the high error rate for alternative production line indicates that the variations between the two storage trials were too high and that the microbial load is not the only factor that has an impact on the collected Raman spectra from the two storage trials. Since fillets of the alternative line had significantly higher protein and lower water and intramuscular fat content in comparison to the conventional production line, and taking into account that the lipid oxidation and autolytic enzymatic spoilage are also considered one of the main mechanisms for meat spoilage; high variations from different storage trials will appear in the collected Raman spectra which will affect the classification ability. The results allow the conclusion that the Raman spectra collected by the portable fiber-optic Raman spectrometer in conjunction with chemometric analysis can be used as a reliable and fast method to characterize and discriminate samples from different poultry meat production systems.

Zusammenfassung

Die Diskriminierung und Klassifizierung von acht Stämmen von Fleischverderb-Mikroorganismen, die üblicherweise in Geflügelfleisch vorkommen, wurde erfolgreich unter Verwendung von zwei dispersiven Raman-Spektrometern (Mikroskop- und tragbare Fiberoptik-Systeme) in Kombination mit chemometrischen Methoden durchgeführt. Die Hauptkomponentenanalyse (PCA, engl. Principal Components Analysis) und Multi-Class Support-Vektor-Maschine-Methode (MC-SVM) wurden zur Entwicklung von Diskriminierungs- und Klassifizierungsmodellen verwendet. Diese Modelle wurden anhand von Validierungsdatensätzen überprüft, die erfolgreich den richtigen bakteriellen Gattungen und sogar dem richtigen Stamm zugeordnet werden konnten. Die Diskriminierung von Bakterien bis auf das Stammniveau wurde für die vorverarbeiteten Spektraldaten unter Verwendung eines 3-stufigen Modells auf PCA-Basis durchgeführt. Die spektralen Merkmale und Unterschiede zwischen den Arten, auf denen die Unterscheidbarkeit beruhte, wurden durch PCA-Loadings identifiziert. Mittels MC-SVM wurden die vorverarbeiteten Spektraldaten einer PCA unterzogen und zur Erstellung eines Klassifizierungsmodells verwendet. Bei Verwendung der ersten beiden Hauptkomponenten betrug die Genauigkeit des MC-SVM-Modells 97,64% und 93,23% für die vom Raman-Mikroskop bzw. vom tragbaren Fiberoptik Raman-System gesammelten Validierungsdaten. Die Genauigkeit erreichte 100% für die Validierungsdaten, indem die ersten acht und zehn PCs aus den Daten verwendet wurden, die vom Raman-Mikroskop bzw. vom tragbaren Fiberoptik Raman-System gesammelt wurden. Die Ergebnisse zeigen, dass die entwickelten Modelle inklusiver der Datenvorverarbeitung und Messmethoden eine hohe Unterscheidbarkeit bei hoher Leistungsfähigkeit der Auswertung ermöglichen und dass auch das in dieser Studie verwendete tragbare Fiberoptik Raman-System mit geringerer Auflösung der spektralen Daten mit dem entwickelten Verfahren ein vergleichbares Ergebnis erzielt.

Unter Verwendung des tragbaren Fiberoptik Raman-Spektrometers (ein QE Pro-Raman-Spektrometer mit einer Laseranregungswellenlänge von 785 nm von Ocean Insight, ehemals Ocean Optics) wurden die Frischeveränderungen in Geflügelfilets während der Lagerung untersucht. Geflügelfilets mit derselben Haltbarkeit (9 Tage) und demselben Verfallsdatum wurden von einem örtlichen Geschäft gekauft und bei 4 °C gelagert. Ihre Raman-Spektren wurden täglich bis zum 21. Tag gemessen. Die komplexen Spektren wurden unter Verwendung von PCA analysiert, was zu einer Trennung der Proben in drei Qualitätsklassen nach ihrer Frische führte: frisch, halbfrisch und verdorben. Diese Klassen

basierten auf den Informationen, die aus dem Produktetikett auf den Verpackungen abgeleitet wurden. Die PCA-Loadings lieferten Hinweise auf eine Abnahme des Proteingehalts des Geflügelfleisches während des Verderbs, eine Zunahme der Bildung freier Aminosäuren, eine Zunahme der Oxidation von Aminosäurerückständen und eine Zunahme des mikrobiellen Wachstums auf der Oberfläche der Geflügelfilets sowie Informationen über hydrophobe Wechselwirkungen um die aliphatischen Rückstände. Ähnliche Gruppierungen (frisch, halbfrisch und verdorben) wurden auch aus den Ergebnissen einer Agglomerativen Hierarchischen Clusteranalyse (AHCA) der ersten fünf Hauptkomponenten gewonnen. Die Ergebnisse lassen den Schluss zu, dass das tragbare Fiberoptik Raman-Spektrometer als zuverlässige und schnelle Methode zur Echtzeit-Auswertung der Frische von Geflügel während der Lagerung eingesetzt werden kann.

Weiterhin wurde die Charakterisierung und Diskriminierung von Filetproben aus verschiedenen Geflügelfleischproduktionslinien (konventionell und alternativ) eines deutschen Geflügelherstellers erfolgreich unter Verwendung von einem tragbaren Fiberoptik Raman-Spektrometer in Verbindung mit chemometrischen Analysen (PCA, Kanonische Diskriminanzanalyse (CDA, engl. Canonical Discriminant Analysis) und AHCA) durchgeführt. Die Untersuchungen wurden zu fünf wiederholten Untersuchungszeiten während der Lagerung durchgeführt, die 24 Stunden nach dem Schlachten bei 0, 72, 120, 168 und 240 Stunden des Experiments begann. Raman-Messungen wurden direkt an Filetoberflächen parallel zur mikrobiologischen Bestimmung und Nährstoffanalyse durchgeführt. Insgesamt 80 Filets wurden in zwei wiederholten Lagerversuchen unter den gleichen Bedingungen untersucht. Das PCA-Modell wurde unter Verwendung des 1. Lagerversuchs (1. Untersuchungszeit; 0 h) konstruiert. Das Modell war in der Lage, die Geflügelproben entsprechend ihrer Produktionslinie in zwei Klassen in konventionell und alternativ zu gruppieren. Die Testdatenpunkte aus dem 2. Lagerungsversuch (1. Untersuchungszeit; 0 h) wurden zur Validierung des Modells verwendet und alle wurden erfolgreich dem richtigen Cluster zugewiesen. Ähnliche Ergebnisse wurden auch von CDA- und AHCA-Modellen erzielt. Der Ursprung der Trennung im PCA-Modell wurde durch die Analyse des Loadingdiagramms untersucht. Die Ergebnisse zeigen, dass die alternative Produktionslinie einen höheren Kollagen-, Protein- und Kohlenhydratgehalt aufweist als die konventionelle. Diese Ergebnisse stimmten mit der Analyse der Nährstoffe in beiden Produktionslinien überein. Die alternative Produktionslinie zeigt auch einen höheren Carotinoidgehalt, der den Farbunterschied zwischen beiden Produktionslinien erklären kann, wobei die alternative Produktionslinie mehr gelbliche Filets anzeigt. Darüber hinaus wurden

für jede Produktionslinie CDA-Modelle bestimmt, um Geflügelfilets nach ihrer Lagerzeit (fünf Untersuchungszeiten) und ihrer mikrobiellen Belastung (drei Qualitätsklassen) zu klassifizieren. Der 1. Lagerversuch (Trainingsdatensatz) wurde verwendet, um die Modelle zu erstellen, und der 2. Lagerversuch (Testdatensatz) wurde verwendet, um diese Modelle zu validieren. Für beide Produktionslinien zeigten alle CDA-Modelle ein gutes Ergebnis, Geflügelfilets nach ihrer Lagerzeit und ihrer mikrobiellen Belastung mit Fehlerraten von weniger als 25,00% zu klassifizieren. Die Klassifizierungsfähigkeit der verwendeten CDA-Modelle zeigte jedoch unterschiedliche Ergebnisse, wenn sie mit der dem 2. Lagerversuch überprüft wurden. Für die Klassifizierung nach Lagerzeit wiesen CDA-Modelle für beide Produktionslinien eine schlechte Klassifizierungsfähigkeit auf (Fehlerquote: 42,06% bzw. 62,99% für konventionelle und alternative Modelle). Die hohen Fehlerraten können mit den hohen Variationen der gemessenen bakteriellen Belastung zwischen den beiden Lagerversuchen für jede Produktionslinie korreliert werden. Für die Klassifizierung nach der mikrobiellen Belastung war die Klassifizierungsfähigkeit der CDA-Modelle für die konventionelle Produktionslinie gut (Fehlerrate: 24,60%) und für die alternative Produktionslinie schlecht (Fehlerrate: 54,33%). Die niedrige Fehlerrate für die herkömmliche Produktionslinie zeigt, dass die Variationen zwischen den beiden Lagerversuchen gering waren,während die hohe Fehlerrate für alternative Produktionslinien darauf hinweist, dass die Variationen zwischen den beiden Lagerversuchen zu hoch waren und dass die mikrobielle Belastung nicht der einzige Faktor ist, der sich auf die gesammelten Raman-Spektren aus den beiden Lagerversuchen auswirkt. Da Filets der alternativen Linie im Vergleich zur herkömmlichen Produktionslinie einen deutlich höheren Protein- und niedrigeren Wasser- und intramuskulären Fettgehalt aufwiesen und unter Berücksichtigung der Tatsache, dass die Lipidoxidation und der autolytische enzymatische Verderb ebenfalls als einer der Hauptmechanismen für den Fleischverderb angesehen werden, wird dies zu großen Unterschieden bei den verschiedenen Lagerversuchen führen, die die Klassifizierungsfähigkeit über die aufgenommenen Raman-Spektren beeinträchtigen wird. Die Ergebnisse lassen aber dennoch den Schluss zu, dass die Raman-Spektren, die vom tragbaren Fiberoptik Raman-Spektrometer in Verbindung mit chemometrischer Analyse gesammelt werden, als zuverlässige und schnelle Methode zur Charakterisierung und Diskriminierung von Proben aus verschiedenen Geflügelfleischproduktionssystemen eingesetzt werden können.

Table of Contents

List of Tables

List of Figures

List of Abbreviations

Acc.	Accuracy
Ade	Adenine
AHCA	Agglomerative hierarchical cluster analysis
a.u.	arbitrary units
α	Polarizability
α_0	Polarizability at the equilibrium position
B. coag	*Bacillus coagulans* DSM 1
B. subt	*Bacillus subtilis* DSM 10
B. ther	*Brochothrix thermosphacta* DSM 20171
C	Regularization parameter
CCDs	Charge-coupled devices
CDA	Canonical Discriminant Analysis
CV	Canonical Variable
DNA	Deoxyribonucleic acid
E	Strength of electric field
E. coli HB101	*Escherichia coli* HB101
E. coli K12	*Escherichia coli* K12
E_0	Amplitude of the electrical field
ELISA	Enzyme-linked immunosorbent assay
FN	False negative
FP	False positive
FT	Fourier transform
γ	Gamma parameter
h	hour
λ_{il}	Wavelengths (in nm) of incident light

λ_{sl}	Wavelengths (in nm) of scattered light
M. lute	*Micrococcus luteus* DSM 20030
MALDI-TOF MS	Matrix assisted laser desorption ionization-time of flight mass spectrometry
MC-SVM	Multi-class support vector machines
v_0	Frequency of incident light
v_m	Frequency of vibration
P	Induce dipole moment
P. fluo 4	*Pseudomonas fluorescens* DSM 4358
P. fluo 5	*Pseudomonas fluorescens* DSM 50090
PCA	Principal components analysis
PCR	Polymerase chain reaction
Phe	Phenylalanine
PMTs	Photomultiplier tubes
q	Displacement of atoms about their equilibrium position
q_0	Vibrational amplitude
RNA	Ribonucleic acid
RS	Raman shift
s	second
SDM	Standard deviation of means
Sens.	Sensitivity
Spec.	Specificity
t	Time
TN	True negative
TP	True positive
Trp	Tryptophan

TVC	Total Viable Count
Tyr	Tyrosine

1 General Introduction

1.1 Background

Muscle foods, including poultry and red meat, are rich sources of protein, essential amino acids and a wide variety of micronutrients essential for human nutrition and health [1–3]. However, fresh meat ranks among the highly perishable food due to its nutritional composition, which transforms it into a susceptible product for the growth of spoilage and pathogenic microorganisms [4–8].

From a consumer and industry perspective, high safety, quality and long shelf life times are the most important criteria for meat and meat products [9].Therefore, the production of high quality and safe meat products with a long shelf life is one of the meat industry's major tasks [10]. Currently, the spoilage and pathogenic microorganisms are determined by culture and colony counting methods which are laborious and time-consuming [11–13]. This is inconvenient in modern food industrial applications [12]. As meat freshness is important to consumers, the meat industry and retailers, a high demand, therefore, remains for the development of effective, rapid, simple, non-destructive and inexpensive sensing technologies for detecting microbial contamination on meat [14–16].

Several methods have been developed to achieve fast and reliable bacterial identification such as Raman spectroscopy [17–23]. Although much research has employed Raman spectroscopy in identifying clinically relevant bacteria [24–27], less has been done with food-related bacteria [28–30]. Several research groups have investigated various methods for the rapid detection of microbiological spoilage on different kinds of meat [31–34]. However, research on and investigations into fast methods for precisely predicting bacterial loads in poultry meat, which production and consumption has risen dramatically in recent years leading to a significant increase in its commercial value [14, 35], are rare even though they are urgently needed for efficient management in the poultry industry [36, 37]. Moreover, Raman spectra usually treated as mathematical data and only little or no attention is paid to interpreting the spectra, which obscures the spectral features and differences among the species on which the classification is made [30, 38–40]. The individual spectral contributions need to be understood better if the field is to move forward.

1.2 Raman Spectroscopy

1.2.1 Theory

Raman spectroscopy is an increasingly popular technique in many areas because it is a non-destructive, non-invasive, rapid, being label-free and relatively inexpensive compared to other methods. Moreover, it requires simple up to no sample preparation and allows for both organic and inorganic substances to be measured in a variety of states. Raman spectroscopy provides information about the concentration, the molecular composition and structure of a sample based on vibrational information. Given these advantages, Raman spectroscopy has already been applied in numerous fields, including physics, chemistry, geology, material sciences, pharmaceutical analysis, and semiconductor technology and many others. Raman spectroscopy is almost insensitive to water, making it an ideal method for biological applications [41–46].

Raman spectroscopy is one kind of spectroscopic technique based on Raman scattering. Raman scattering is a phenomenon results from the interaction of the light with molecules through inelastic scattering of light, in which the incident light induces molecular vibrations in the sample. The phenomenon of inelastic scattering of light was predicted theoretically in 1923 by A. Smekal, and experimentally confirmed in 1928 by C. V. Raman, which is the reason why the inelastic scattering is called Raman scattering. For which discovery, Prof. Raman received the 1930 Nobel Prize in Physics [44, 47–51].

When light interact with matter this will lead to several different processes such as transmission, reflection, absorption or scattering. In the process of scattering, the incident light interacts with molecules by distorting (polarizing) the electron cloud, as a result, promotes the system to a higher-energy state generally identify as a ‘virtual state’. This ‘virtual state’ is not stable, the photons are scattered immediately to another state which is relatively stable, giving rise to the phenomenon of light scattering [47, 52, 53].

There are two types of scattering that may occur, Rayleigh (elastic) and Raman (inelastic) scattering. The predominant form is Rayleigh scattering, approximately one in 10^3 photons undergoes Rayleigh scattering. Rayleigh scattering occurs when the scattered light is of the same frequency as the incident light. Since there is no change in energy or frequency, Rayleigh scattering are called elastic scattering. As shown in Figure 1.1(a), an incident light excites a molecule from an initial vibrational state to the ‘virtual state’. After being excited,

the molecule spontaneously drops back to the same initial state [44, 48, 52, 54–57]. The other type of scattered light called Raman scattering which is a weak phenomenon, approximately one of about 10^6 to 10^8 photons undergoes Raman scattering. Raman scattering occurs if the scattered light have energy or frequency different from that of the incident light. As there is a change in energy (lost or gained), Raman scattering are called inelastic scattering. As shown in Figure 1.1(b) and (c), Raman scattering can be classified into two types, Stokes and Anti-Stokes Raman scattering. In the case of Stokes Raman scattering (Figure 1.1(b)), a molecule is excited from the ground vibrational state to the 'virtual state' and spontaneously relaxes to a higher energy vibrational state in the ground state, thus scattered light holds a lower frequency than the incident light. While in the case of Anti-Stokes Raman scattering (Figure 1.1(c)), the molecule is already in excited vibration state, after interacting with the incident light the molecule excited to the 'virtual state' and spontaneously relaxes to a lower energy vibrational state in the ground state, thus scattered light holds a higher frequency than incident light. The difference in energy between incident and scattered photons is equal to the energy of transition between two vibrational modes. Accordingly; the energy of emitted photons (being shifted down or up) gives information about the vibrational structure of the sample [44, 47, 48, 52–55, 57].

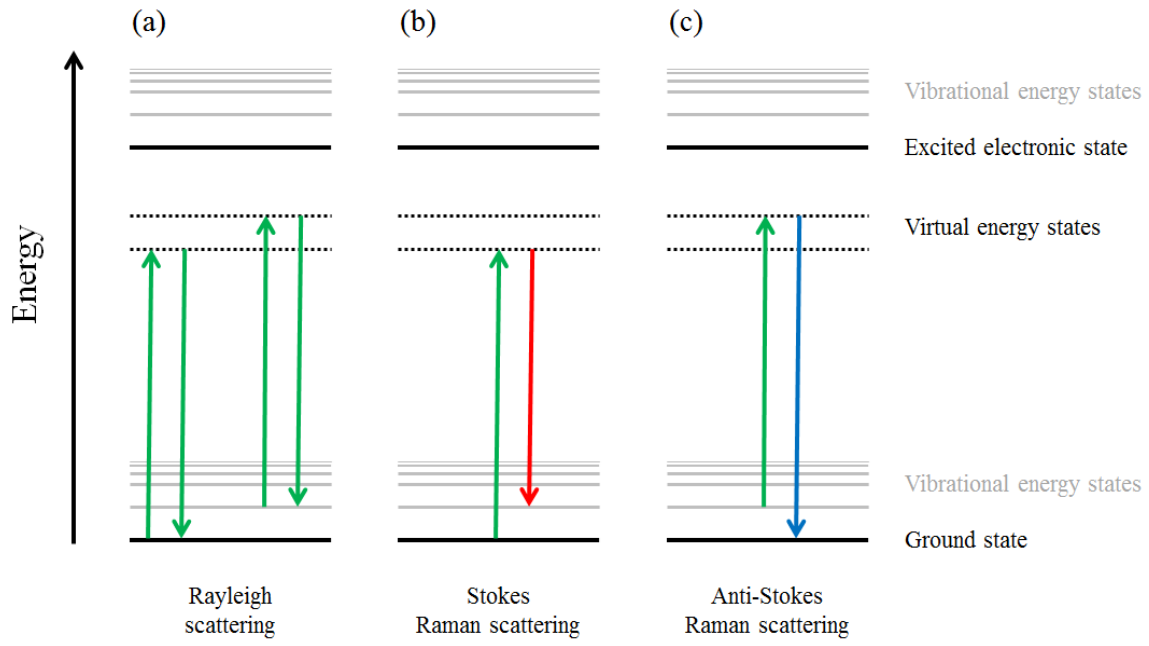

Figure 1.1: Energy level diagram for: (a) Rayleigh scattering, (b) Stokes Raman scattering and (c) Anti-Stokes Raman scattering.

According to classical theory, the polarizability (α) of a molecule represents the ability of an external electric field of strength E to induce a dipole moment (P) in the molecule. The induce dipole moment can be defined by:

$$P = \alpha E \tag{1.1}$$

and the strength of the electric field of the incident light of frequency v_0 is given by:

$$E = E_0 \cos 2\pi v_0 t \tag{1.2}$$

where E_0 is the amplitude of the electrical field at time t. For any molecular bond, the individual atoms in a molecule are confined to specific vibrational modes. The displacement (q) of atoms about their equilibrium position due to a particular vibrational mode can be expressed as:

$$q = q_0 \cos 2\pi v_m t \tag{1.3}$$

where q_0 is the vibrational amplitude and v_m is the frequency of vibration. For a small amplitude of vibration, α is a linear function of q. Thus, it can be approximated as a Taylor series expansion in normal coordinates as follows:

$$\alpha = \alpha_0 + \left(\frac{\partial \alpha}{\partial q}\right)_0 q + \ldots . \tag{1.4}$$

where α_0 stands for the polarizability at the equilibrium position, and $(\partial\alpha/\partial q)_0$ is the rate of change of α with respect to the change in q evaluated at the equilibrium position. Approximating equation (1.4) to the first order term and substituting it and equations (1.2) and (1.3) into equation (1.1) yields:

$$P = \alpha_0 E_0 \cos 2\pi v_0 t + \frac{1}{2}\left(\frac{\partial \alpha}{\partial q}\right)_0 q_0 E_0 [\cos\{2\pi(v_0 + v_m)t\} + \cos\{2\pi(v_0 - v_m)t\}] \tag{1.5}$$

From a classical approach, the first term in equation (1.5), $(\alpha_0 E_0 \cos 2\pi v_0 t)$, represents Rayleigh scattering in which the scattered radiation has a frequency, v_0, equal to the incident light. The second term in the equation, $\left(\frac{1}{2}\left(\frac{\partial \alpha}{\partial q}\right)_0 q_0 E_0 \cos\{2\pi(v_0 + v_m)t\}\right)$, corresponds to the Anti-Stokes Raman scattering in which the scattered radiation has a frequency, $(v_0 + v_m)$, higher than the incident light (blue shifted). The third term in the equation, $\left(\frac{1}{2}\left(\frac{\partial \alpha}{\partial q}\right)_0 q_0 E_0 \cos\{2\pi(v_0 - v_m)t\}\right)$, represents Stokes Raman scattering in which the scattered radiation has a frequency, $(v_0 - v_m)$, lower than the incident light (red shifted).

As indicated by equation (1.5) the Stokes or Anti-Stokes Raman scattering will vanish if the differential term is equal to zero. This gives rise to the selection rule of Raman spectroscopy, which states that, in order to be Raman active, a vibration must involve a

change in the polarizability of the system, i.e.: $(\partial\alpha/\partial q)_0 \neq 0$. The Quantum description and more detailed aspects of Raman are discussed elsewhere [44, 52, 58–60]

The intensity of Stokes and Anti-Stokes Raman scattering light is proportionate to the number of scattering molecules. As different departure vibrational levels involved, the intensity of the two processes will be different. At room temperature, the Boltzmann distribution of vibrational states has the majority of molecules in their ground vibrational states and therefore; the intensity of Stokes scattering light is greater than the intensity of the Anti-Stokes. As the Stokes scattering light is the more intense and since the same information can be obtained from both processes; Stokes scattering light is typically measured in the conventional Raman spectroscopy [47, 48, 52, 57–59].

The Raman scattering process as illustrated above occurs spontaneously. Thus, this process is called spontaneous Raman scattering. Since this process is very weak; it has a very small cross-section ($\sim 10^{-30}$ cm^2). Therefore, numbers of various techniques of Raman Spectroscopy such as Surface Enhanced Raman Spectroscopy, Coherent Anti-Stokes Raman Scattering, Resonance Raman Spectroscopy, Transmission Raman Spectroscopy, Stimulated Raman scattering, Tip-Enhanced Raman Spectroscopy have been developed to enhance sensitivity, to improve intensity, to reach better spatial resolution and other improvements [44, 58, 59, 61–64]. This thesis deals only with spontaneous Stokes Raman scattering.

A typical Raman spectrum is obtained by plotting the intensity of the scattered light (in arbitrary units (a.u.)) on the vertical axis against the Raman shift on the horizontal axis. Raman shift defined as the difference in frequency between the incident and scattered light, and it is usually in units of wavenumbers (cm^{-1}). Raman shift is determined by:

$$\text{Raman shift} = \left(\frac{1}{\lambda_{il}} - \frac{1}{\lambda_{sl}}\right) \times 10^7 \tag{1.6}$$

where λ_{il} and λ_{sl} are the wavelengths (in nm) of incident light and scattered light, respectively. As an example; see Figures 1.2(a) and (b) for Raman spectra of polystyrene and fresh boneless skinless chicken breast fillet, respectively. The Raman spectra are typically featured by a series of narrow and sharp peaks. The position of each peak is related to a particular molecular vibration at a fixed frequency, which can be used to analyse the composition of a sample. The intensity of the Raman peak is linearly proportional to the concentration of molecules, which can be used for quantitative analysis of the analyte. Since it is a difference value, the Raman shift of materials is usually independent of the wavelength of the incident light. Therefore; Raman shift is an intrinsic property of a molecule, which makes the Raman spectroscopy a powerful experimental tool for analytical studies [47, 52, 56, 59, 62, 65–68].

As shown in Figures 1.2(a) and (b), Raman spectra for organic and biological molecules can be divided into three parts: the fingerprint region (below 1800 cm^{-1}), the silent region (from 1800 cm^{-1} to 2800 cm^{-1}) and the high frequency region (above 2800 cm^{-1}). For biological samples, approximately 90% of the peaks are found in the fingerprint region and associated with bond vibrations of nucleic acids (DNA and RNA), proteins, carbohydrates, lipids and additional cellular biomolecules. This region gets its name from the diversity of sharp and localized spectral features that give molecules unique fingerprints. These molecular fingerprints can allow sample classification and chemometric analysis. The silent region is mostly empty of contributions from biological molecules. The remaining of the peaks are found in the high frequency region and associated with bond vibrations of CH, NH and OH stretching in lipids, proteins and water. Bands in this region are much broader, leading to increased spectral overlap [44, 58, 69–72].

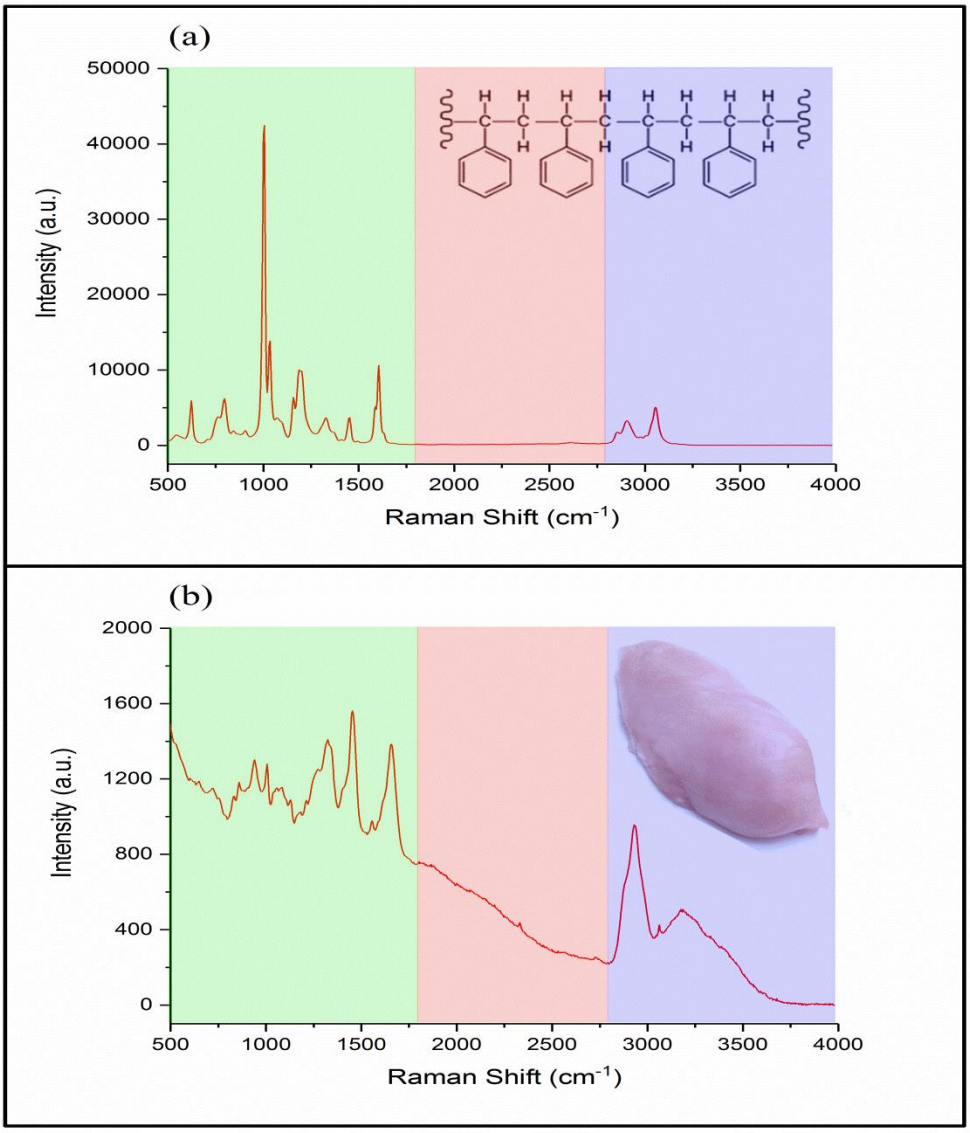

Figure 1.2: Mean Raman spectra of: (a) Polystyrene, (b) Fresh boneless skinless chicken breast fillet. The spectra were collected by Portable Fiber-Optic Raman system (QE Pro-Raman system, Ocean Optics, Netherlands) using a 785 nm laser at 250 mW power. The exposure time was 1 s for polystyrene and 10 s for the fresh boneless skinless chicken breast fillet. The fingerprint region is highlighted in green, the silent region in red and the high frequency region in violet.

1.2.2 Instrumentation

1.2.2.1 Raman Spectrometer

A spectrometer is the instrument used to collect Raman spectra. The major typical components of Raman spectrometer are an excitation source, light collection system, monochromator and a detector. A typical Raman spectrometer is shown schematically in

Figure 1.3. The excitation light is delivered to the sample and Raman scattered light is collected back and directed towards the detector by some intermediate optics. These intermediate optics can include lenses, mirrors and filters [54, 64, 73, 74]. The main elements of a Raman spectrometer and their roles are summarized below.

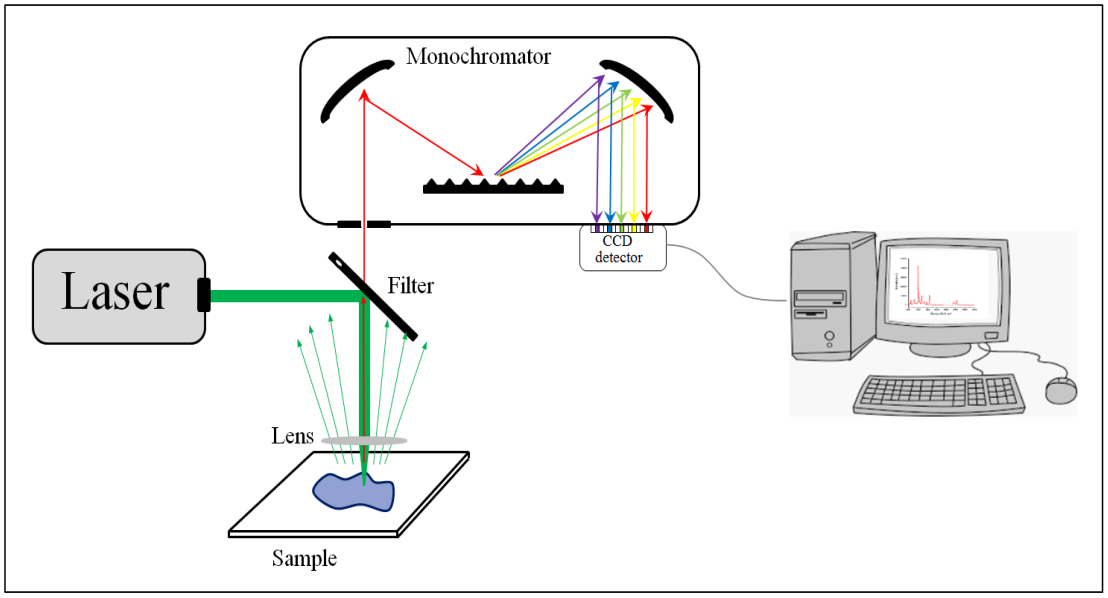

Figure 1.3: Schematic layout of a typical Raman spectrometer.

1.2.2.1.1 Excitation Source

Since the Raman effect is a very weak process, lasers are preferable as an excitation source to produce quality Raman spectra. Lasers offered many advantages such as monochromaticity, brightness, high accuracy of collimation and power density. The wavelengths of most used lasers in Raman spectroscopy are listed in Table 1.1. The intensity of the Raman scattering is linearly proportional to the laser power, but it depends on the fourth power of the excitation light frequency, hence shorter wavelength provides higher Raman signal. However, with a short excitation wavelength a thermal decomposition of a biological sample can occur. For most biological samples, Autofluorescence is an additional issue associated with the excitation laser emitting in the visible range. Fluorescence usually occurs when the laser light is absorbed by the analyte or chromophore group, as well as crystal defects. The appropriate selection of the incident laser wavelength is necessary to avoid this problem. A lower energy excitation laser reduces the likelihood of fluorescence excitation. Hence, Fluorescence is suppressed or even diminished when the excitation wavelength moves to the Near-Infrared for biological samples. Thus, Near-Infrared lasers,

most commonly at 785 and 830 nm, have been extensively applied in biological studies [48, 54, 55, 58, 70, 73–76].

Table 1.1: List of wavelengths in nm of the most used lasers in Raman spectroscopy.

Ultra-Violet	Visible	Near-Infrared
244 (Argon ion)	488 (Argon ion)	785 (Diode laser)
325 (Helium–Cadmium)	514.5 (Argon ion)	830 (Diode laser)
363 (Argon ion)	532 (Neodymium–Yttrium Aluminum Garnet)	1064 (Neodymium–Yttrium Aluminum Garnet)
	632.8 (Helium–Neon)	
	647.1 (Krypton ion)	

1.2.2.1.2 Monochromators

Single monochromator comprise a diffraction grating, which is used to disperse the Raman scattered light. Dispersive Raman spectroscopy and Fourier transform (FT) Raman spectroscopy are the two main techniques used to collect Raman spectra. Dispersive Raman spectroscopy uses gratings and multistage monochromators to disperse the signal into its spectral components, whereas FT-Raman spectroscopy involves the use of a multiplexing spectrometer system, such as a Michelson interferometer, to detect and analyse the radiation scattered from a sample [70, 73].

1.2.2.1.3 Light Collection System

1.2.2.1.3.1 Fiber Optics

Fiber optics are often used to deliver the excitation light to the sample and to deliver collected Raman scattered light back to the instrument. Nearly all Raman fiber optic probes use multimode silica fiber optics. Even though silica fibers are very efficient across the visible and Near-Infrared portions of the spectrum, it is also generates a spectral background due to the Raman scattering of the silica and a fluorescence background. This spontaneous background can be reduced through the use of low hydroxyl content optical fibers and further suppress by using optical filters at the end of the probe. The excitation laser light is filtered

using a short-pass or a notch filter, while the collected Raman scattered signal is filtered with a long-pass or a notch filter. The optical paths for excitation and collection can be overlapped using a dichroic or a notch filter, either of which can be used to reflect the laser beam but transmit the Raman scattered light [74].

1.2.2.1.3.2 Filters

Filters such as interferential, edge and density filters can be integrated into the spectrometer. The interference filter used to eliminates the parasitic radiation emitted by the laser. The interference filter located just after the laser source, thus improving the quality of the excitation beam. The edge rejection filter eliminates the contribution of the Rayleigh scattering. Since Rayleigh scattering is more intense than Raman scattering, it can easily overwhelm the Raman scattering signal, so it must be optically filtered. The most commonly used Rayleigh filters are holographic notch and dielectric edge filters. Edge filters only transmit light wavelengths above that of the laser in use, while notch filters will effectively filter only the laser wavelength, allowing both Stokes and Anti-Stokes measurements. The density filter used to control the power of the laser according to the analysis requirement [54, 70].

1.2.2.1.4 Detector

The detector included in the Raman system needs to be extremely sensitive to detect the weak intensity of Raman scattering. The detector was initially the human eye, later more sensitive detectors in the form of photomultiplier tubes (PMTs), which are characterized by single-channel recording, were available. By contrast, the multichannel technique can record a large number of spectral elements simultaneously with a sensitivity per channel that is comparable to a photomultiplier, which delivers a drastic reduction in the amount of time required to obtain Raman data. The availability of charge-coupled devices (CCDs) led to the development of a new generation of multichannel Raman spectrometers. CCDs are multichannel arrays made up of thousands of pixels, each of which can collect charge from scattered photons. This charge is directly proportional to the Raman scattering intensity. CCDs are commonly integrated in Raman systems, because they exhibit high quantum efficiencies and low signal-to-noise ratios, compared with early alternative detectors such as

PMTs. Dark, or thermal, noise can be notably improved by detector cooling, often by using liquid nitrogen cryogenic or thermoelectric Peltier cooling [70, 73].

1.2.2.1.5 Computer System

The computer system transforms the electrical signal into a signal which can be used by the user, enabling the device control with different commands and processing the data with the dedicated software [54].

1.2.2.2 Raman Microspectroscopy

Raman microspectroscopy used to investigate very small quantities of materials, or even domains within materials, at a resolution of a few square micrometers. In Raman microspectroscopy, Raman spectrometer is interfaced to a standard microscope. The microscope is used to focus the laser beam onto the sample via a microscope objective lens and then collects scattered photons and redirects them to the spectrometer. This enables the visual inspection of sample and facilitates spectroscopic analysis of a limited amount of sample or a selected small region within a sample. Raman microspectroscopy enables both visual and spectroscopic examinations, either as single point, mapping or imaging measurements. To reduce interference from Fluorescence emission, avoid sample damage and achieve reasonable experiment times in Raman microspectroscopy measurements, parameters such as the laser wavelength, laser power, focusing element (objective lens), spectrometer grating, the acquisition time and pixel size and number have to be carefully selected [48, 54, 73, 74, 76, 77].

1.2.2.3 Raman Systems Used in this Work

1.2.2.3.1 Portable Fiber-Optic Raman System

As shown in Figure 1.4, the Portable Fiber-Optic Raman system used in this work consists of four components: a QE Pro-Raman spectrometer, a Turnkey Raman laser of 785 nm excitation wavelength, an RPB785 fiber-optic probe and a computer running OceanView version 1.4.1 software. All four components are from Ocean Optics (Ocean

Optics, Netherlands). A more detailed description of this system can be found in chapter 3, section 3.2.2.

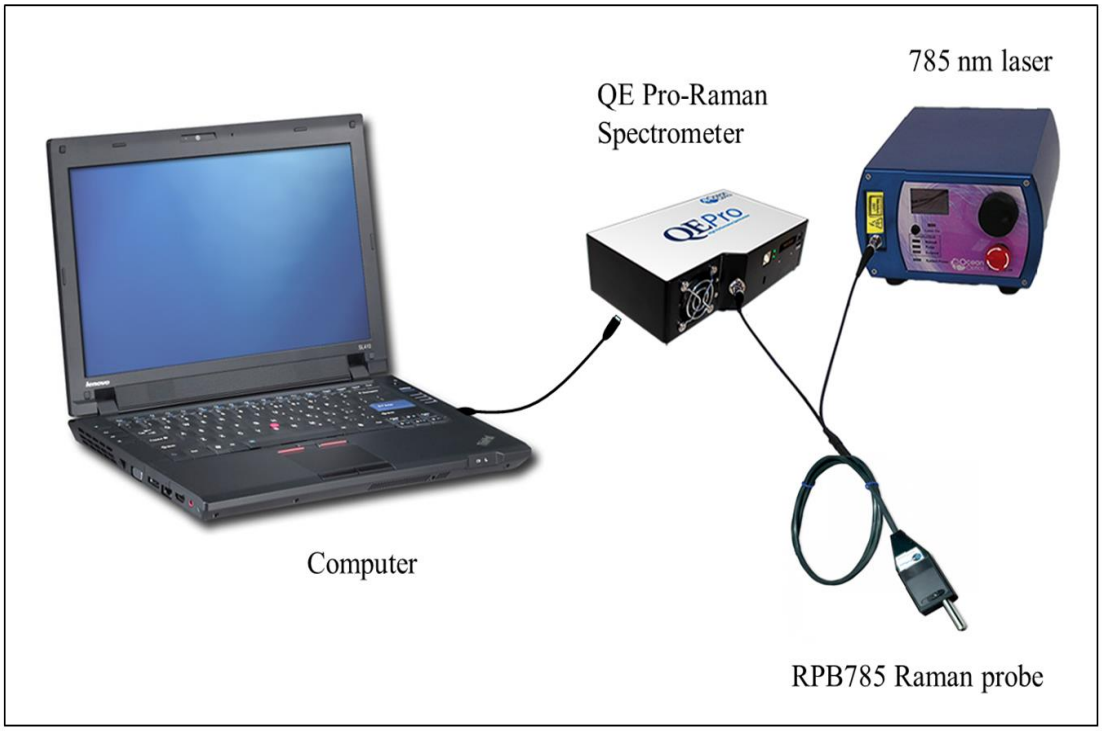

Figure 1.4: Components of Portable Fiber-Optic Raman system used in this work.

1.2.2.3.2 Raman Microscope System

The Raman microscope system used in this work is SENTERRA Raman microscope. SENTERRA Raman microscope (see Figure 1.5) is a bench-top model of dispersive Raman spectrometer (Bruker Optics, Ettlingen, Germany), hereafter referred to as 'SENTERRA'. It is equipped with 488, 532 and 785 nm laser sources. The spectral range depends on the frequency of the laser and on the resolution mode. In the low resolution mode (9-15 cm^{-1}) the spectral ranges for 488, 532 and 785 nm laser sources are 80-4500 cm^{-1}, 60-4450 cm^{-1} and 60-3500 cm^{-1} respectively. While in the high resolution mode (3-5 cm^{-1}), several spectral windows are exist within the spectral range for each laser source. To reduce the intensity of the laser light SENTERRA spectrometer uses neutral density filters. The intensity can be reduced from 100% (no filter) down to 50%, 25%, 10% and 1% of the original laser intensity. In SENTERRA spectrometer an Olympus microscope (model BX51) is used to visualise the sample and to focus the laser beam on it. A digital video camera is coupled to the microscope, delivering digital images of the samples. The laser light or the visible light is focussed on the sample using the objectives of the microscope. The microscope has 5×, 20×, 50× and 100×

objectives, with spot sizes of approximately 50, 10, 4 and 2 μm, respectively. SENTERRA spectrometer has an XYZ motorised stage which is used to select the region of interest of the sample. This motorised stage can be controlled by the OPUS software and by a joystick. The motorised stage provides automatic point measurements of a list of predefined spots on the sample. SENTERRA spectrometer has two different types of apertures: a slit-type aperture of 25 x 1000 μm and one of 50 x 1000 μm for high-throughput; and two pinhole-type apertures of 25 μm and 50 μm for confocal spectroscopy and depth profiling. SENTERRA spectrometer contains two different diffraction gratings: one with 400 lines/mm to measure in low resolution mode (9-15 cm^{-1}) and one with 1200 lines/mm to measure in high resolution mode (3-5 cm^{-1}). The system uses a thermoelectrically cooled CCD detector, operating at -70 °C. The format of the CCD in the SENTERRA spectrometer is 1024 x 256 pixels. The instrument is controlled via the OPUS software version 7.5 [78–80].

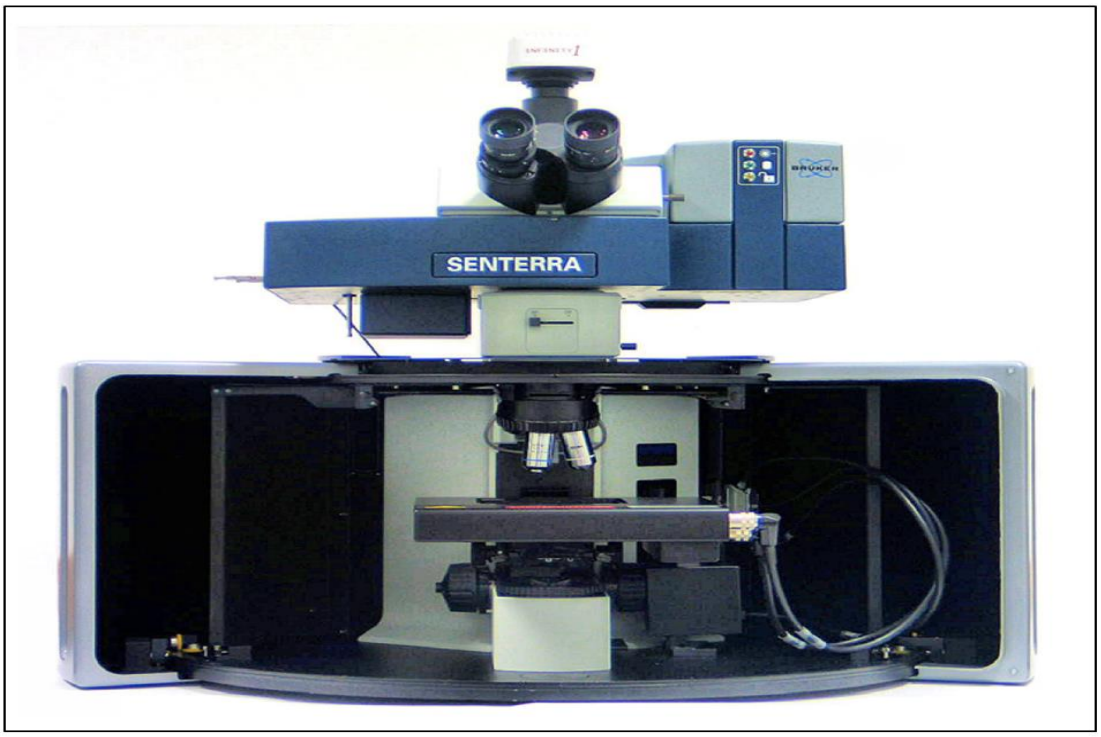

Figure 1.5: SENTERRA Raman microscope.

1.3 Meat

1.3.1 Meat Composition

Meat is the edible postmortem component originating from live animals, such as domesticated cattle, hogs, sheep, goats and poultry, as well as wildlife such as deer, rabbit and fish. During the postmortem period, complex changes take place in the muscle that results in its conversion to meat. The composition of the carcass relies on the market segment for which the meat is destined. Traditionally, carcass composition refers to the absolute or relative amounts of muscle, fat and bone, or of protein, lipid, ash and water. From a processor point of view, this definition can be refined to include quantities of retail meat, fat trim and bone. The meat of any animal has a composition associated with the age and nutritional state of the animal. Meat is a muscular tissue that is composed of skeletal muscles, connective tissue, fat, and little amounts of smooth muscles like veins and arteries. As shown in Figure 1.6, skeletal muscles are, in turn, composed of muscle fibers, that consist of rod-shaped myofibrils. Myofibrils and connective tissues are the major structural components of muscles. The animal muscle is generally composed of 60–80% water, 18–20% proteins, 0.5–19% lipids, 1–1.5% minerals and a very small amount of carbohydrate [81–85].

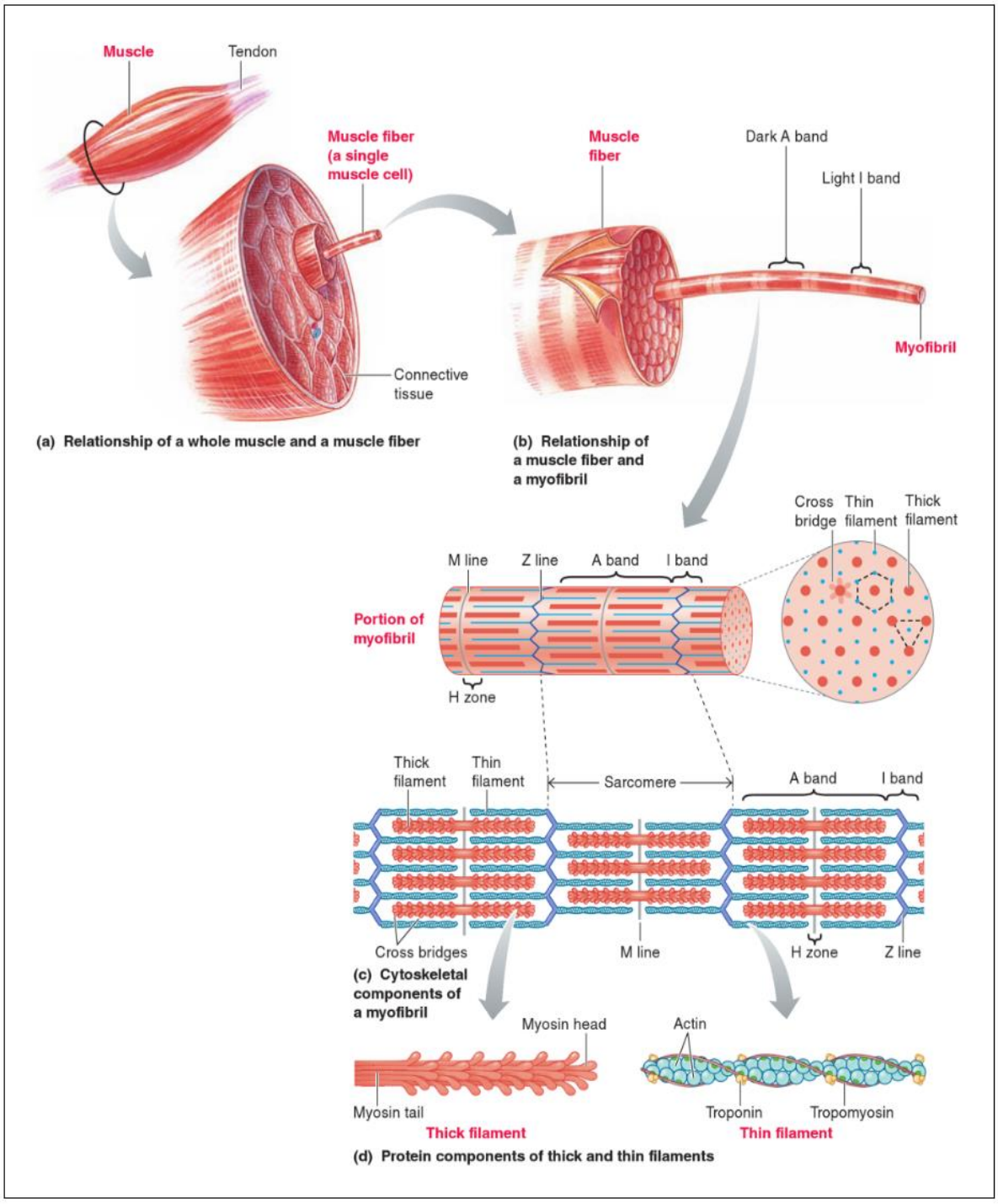

Figure 1.6: The structure of muscle (From: Frontera and Ochala [86], Figure 3).

1.3.2 Meat Quality

The quality can be described as the measure of traits that are sought and valued by the consumer. The meat quality is a wide term and covers a variety of characteristics and can be defined in various ways from palatability to technological aspects to safety. The properties

used to define the quality of meat can be divided into four groups of parameters (Figure 1.7); animal nutrition, hygiene and toxicological, meat processing and sensory parameters which have the highest influence on the consumers' purchase decision [87–89].

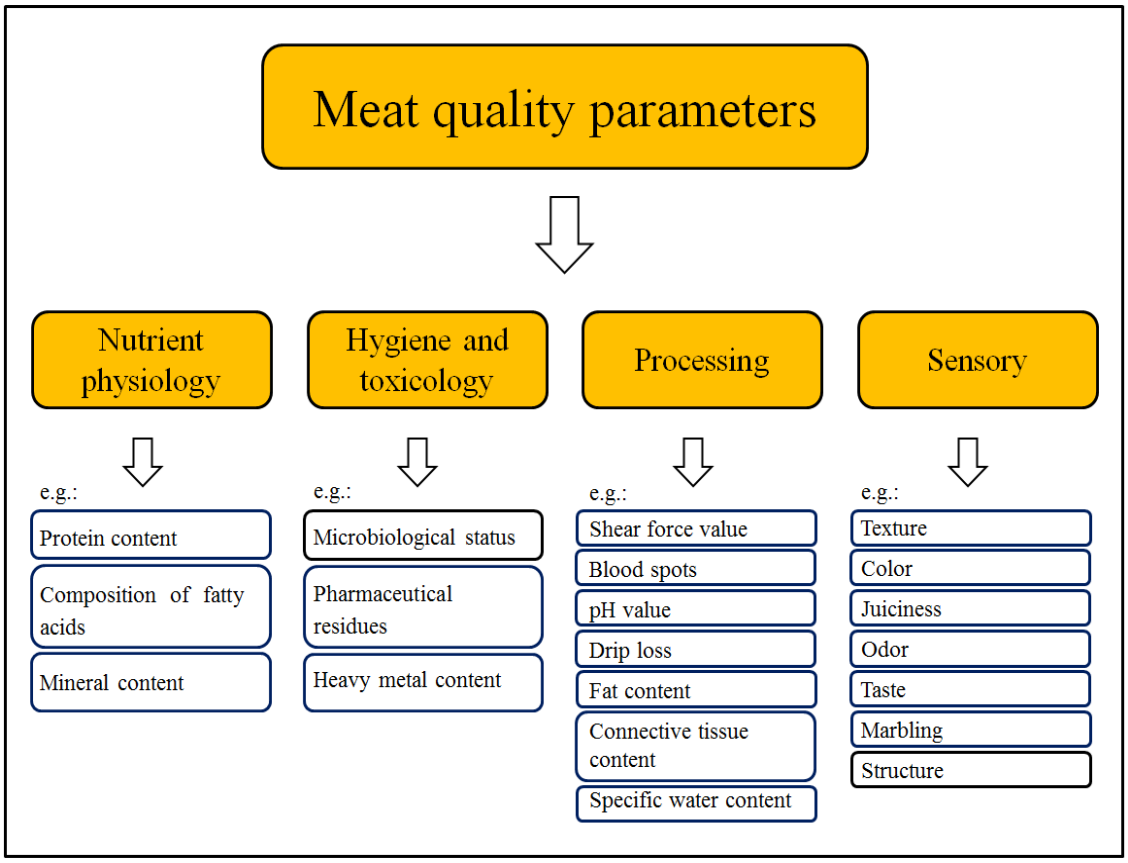

Figure 1.7: Parameters of meat quality for meat-producing animals.

In the first half of the 20th century, the intrinsic set of quality factors (i.e., the characteristics of the product itself) were the most important factors used to judge meat at its point of purchase or on consumption after cooking. To minimize variability in these intrinsic factors, much of the work done on best practices for genetic selection, animal production, slaughter methods and post-mortem handling of meat. A further set of extrinsic factors gained a remarkable position in the minds of current consumers of meat and meat products. These factors can't immediately be detected by physical or sensory examination of the meat itself, but are associated with the way that the meat is produced. These extrinsic parameters center on animal welfare, the nutritional values of meat in the human diet and the ecological sustainability of production systems [87, 90].

The microbial spoilage regarded as the main cause of quality deterioration in meat, and it is causes pH change, off odors, slime formation, structural components degradation and appearance change [91–93].

1.3.3 Microbial Spoilage and Shelf Life of Meat

Food spoilage is the process which decreases the desirability of food for consumption by changing several biochemical properties of food caused by microbiological, chemical or physical changes. Microbiological food spoilage is a result of the growth of microorganisms which produce enzymes that lead to undesirable by-products in the food [94, 95]. Meat is one of the most sensitive food products regarding spoilage and prediction of minimum shelf life. Fresh meat is excellent basic nutrients for microbial activity as it is rich in nutrients (sugars, amino acids, nucleotides, peptides, vitamins, etc.), it possesses a pH between 5.5 and 6.5 and a high water activity which supports the growth of a wide variety of microorganisms [96–99]. The shelf life of meat and meat products is the period of time a product can be stored without becoming unacceptable for human consumption or becoming a health risk. The main reason for meat spoilage is the presence of microorganisms and their metabolites [97, 100, 101].

A maximum acceptable microbial level and (or) unacceptable off-odor and off-flavor identify the exact point of spoilage, which is rigidly dependent on the initial numbers and types of contaminating microorganisms and their growth, lipid oxidation and autolytic enzymatic reactions. Commonly, the initial microbial count of fresh meat and meat products is about 4-5 log CFU/cm^2 and the spoilage is determined by up to 10^8-10^9 CFU/g of different microorganisms. If the meat is maintained in air at temperatures lower than 5 °C, the shelf life of the meat will be limited by microbial growth. The unpleasant odors develop when the number of microorganisms reaches about 10^7 CFU/cm^2 and a slimy coating appears with the count of 10^8 CFU/cm^2 [97].

Fresh meat can be contaminated by a large variety of microorganisms. The composition of these microorganisms depends on several factors: (a) preslaughter husbandry practices, (b) age of the animal at the time of slaughtering, (c) handling during slaughtering, evisceration and processing, (d) temperature controls during slaughtering, processing and distribution, (e) preservation methods, (f) type of packaging and (g) handling and storage by consumer. Or in other words; these factors can be categorized into five groups: intrinsic, extrinsic, processing, implicit and the emergent. These factors can influence the growth and predominance of specific microbial groups [93, 96–98, 102]. Meat spoilage depends on the composition of a heterogeneous microflora, but in some cases, spoilage is caused by one specific organism. The groups of microorganisms responsible for the spoilage of meat and poultry under different storage conditions are mainly belonging to a few genera, including: *Pseudomonas*, *Shewanella*, *Psychrobacter*, *Moraxella*, *Acinetobacter*, *Bacillus*, *Escherichia*,

Enterobacteriaceae, *Flavobacterium*, *Staphylococcus*, *Micrococcus*, *Corynebacterium*, *Clostridium*, *Brochothrix* and *Lactic acid bacteria* [41, 93, 97, 98, 100, 101, 103].

1.3.4 Microbial Spoilage Detection Methods

Traditionally, evaluating the spoilage process of fresh meat has focused on evaluating the presence of microorganisms by detection and enumeration. The conventional analytical methods, such as colony counting methods, have been used almost exclusively in the actual evaluation of spoilage. The conventional methods were developed many years ago and have been in use ever since as the official methods of most food microbiology laboratories, that's why it's called 'conventional'. These methods are well established, reliable and accurate. However, these methods have major drawbacks related to excessive laboratory work, time consumption, culture media, technique failures associated with high agar temperature, laboratory glassware requirement and high risk of contamination due to all the stages involved in culture medium preparation and inoculation. This is an explicit inconvenience in modern food industrial applications since those methods are not appropriate for on-line and real-time detection of microbial spoilage in a fast and non-destructive or non-invasive means. Therefore, demand remains high for the development of cost effective, rapid, simple, reagent-free and non-destructive methods to detect microbial contamination on meat [41, 95, 104–109].

Several methods have been developed to achieve fast and reliable bacterial identification, such as Matrix Assisted Laser Desorption Ionization-Time Of Flight Mass Spectrometry (MALDI-TOF MS) [110], Polymerase Chain Reaction (PCR) based methods [111] and Enzyme-Linked Immunosorbent Assay (ELISA) techniques [112]. These methods are objective, reliable, highly specific and rapid [17, 113–116]. However, they are destructive [115, 117] and require complex sample preparation steps [117, 118]. Moreover, PCR and ELISA methods require specific primers and antibodies [118].

As an alternative to those methods, bacteria are increasingly being identified using Raman spectroscopy based detection techniques such as conventional Raman spectroscopy and surface-enhanced Raman spectroscopy [17–23, 117, 119–122]. Raman spectroscopy has several advantages over other methodologies as it is a non-destructive, non-invasive, relatively inexpensive compared to other methods, rapid and being a label-free method. Furthermore, it requires simple up to no sample preparation. Moreover, the presence of

microorganisms or DNA in the laboratory environment is not a concern in Raman spectroscopy. Additionally, strains can be identified extremely accurately [24, 121, 123, 124].

1.4 Raman Spectral Data Analysis

In general, Raman spectral data analysis can be divided into two steps: (1) data set pre-processing and (2) information extracting using chemometric techniques.

1.4.1 Data Pre-processing

Raman spectra can provide a molecular structural signature of a substance. Despite Raman fingerprint information, the Raman spectrum contains other contributions that influence the Raman signal and thereby obscure the desirable information. A variety of common contaminants can be observed in Raman spectra, some of which can be sample or instrument dependent. Contributions such as fluorescence background, substrate background, cosmic spikes, Gaussian noise, CCD background noise, varying in sampling geometries and other effects dependent on experimental parameters; have to be corrected or removed before the analysis, in order to ensure that the analysis is based on the Raman measurements and not on other effects. The effect of these interferents can be reduced by applying pre-processing methods such as visually assessing the quality of the spectra, outliers detection and elimination, cosmic spikes corrections or removal, baseline corrections, smoothing and normalization. Pre-processing the raw data helps eliminate unwanted variation such as instrumental and experimental artifacts, enhances Raman spectral features and allows more reproducible data for qualitative and quantitative analysis [41, 59, 70, 105, 125–128].

Since there is no single standard method for pre-processing Raman spectra, and the choice of pre-processing steps and the order in which they are conducted has been shown to have a major impact on the outcomes of spectral analysis [105]; several pre-processing steps with different orders were applied in this work to the raw Raman spectra to achieve the optimal results.

1.4.2 Chemometric Techniques

Raman data can be analysed through two main approaches: univariate and multivariate (chemometrics). Raman band features (e.g. area, intensity and center of gravity) are used in

the univariate approach to understand the sample chemistry. Despite that a univariate data analysis is straightforward to utilize; it needs that the components of interest have distinctive and unique Raman bands. Since biological samples are heterogeneous mixtures of different biomolecules; their Raman spectra have a complex structure. They have numerous peaks in a broad band. Only slight spectral differences are visible if Raman spectra of different biological states are measured and compared. A manual differentiating and rating of these slight changes are not possible or practical. Consequently, the use of chemometrics techniques is required [45, 128–130].

Chemometric techniques can be defined as the chemical discipline that uses mathematical, statistical and other methods to design or select optimal measurement procedures and experiments, and to provide maximum relevant chemical information by analysing chemical data. Chemometric techniques enhance the sensitivity of Raman spectroscopy, which are capable of distinguishing subtle spectral differences between classes. Furthermore, chemometric techniques make biological diagnostics more objective since little to no human intervention is required. In addition, chemometrics dramatically speed up biological diagnostic procedures, making it possible to deal with large-size Raman spectral datasets within an acceptable time [41, 131, 132].

In this work, the following chemometric methods were used to analyse the collected Raman data: (a) Principal Components Analysis (PCA) using the covariance matrix; unsupervised chemometric method (i.e., it makes no a priori assumptions about the data set), (b) Hierarchical Cluster Analysis (HCA); unsupervised chemometric method, (c) Support Vector Machines (SVM); supervised chemometric method and (d) Canonical Discriminant Analysis (CDA); supervised chemometric method [41, 76, 133].

1.5 Objective, Research Questions and Outline of the Thesis

The main objective of this thesis is to investigate the feasibility of Raman spectroscopy in conjunction with chemometric methods for the characterization and analysis of quality and shelf life of poultry meat. For this purpose, the following research questions are proposed:

1. Can two dispersive Raman spectrometers with different characteristics (Microscope and Portable Fiber-Optic systems) be used to characterize, discriminate and classify important strains of meat spoilage microorganisms commonly found in poultry meat?

2. Can the accuracy of the used Raman systems affect the accurate discriminating and classifying of bacteria down to the strain level?
3. Can Raman spectral features and differences on which the discrimination is made be identified?
4. Is Raman spectroscopy able to monitor the spoilage process of poultry fillets through the evaluation of their freshness quality?
5. Is Raman spectroscopy able to investigate the influence of different production systems on the quality and shelf life of poultry meat?

Besides the introduction (chapter 1), this thesis contains four more chapters. In the second part of this thesis (chapter 2); characterization, discrimination and classification of eight important strains related to meat spoilage microorganisms, commonly found in poultry meat, were carried out using two dispersive Raman spectrometers (Microscope and Portable Fiber-Optic systems) in combination with chemometric methods. From each bacterial strain, a small amount of the biomass was placed on a disinfected stainless steel slide and was used for the Raman measurements. After the pre-processing step for the data collected by each system, chemometric methods were applied to develop discrimination and classification models. Thereafter, the obtained results from both systems were compared. Furthermore, the influence of the accuracy of the used Raman systems on the accurate discrimination and classification of bacteria down to the strain level was investigated, and the spectral features and differences on which the discrimination is made were identified.

Chapter 3 was based on the findings in chapter 2 in which the same portable fiber-optic Raman spectrometer was used to study the ability of Raman spectroscopy to monitor the spoilage process of poultry fillets through the evaluation of their freshness quality. The collected time-dependent Raman spectra were pre-processed and then combined with chemometric methods to investigate information about the quality and the remaining shelf life. The fillets samples were successfully separated into three quality classes according to their freshness: fresh, semi-fresh, and spoiled. These classes were based on the information inferred from the product label on the packages of poultry fillets. Furthermore, a conclusion was drawn on the poultry meat spoilage mechanism.

The aim of chapter 4 is to confirm the findings and investigate other scenarios. Therefore, the influence of two commercial production lines (conventional and alternative) of a German poultry producer on the quality and shelf life of poultry meat were studied using Raman spectroscopy. In two repeated storage trials; Raman spectra of a total of 80 fillets (40

conventional and 40 alternative) were collected using portable fiber-optic Raman spectrometer. The investigations were conducted at five repeated investigation times during storage. Raman measurements were conducted directly on fillets surfaces parallel to the microbiological and nutrients analysis. The duration of each trial was 11 days. After the pre-processing step for the collected data from each production line was done; chemometric methods (PCA, CDA and AHCA) were applied to study the ability of Raman spectroscopy to assess the quality parameters and shelf life. The results were compared to the data obtained from the physicochemical parameters' measurements and microbiological analyses.

The models were constructed using the 1st storage trial (first investigation time) and were able to group the poultry samples according to their production line into two classes; conventional and alternative. The testing data points from the 2nd storage trial (first investigation time) were used to validate the models and all have been successfully assigned to the correct cluster. The origin of the separation in PCA model was investigated by analysing the loading plots. The results were consistent with the analysis of nutrients in both production lines.

Further, CDA model was constructed for each production line to classify poultry fillets according to their storage time (five investigation times) and their microbial load (three quality classes). For both production lines, the constructed models showed good ability to classify poultry fillets according to their storage time with error rates less than 25.00%. However, the constructed models showed poor classification ability when tested with the 2nd storage trial. The high error rates could be correlated to the high variations of the bacterial load between the two storage trials for each production line. The data were regrouped according to their microbial load to three quality classes (fresh, semi-fresh and spoiled) to minimize these variations. For the conventional production line, the constructed model showed good ability to classify poultry fillets according to their microbial load with error rates less than 25.00% for the training set and for the testing set. This indicates that the variations between the two storage trials are not high. The alternative production line showed good ability to classify poultry fillets according to their microbial load. Nevertheless, the model failed to classify poultry fillets when tested with the 2nd storage trial. This indicates that the variations between the two storage trials are too high and that the microbial load is not the only factor that has an impact on the collected Raman spectra from the two storage trials.

The last chapter (chapter 5) displays the conclusion of the entire thesis. It answers the research questions in regard to the empirical results.

2 In Vitro Discrimination and Classification of Microbial Flora of Poultry Using Two Dispersive Raman Spectrometers (Microscope and Portable Fiber-Optic Systems) in Tandem with Chemometric Analysis

This chapter is adapted from: S. Jaafreh, O. Valler, J. Kreyenschmidt, K. Günther, P. Kaul, In vitro discrimination and classification of Microbial Flora of Poultry using two dispersive Raman spectrometers (microscope and Portable Fiber-Optic systems) in tandem with chemometric analysis, *Talanta*. 202 (2019) 411–425. doi:10.1016/j.talanta.2019.04.082.

2.1 Introduction

Global production and consumption of poultry meat has increased over the last decades, and per capita consumption is expected to grow [4, 35, 105]. However, fresh poultry meat ranks among the highly perishable food due to its nutritional composition, which transforms the poultry meat to a susceptible product for growth of spoilage and pathogenic microorganisms [4–6]. Worldwide more than 20% of the meat produced is not consumed [134]. This waste leads to economic losses, food waste and loss of consumer confidence in the meat market. Therefore, the production of high quality and safe meat products with a long shelf life is one of the meat industry's major tasks. By supplying meat of high quality and an adequate shelf life, the industry can optimize its storage management and thus reduce losses [10, 134–136].

The microorganisms commonly found in meat and poultry are *Acinetobacter*, *Campylobacter*, *Flavobacterium*, *Micrococcus*, *Brochothrix*, *Bacillus*, *Pseudomonas* and *Escherichia* [28, 83, 137, 138]. Currently, the gold standards in determining the spoilage microorganisms and foodborne pathogens are culture and colony counting methods [11, 12]. These methods are well established and reliable but at the same time laborious and time-consuming, which is inconvenient in modern food industrial applications [11–13, 28, 94].

Several methods have been developed to achieve fast and reliable bacterial identification, such as Polymerase Chain Reaction (PCR) based methods [111], Enzyme-linked immunosorbent assay (ELISA) techniques [112] and Matrix Assisted Laser Desorption Ionization-Time Of Flight Mass Spectrometry (MALDI-TOF MS) [110].

These methods are objective, reliable, highly specific and rapid [17, 113–116]. However, they are destructive [115, 117] and require complex sample preparation steps [117, 118]. Moreover, PCR and ELISA methods require specific primers and antibodies [118].

As an alternative to those methods, bacteria are increasingly being identified using Raman spectroscopy based detection techniques such as conventional Raman spectroscopy and surface-enhanced Raman spectroscopy [17, 18, 121, 122, 19–23, 117, 119, 120]. Raman spectroscopy has several advantages over other methodologies as it is a non-destructive, non-invasive, relatively inexpensive compared to other methods, rapid and being a label-free method. Furthermore, it requires simple up to no sample preparation. Moreover, the presence of microorganisms or DNA in the laboratory environment is not a concern in Raman spectroscopy. Additionally, strains can be identified extremely accurately [24, 121, 123, 124]. The Raman spectra of each microorganism are highly specific because each microorganism has a unique spectral pattern. Raman and Micro-Raman Spectroscopy have the potential to investigate bulk samples as well as a single cell. The analyses can be performed directly from colonies grown on culture plates or from bacterial smears on an optical substrate [19, 25, 139, 140].

To provide specificity to minute biochemical differences between samples and to enable the bacteria to be characterized, discriminated and identified, the Raman spectra have to be analysed by chemometric techniques [139, 140].

Although much research has employed Raman spectroscopy in identifying clinically relevant bacteria [24–27], less has been done with food-related bacteria [28–30]. Using Raman microspectroscopy, Meisel *et al.* identified meat-associated pathogens [28]. On a single-cell level, they created a spectral database of 19 bacterial species of the most important harmful and nonpathogenic bacteria associated with meat and poultry. Despite their promising recognition rate, single-cell analysis of bacteria by Raman microscopy requires a larger amount of spectra to include variations between individual cells or variations caused by different cultivation conditions. Furthermore, when using Raman microscopy, the methods used to isolate microorganisms can affect their identification. Moreover, spectra are treated as mathematical data and only little or no attention is paid to interpreting the spectra, which obscures the physical evidence (spectral features and differences among the species) on which the classification is made. Additionally, Raman microscopy needs much more time to analyse an individual cell, which leads to inadequate evaluation of large samples [30, 38–40, 141].

The objective of this study was to discriminate and classify important strains of meat spoilage microorganisms commonly found in poultry meat. The usability of two dispersive Raman spectrometers with different characteristics (Microscope and Portable Fiber-Optic systems) were compared by conducting the measurements directly from a stainless steel slide without the need for any pretreatments like purification or singulation steps. The possibility of accurately discriminating and classifying bacteria down to the strain level using the less accurate measurement system (Portable Fiber-Optic) was investigated as well. Furthermore, the study aimed to identify the spectral features and differences on which the discrimination is made.

2.2 Material and Methods

2.2.1 Bacterial Strains, Growth Conditions and Sample Preparation

The eight bacterial strains selected for the study, *Micrococcus luteus* DSM 20030 (*M. lute*), *Brochothrix thermosphacta* DSM 20171 (*B. ther*), *Bacillus coagulans* DSM 1 (*B. coag*), *Bacillus subtilis* DSM 10 (*B. subt*), *Pseudomonas fluorescens* DSM 4358 (*P. fluo* 4), *Pseudomonas fluorescens* DSM 50090 (*P. fluo* 5), *Escherichia coli* K12 (*E. coli* K12) and *Escherichia coli* HB101 (*E. coli* HB101), were obtained from culture collections available in the Department of Natural Sciences of Bonn-Rhein-Sieg University of Applied Sciences and in the Institute of Animal Sciences of Bonn University. The bacteria were cultivated under aerobic conditions on nutrient agar containing 10 g/l peptone from meat, 10 g/l meat extract, 5.0 g/l sodium chloride and 18.0 g/l agar-agar (Merck, Darmstadt, Germany) for 24 hours at 37 °C except *B. coag*, which was incubated for 48 hours at 55 °C (to increase the biomass accumulation). An overview of the genera, species and strains used throughout this study is provided in Table 2.1.

Table 2.1: List of used bacteria, abbreviations, number of spectra collected by each system and standard deviation of means (SDM) per strain. For more details on SDM, see Section 2.3.2 Chemometric techniques.

Genus	Species	Strain	Abbr.	Microscope		Portable Fiber-Optic	
				No. of Spectra	SDM	No. of Spectra	SDM
Micrococcus	*luteus*	DSM 20030	*M. lute*	115	0.08	25	0.18
Brochothrix	*thermosphacta*	DSM 20171	*B. ther*	114	0.07	25	0.26
Bacillus	*coagulans*	DSM 1	*B. coag*	98	0.13	25	0.11
	subtilis	DSM 10	*B. subt*	87	0.14	24	0.12
Pseudomonas	*fluorescens*	DSM 4358	*P. fluo* 4	112	0.12	22	0.14
		DSM 50090	*P. fluo* 5	111	0.12	25	0.12
Escherichia	*coli*	K12	*E. coli* K12	115	0.06	25	0.10
		HB101	*E. coli* HB101	115	0.08	24	0.15

2.2.2 Raman Spectrometers and Acquisition Parameters

For the Raman Microscope system; all measurements were carried out using the SENTERRA Raman microscope (Bruker Optics, Ettlingen, Germany) [78], hereafter referred to as 'Microscope system'. The acquisition parameters were a laser wavelength of 785 nm for excitation, a laser power of 100 mW, a 50X long working distance objective with a laser spot size of ~4 µm, an aperture of 50x1000 µm, a 1200 lines/mm grating (high resolution mode of 3-5 cm^{-1}), an integration time of 15 seconds and with five co-additions. To cover the most relevant bacterial Raman features, the spectral window covering the spectral range of 410-1790 cm^{-1} was chosen. Raman spectra were acquired using OPUS software (Bruker Optics, Ettlingen, Germany).

For the Portable Fiber-Optic Raman system; all measurements were carried out using the QE Pro-Raman system (Ocean Optics, Netherlands) [105], hereafter referred to as 'Portable Fiber-Optic system'. The Portable Fiber-Optic system has an RPB785 fiber-optic probe. The fiber probe configuration consists of a permanently aligned combination of two single fibers (105-µm excitation fiber and a 200-µm collection fiber) with filtering and steering micro-optics (Numerical Aperture = 0.22), in a rugged polyurethane jacket. No objectives were used in the Portable Fiber-Optic system. The acquisition parameters were a laser excitation wavelength of 785 nm and a laser power of 250 mW; the distance between the sample and the laser fiber optic probe was 7.5 mm, with a laser spot size of ~155 µm, and the integration time was 10 seconds. The average of five scans was used in each collected

spectrum. Raman spectra were acquired using OceanView software (Ocean Optics, Netherlands).

To take into account both biological variability and possible daily variations during Raman measurements, Raman bulk spectra of bacteria were recorded from four independently prepared batches of each strain. From each batch; a small amount of the biomass was scraped off the Agar plates using a sterile disposable loop. The collected biomass was then placed on a disinfected stainless steel slide and used for the Raman measurements (this step was repeated three times). For the Microscope system nine to ten Raman spectra were collected from each bacterial bulk sample. In this manner, around 115 Raman spectra for each bacterial strain were collected. For the Portable Fiber-Optic system only two or three Raman spectra were collected from each bacterial bulk sample due to the larger laser spot. Thus, around 25 Raman spectra for each bacterial strain were collected. More details are provided in Table 2.1.

For both Raman systems, the spectra were collected from random positions chosen manually and with a new bacterial smear for each instrument system. To eliminate ambient light from Raman spectra, all Raman measurements were taken inside a dark enclosure. For both Raman systems, the dark spectrum subtraction was performed during the spectral acquisition. Bacterial bulk samples were measured directly without air drying. No further sample treatments were required. All of the Raman spectra were collected in a sterile environment and under ambient conditions.

2.2.3 Raman Data Evaluation

2.2.3.1 Data Pre-processing

To reduce the wavenumber region to the fingerprint region, the spectra for the Portable Fiber-Optic system was cut to the wavenumber region from 497 to 1803 cm^{-1} while, for the Microscope system, the wavenumber region was kept the same as the chosen spectral window (from 410 to 1790 cm^{-1}). Subsequently, the same pre-processing steps were performed for both systems. All spectra with cosmic spike(s) were searched for by visual inspection. These spectra were then eliminated from further analysis. Then, the baselines of all spectra were corrected using the concave rubber band correction method [20] (available in OPUS software; Bruker Optics) with 10 iterations and 64 baseline points. The spectra were then smoothed based on the Savitzky-Golay algorithm; the number of smoothing points was 7 with a second-

order polynomial. Subsequently, the area under curve for each spectrum was normalized to one. Finally, the second-order derivative was calculated for each spectrum to improve resolution and minimize baseline variability [70, 105, 123, 142]. For each Raman system, the pre-processed spectral data were consecutively numbered in the order of their recording. Then, the data were divided into two sets: a training set (75%) and a validation set (25%). All the multiples of the measurement number four were placed in the validation set while the remaining measurements were placed in the training set. The training set was used to build the models for bacterial discrimination or classification, and the validation set was used to validate the presented pre-processing method and to test the models for their robustness. Data pre-processing were performed using OPUS software for the concave rubber band correction method and OriginPro 2018 software (OriginLab Corporation, United States) for all other steps.

2.2.3.2 Chemometric Techniques

To distinguish between the bacterial strains, chemometric techniques were applied to the data. These techniques enhance the sensitivity of Raman spectroscopy, which are capable of distinguishing subtle spectral differences between classes. Furthermore, chemometric techniques make biological diagnostics more objective since little to no human intervention is required. In addition, chemometrics dramatically speed up biological diagnostic procedures, making it possible to deal with large-size Raman spectral datasets within an acceptable time [21, 143]. In this study, the unsupervised chemometric method PCA and the supervised chemometric method SVM were used to differentiate between bacterial strains.

2.2.3.2.1 Principal Components Analysis, PCA

PCA is an unsupervised classification method used to reduce the dimensionality as well as to investigate and visualize the grouping of different samples into different clusters. Briefly, PCA linearly transforms the original data (Raman spectra in this work) into new orthogonal variables called principal components (PCs). Potentially, there are as many PCs extracted from the data matrix as there are original variables (Raman wavenumbers in this work). The first PCs explain the largest amount of variance observed in the features, which can be used to identify the samples' differences [105, 144, 145]. For each Raman system in this work, bacterial samples were discriminated through a 3-stage PCA model. Before

performing the PCA calculation in each stage, the standard normal variate [146] was calculated for the training and the validation data sets. Standard normal variate and PCA calculations were performed using OriginPro 2018 software.

2.2.3.2.2 Support Vector Machines, SVM

SVM are supervised machine learning algorithms that have been widely used in data classification and regression analysis. The strategy of SVM is to find an optimal separating hyperplane or hyperplanes with the maximum margin between two or more classes by focusing on the training samples located at the edge of the class distribution and minimizing the classification error between each class. SVM are not relatively sensitive to training sample size. SVM can be built to discriminate between both linear and non-linearly separable data by using different kernel functions. Each kernel function has a particular parameter that must be optimized to obtain the optimal performance. For the linear kernel function, two parameters have to be defined: the regularization parameter (C) and gamma (γ) [147–153]. The high dimension of Raman spectral space may result in computational complexity and inefficiency when optimizing and implementing the SVM algorithms. As such, PCA was performed on the pre-processed spectra to reduce the dimensionality of the Raman spectral space while retaining the most diagnostically significant information for bacterial classification.

To eliminate the influence of inter and (or) intra-subject spectral variability on PCA, the entire spectra were standardized by using the standard normal variate [146]. PC scores were used as an input to develop SVM models for multi-class classification using the following number of consecutive components: 2, 4, 6, 8, 10, 15 and 20. The maximal number of PCs was calculated using Kaiser-Guttman test. Classification was accomplished through a linear SVM (One-Against-One strategy [146]) with a linear kernel function. The C value was set to 1.0, while the γ value was adjusted to 1/n features (n is the number of principle components used). To evaluate model performance, the metrics accuracy, sensitivity and specificity were calculated using a confusion matrix, which was computed for the classification (75%) and validation (25%) datasets. SVM implementations were based on the Python Package Scikit-learn [154].

2.3 Results and Discussion

2.3.1 Raman Measurements and Analysis

Raman scattered light quantitatively reflects the chemical composition of bacterial samples. However, Raman spectra contain other contributions that influence the Raman signal and thereby obscure the desirable quantitative information. For instance, Raman spectra of bacterial bulk samples are often masked by the appearance of fluorescence and substrate background. To minimize the fluorescence background, we chose the operation wavelength of the Raman excitation laser in the near-infrared spectral region at 785 nm for both Raman systems. To reduce the substrate background, stainless steel was used because of its low Raman background contribution, low cost and robust durability instead of the traditional substrates like fused silica or CaF_2. Cosmic spikes and other effects dependent on experimental parameters also influence the Raman signal. By applying pre-processing methods, these effects were reduced prior to the analysis, thus ensuring that the chemometric analysis was based on the Raman measurements and not on other effects. The pre-processing step is crucial to obtain robust and accurate quantitative information from Raman spectra. The pre-processing method used in this work is described in the Data Pre-processing subsection. All collected Raman spectra from both Raman systems were pre-processed by the same procedure to ensure sufficient comparability [105, 155–159].

Figures 2.1(a) and (b) show the average, baseline corrected, smoothed and intensity-normalized Raman spectra from each bacterial strain collected using Microscope and Portable Fiber-Optic systems, respectively. To determine the variations within the Raman spectra in each strain, the double standard deviation for each mean spectrum has been added as gray coronas to the mean spectra [28] (the mean spectrum for a certain strain represents the mean of all Raman spectra collected for that strain). As shown in Figure 2.1(a), the Raman spectra collected using the Microscope system share similar characteristic peaks. The peak at 1661 cm^{-1} could be attributed to the amide I band [105, 122, 160, 161]. Another important peak at 1448 cm^{-1} corresponding to a CH_n deformation vibration (δCH_2, δCH_3) originates from the CH bindings in lipids, proteins and carbohydrates [105, 122, 158, 161–164]. The band at 1337 cm^{-1} is assigned to Amide III, CH deformation and to the ring breathing modes in the DNA bases adenine and guanine [122, 161, 163, 164]. An additional broad band centered at around 1250 cm^{-1} was observed and could be attributed to Amide III [122, 161–163]. In this work, this band is always notable and unavoidable whenever

weak Raman scatterer, such as bacterial samples, is measured. It is suspected that this band appears because of the microscope objective and (or) the internal parts of the microscope. The =C–C= vibration of unsaturated fatty acids in the lipids band, C-C stretching (νCC) and C-N stretching (νCN) are also observed at 1124 cm^{-1} [119, 122, 165, 166]. Another notable band at 1100 cm^{-1} could be attributed to the PO_2^- stretching of DNA/RNA and the C–C stretching (νCC) or C–O–C stretching (νCOC) of carbohydrates [122, 163–165]. Furthermore, the peak at 1004 cm^{-1} corresponds to the ring breathing vibration of the amino acid phenylalanine [105, 122, 158, 160–162]. An additional band can be seen at 782 cm^{-1}; it could be attributed to Guanine, Thymine, Cytosine and Uracil ring stretching vibration [122, 158, 161, 163, 164, 166]. Further vibrations attributed to adenine at 725 cm^{-1} were recognizable [122, 161–164]. Moreover, additional notable band around 521-542 cm^{-1} could correspond to S-S stretching (νSS) and C–O–C glycosidic ring deformation (δCOC) [119, 167, 168]. Another band around 410-482 cm^{-1} was recognizable and could be attributed to carbohydrates [119, 167, 168]. However, subtle differences between spectra can be still observed. One of the obvious differences found in the spectrum of *M. lute*, that are absent in the other strains, are peaks associated with carotene-like pigments at 1157 cm^{-1} and 1529 cm^{-1} [22, 120, 160, 169]. In Figure 2.1(b), the spectra collected using the Portable Fiber-Optic system also shared similar characteristic bands. Moreover, the peaks associated with carotene-like pigments were notable and only found in the spectrum of *M. lute* (see Figure 2.1(c)).

The spectral features for the spectra collected by the Portable Fiber-Optic system compared to the Microscope system are not all cleanly resolved; the bands are broader due to the lower resolution spectrometer (~13 cm^{-1}) while in the Microscope system, the resolution is 3-5 cm^{-1}. The broad band centered at around 1250 cm^{-1} in the spectra collected by the Microscope system was absent in the Fiber-Optic system. Variations in bands intensity were also notable. These variations may occur due to the fluorescence backgrounds, which can limit or prohibit the relatively weaker Raman signal and thus make the detection of useful spectral lines difficult. Fluorescence backgrounds are usually removed in the pre-processing step by computational methods. However, the resulting spectrum can be distorted and may contain artifacts, especially in weak Raman signals [105]. The intensity and variations of the fluorescence backgrounds were higher in the Raman spectra collected by the Portable Fiber-Optic system compared to the spectra collected by the Microscope system (see Figure 6.1 in the Appendix). This may possibly be the reason behind the relatively high standard deviation for the spectra collected by the Portable Fiber-Optic system. Unlike the Portable Fiber-Optic system, which has a large laser spot size (~155 μm), the objective lenses of the Microscope

system focus the laser beam to ~4 μm, which enhances fluorescence quenching [170]. The high fluorescence background problem that appears when using the Portable Fiber-Optic system can be reduced by photobleaching, in which the sample is irradiated for a period of time before the spectrum is acquired. The Raman spectrometer's laser acts as the light source for the photobleaching [171, 172]. Despite the differences and divergences described above, there is some similarity among the spectra collected by the two systems.

The spectral features were compiled with a more detailed tentative assignment of the Raman signals in the Appendix in Tables 6.1 and 6.2 for spectra collected using Microscope and Portable Fiber-Optic systems, respectively. The spectral features were found to be consistent with those in the literature. Nonetheless, most signals are a superposition of bands from several compounds, as the entirety of biochemical compounds in a bacterial cell contributes to the Raman spectrum [23].

On the basis of the spectra collected using the Microscope and the Portable Fiber-Optic systems, it was assessed whether it is possible to maintain accurate discrimination and classification of bacteria down to the strain level.

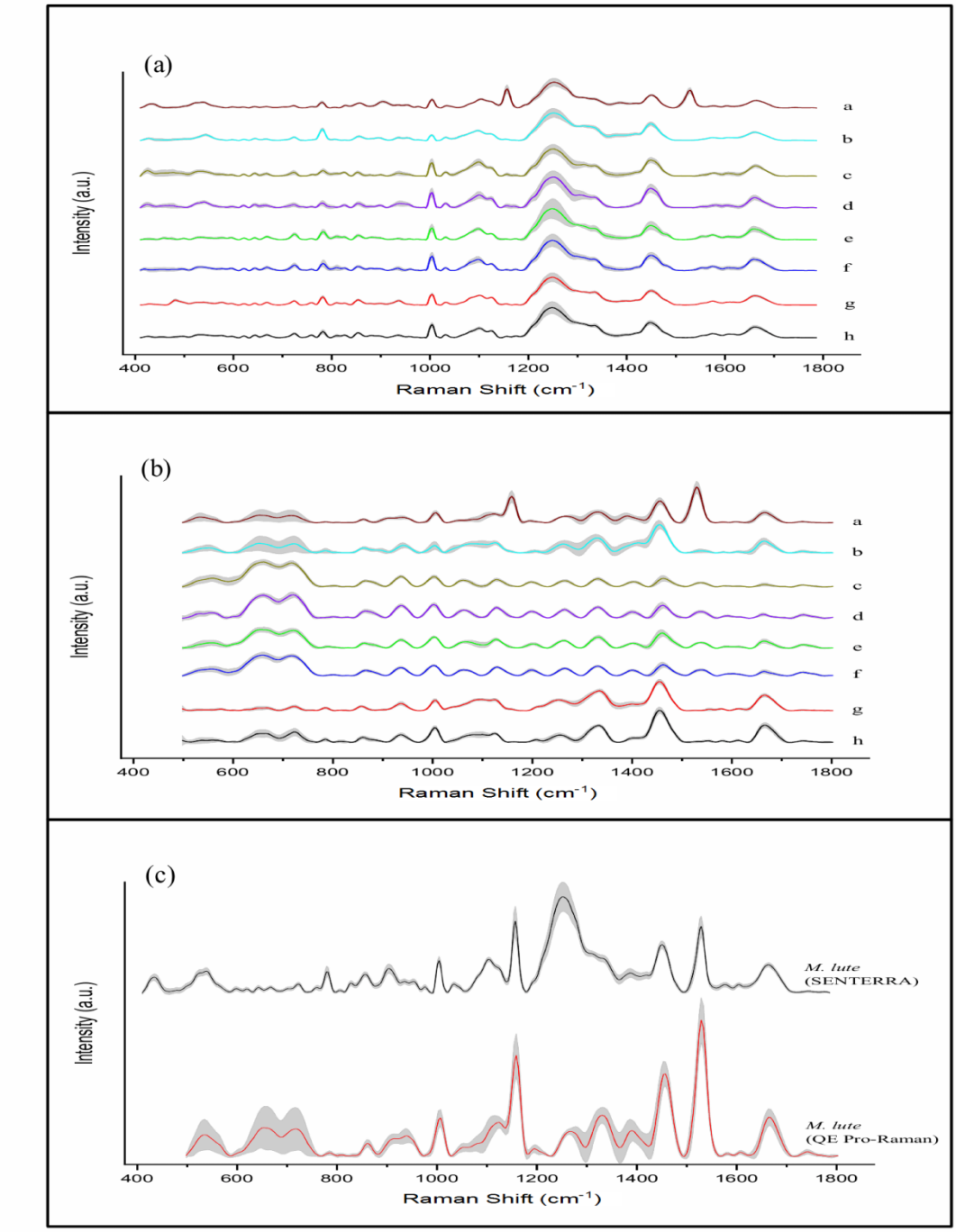

Figure 2.1: Mean Raman spectra collected by the Microscope system (a) and the Portable Fiber-Optic system (b): (a) *Micrococcus luteus*, (b) *Brochothrix thermosphacta*, (c) *Bacillus coagulans*, (d) *Bacillus subtilis*, (e) *Pseudomonas fluorescens* DSM 4358, (f) *Pseudomonas fluorescens* DSM 50090, (g) *Escherichia coli* K12, (h) *Escherichia coli* HB101. (c) Mean Raman spectra for *Micrococcus luteus* collected by the Microscope system and the Portable Fiber-Optic system. All spectra were baseline corrected, smoothed and intensity-normalized (area under curve normalized to one). The double standard deviation is depicted as gray corona of all analysed bacterial strains. The spectra are offset for clarity.

2.3.2 Chemometric Techniques

To compare the bacterial strains and to check whether the pre-processed data could be used to create a discrimination and classification system, the mean of the standard deviation per channel (Raman wavenumber) within each bacterial strain was normalized to the standard deviation of the channel means, resulting in a standard deviation of the means (SDM). Thus, the standard deviation per channel was placed into a relation of a mean spectrum statistical property. High SDM numbers (i.e. nearly 1) denote high intensity variations per channel. In contrast, low SDM numbers represent low variations per channel and therefore indicate high reproducibility and reliability of the statistical dataset. The calculated SDM for each strain are given in Table 2.1. In both Raman systems, the calculated SDM are significantly lower than 1. For the Raman spectra collected using the Microscope system, SDM values lie between 0.06 and 0.14, while, for the Portable Fiber-Optic system, SDM values lie between 0.10 and 0.26. Thus, the spectral dataset show a high reproducibility for both Raman systems. Consequently, the mean Raman data collected by Microscope and Portable Fiber-Optic systems could be used to create a discrimination and classification systems [173, 174].

2.3.2.1 Principal Components Analysis

In both systems, the discrimination of bacteria down to the strain level was successfully accomplished for the pre-processed spectral data using a 3-stage PCA model. The PCA model was validated using the validation data samples, which were successfully assigned to the correct bacterial genera and even to the right strain. Figure 2.2 shows a schematic representation of the PCA model for both systems.

2.3.2.1.1 PCA Stage 1

Figures 2.3(a) and 2.4(a), solid circles, show the PCA stage 1 scores plots obtained from the training sets for the Raman spectra of all 8 types of bacteria collected using the Microscope and Portable Fiber-Optic systems, respectively. Three separated clusters were visible in the scores plots. *M. lute* and *B. ther* were clustered into two distinct groups, while *Bacillus* subspecies (*B. coag* and *B. subt*), *Escherichia* strains (*E. coli* K12 and *E. coli* HB101) and *Pseudomonas* strains (*P. fluo* 4 and *P. fluo* 5) were clustered together into the same group. The ellipses depict the 95% Prediction Interval for each class. Subsequently, validation sets were rotated into the PCA space of the training data by the respective PCA

loadings from each system. Figures 2.3(a) and 2.4(a), empty circles, show that nearly all validation data points have been assigned to the correct cluster. To investigate the origin of the separation of the scores plots, the loading plots were analysed. The loadings values from stage 1 are plotted in Figures 2.5(a) and 2.6(a) for Microscope and Portable Fiber-Optic systems, respectively. The spectral features that represent the differences among the bacterial species are summarized in Table 2.2. These spectral features explain the distinct cluster of *M. lute* and *B. ther* in comparison to other bacterial species. Owing to the more discrete spectral features of *M. lute* and *B. ther* compared to other bacteria species, the PCA scores of the latter (*Bacillus*, *Escherichia* and *Pseudomonas*) were closely spaced in the presence of *M. lute* and *B. ther*; showing non-significant grouping. Hence, another PCA (stage 2) was performed for *Bacillus*, *Escherichia* and *Pseudomonas* to confirm the PCA's ability to discriminate these genera.

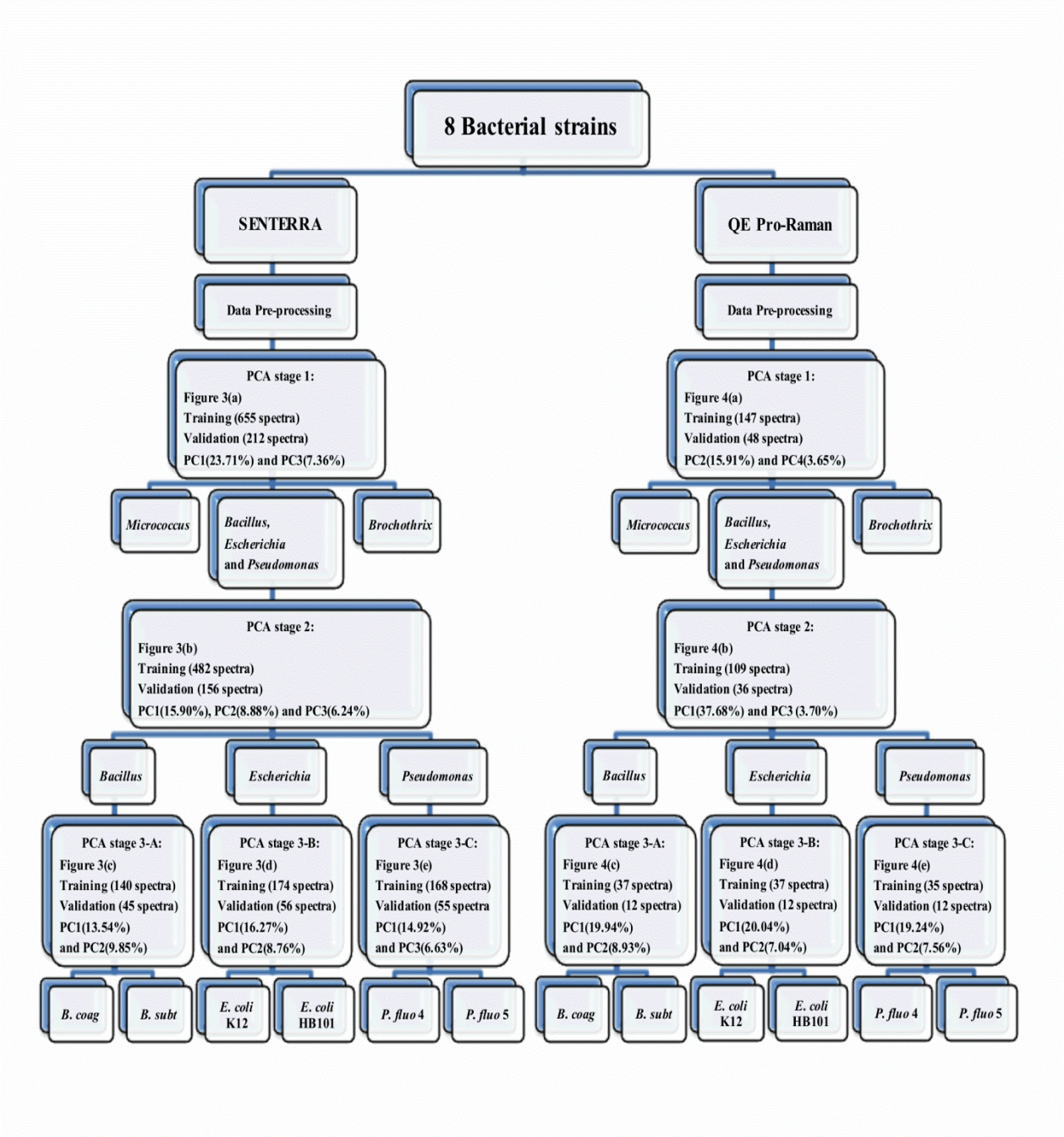

Figure 2.2: Schematic representation of the PCA model for bacterial spectra collected by the Microscope system (SENTERRA) and the Portable Fiber-Optic system (QE Pro-Raman). Stage 1: discrimination of bacterial genera to three groups; group 1 (*Micrococcus*), group 2 (*Brochothrix*) and group 3 (*Bacillus*, *Escherichia* and *Pseudomonas*). Stage 2: discrimination of bacterial genera from group 3 in stage 1 into three groups; group 1 (*Bacillus*), group 2 (*Escherichia*) and group 3 (*Pseudomonas*). Stage 3-A: discrimination of *Bacillus* subspecies into two groups; group 1 (*Bacillus coagulans*) and group 2 (*Bacillus subtilis*). Stage 3-B: discrimination of *Escherichia* strains into two groups; group 1 (*Escherichia coli* K12) and group 2 (*Escherichia coli* HB101). Stage 3-C: discrimination of *Pseudomonas* strains into two groups; group 1 (*Pseudomonas fluorescens* DSM 4358) and group 2 (*Pseudomonas fluorescens* DSM 50090).

Table 2.2: Analysis of stage 1 loading plots for Microscope and Portable Fiber-Optic systems. The spectral differences among the bacterial species were based on the Raman bands with the highest variance values. The values of Raman shift (RS) were sort in ascending order.

Microscope		**Portable Fiber-Optic**	
PC1 and PC3; Figure 2.5(a)		**PC2 and PC4; Figure 2.6(a)**	
RS (cm^{-1})	**Observations**	**RS (cm^{-1})**	**Observations**
515-530	Absent in *B. ther*	. . . . .	. . . . .
827	*B. ther* has the lowest intensity value	. . . . .	. . . . .
905	*M. lute* has the highest intensity value and a slight shift in position compared to the other bacterial species	. . . . .	. . . . .
. . . . .	. . . . .	940	*M. lute* has the lowest intensity value
1004	*B. ther* has the lowest intensity value	1003	*B. ther* has the lowest intensity value
1031	*M. lute* has the lowest intensity value	. . . . .	. . . . .
1100	*M. lute* has the lowest intensity value	. . . . .	. . . . .
1157	*M. lute* has a strong intensity value	1159	Present only in *M. lute*
1175	Absent in *M. lute* and *B. ther*	. . . . .	. . . . .
1190	Present only in *M. lute*	. . . . .	. . . . .
. . . . .	. . . . .	1403	*B. ther* followed *M. lute* has the highest intensity value and a slight shift in position compared to other bacterial species
1529	Present only in *M. lute*	1529	*M. lute* has a strong intensity value

2.3.2.1.2 PCA Stage 2

Before performing a second PCA (stage 2), the spectra of *M. lute* and *B. ther* were excluded from the training as well as from the validation sets. Figures 2.3(b) and 2.4(b), solid circles, show the PCA stage 2 scores plots obtained for the training sets for all 3 types of bacteria collected using Microscope and Portable Fiber-Optic systems, respectively. As shown in the scores plots, *Bacillus*, *Escherichia* and *Pseudomonas* were clustered into three distinct groups. Subsequently, the validation spectra were rotated into the PCA space of the training data by the respective PCA loadings from each system. Figures 2.3(b) and 2.4(b), empty circles, show that nearly all validation data points were assigned to the correct cluster. To investigate the origin of the separation of the scores plots, the loading plots were analysed. The loadings values from stage 2 are plotted in Figures 2.5(b) and 2.6(b) for Microscope and Portable Fiber-Optic systems, respectively. The spectral features that represent the differences among the bacterial genera are summarized in Table 6.3 in the Appendix. In this stage, the PCA scores of each cluster were closely spaced in the presence of other clusters, showing

non-significant grouping with respect to subspecies (*Bacillus*) and strains (*Escherichia* and *Pseudomonas*). Hence, PCA stage 3-A, 3-B and 3-C were performed to discriminate *Bacillus* subspecies (*B. coag* and *B. subt*), *Escherichia* strains (*E. coli* K12 and *E. coli* HB101) and *Pseudomonas* strains (*P. fluo* 4 and *P. fluo* 5), respectively.

2.3.2.1.3 PCA Stages 3-A, 3-B and 3-C

The PCA stages 3-A, 3-B and 3-C were similar, but they differ in the subspecies, strains, training and validation sets where 3-A is for *Bacillus* subspecies (*B. coag* and *B. subt*), 3-B is for *Escherichia* strains (*E. coli* K12 and *E. coli* HB101) and 3-C is for *Pseudomonas* strains (*P. fluo* 4 and *P. fluo* 5). Figures 2.3(c), (d) and (e) for the stages 3-A, 3-B and 3-C, respectively show the PCA scores plots obtained for the training sets (solid circles) for the Microscope system, and Figures 2.4(c), (d) and (e) for the stages 3-A, 3-B and 3-C, respectively show the PCA scores plots obtained for the training sets (solid circles) for the Portable Fiber-Optic system. As shown in the scores plots, each strain was clustered into a distinct group. Subsequently, in each of these stages, the validation sets were rotated into the PCA space of the training data by the respective PCA loadings from each system. Figures 2.3(c), (d) and (e) for the stages 3-A, 3-B and 3-C, respectively show that nearly all validation data points (empty circles) for the Microscope system were assigned to the correct cluster. The same result is obtained for the Portable Fiber-Optic system which can be seen in Figures 2.4(c), (d) and (e) for the stages 3-A, 3-B and 3-C, respectively. To investigate the origin of the separation of the scores plots, the loading plots were analysed. The loadings values from each of these stages for the Microscope system are plotted in Figures 2.5(c), (d) and (e) for the stages 3-A, 3-B and 3-C, respectively, while for the Portable Fiber-Optic system the loadings values are plotted in Figures 2.6(c), (d) and (e) for the stages 3-A, 3-B and 3-C, respectively. The spectral features that represent the differences among the bacterial subspecies and strains for each of these stages are summarized in the Appendix in Tables 6.4, 6.5 and 6.6 for the stages 3-A, 3-B and 3-C, respectively.

2.3.2.1.4 Comparison between Both Systems

The results show that both systems were able to separate the bacterial strains in the 3-stage PCA model. Both systems show that almost all training and validation data were assigned to the right cluster. Furthermore, the physical evidence on which the discrimination

was made was clarified through the loadings profiles e.g., presence or absence of certain peaks in a certain strain, variation in peaks intensity, peaks splitting and peaks shifting. For instance, from the spectra collected by the Microscope system, the peaks at 1190 and 1529 cm^{-1} are present only in *M. lute*, the peak at 1175 cm^{-1} is absent in *M. lute* and *B. ther*, the peak at 1484 cm^{-1} is absent in *B. coag* and *B. subt*, the peak at 455 cm^{-1} is absent in *E. coli* K12, the peak at 977 cm^{-1} is absent in *P. fluo* 5, at the peak 1004 cm^{-1} *B. ther* has the lowest intensity among the examined bacterial species and at the peak 905 cm^{-1}, *M. lute* has the highest intensity value and a slight shift in position when compared to the other bacterial species. The origin of the separation of the bacterial strains resulting from each Raman system was not always similar; there were some differences especially in the variations in bands intensity. These variations may be caused by the fluorescence backgrounds (see Section 2.3.1 Raman Measurements and Analysis). Nevertheless, the results show that the broader bands due to the low resolution spectrometer and the relatively high fluorescence backgrounds in the Portable Fiber-Optic system do not adversely affect the discriminative power of the developed PCA model. The results also show that the broad band which is centered at around 1250 cm^{-1} in the spectra collected by the Microscope system (see Section 2.3.1 Raman Measurements and Analysis) does not affect the developed PCA model as shown in the loadings profiles.

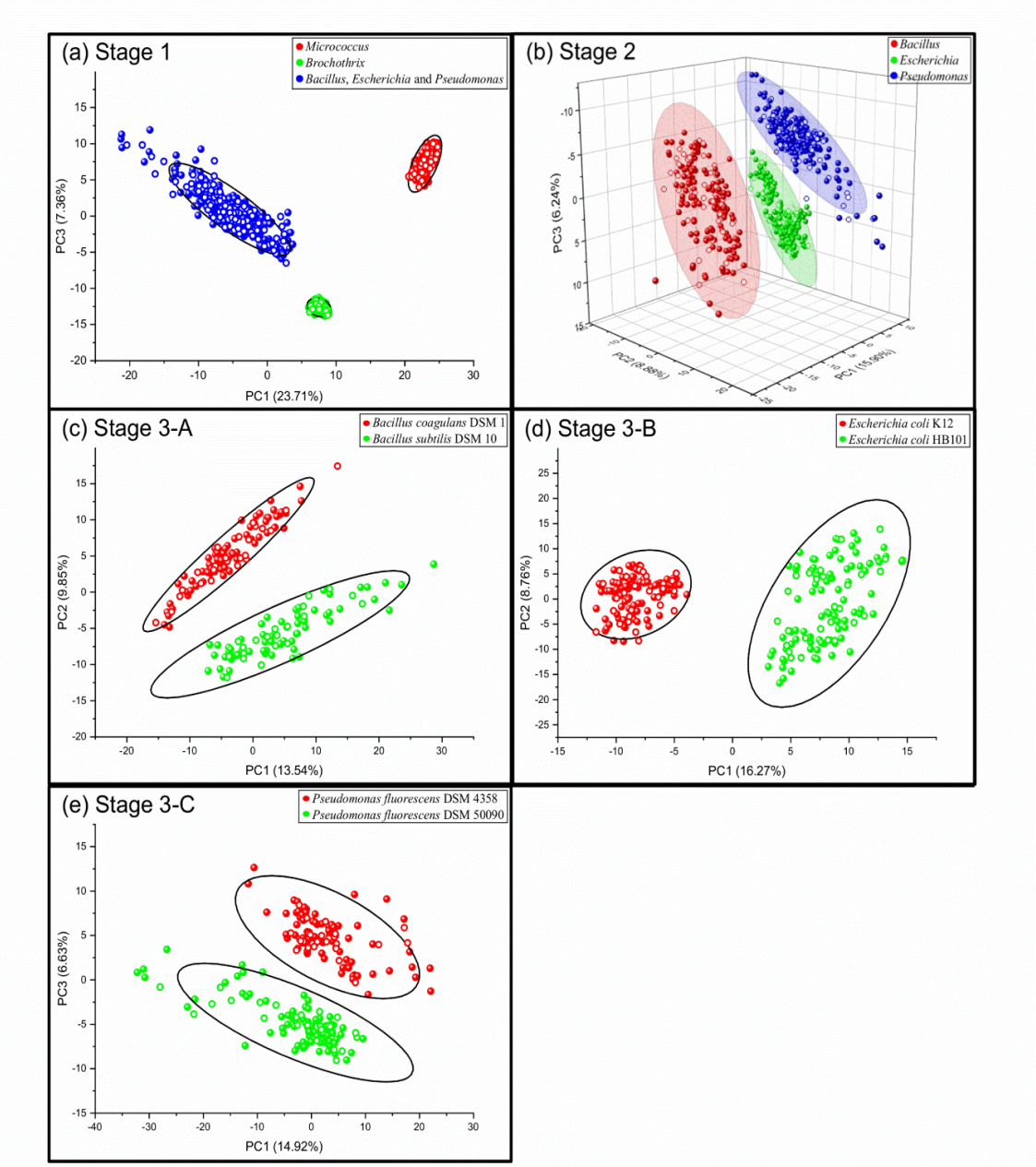

Figure 2.3: Stages and scores of PCA for bacterial spectra collected by the Microscope system: (a) Stage 1, discrimination of bacterial genera to three groups; group 1 (*Micrococcus*), group 2 (*Brochothrix*) and group 3 (*Bacillus*, *Escherichia* and *Pseudomonas*). (b) Stage 2, discrimination of bacterial genera from group 3 in stage 1 into three groups; group 1 (*Bacillus*), group 2 (*Escherichia*) and group 3 (*Pseudomonas*). (c) Stage 3-A, discrimination of *Bacillus* subspecies from group 1 in stage 2 into two groups; group 1 (*Bacillus coagulans*) and group 2 (*Bacillus subtilis*). (d) Stage 3-B, discrimination of *Escherichia* strains from group 2 in stage 2 into two groups; group 1 (*Escherichia coli* K12) and group 2 (*Escherichia coli* HB101). (e) Stage 3-C, discrimination of *Pseudomonas* strains from group 3 in stage 2 into two groups; group 1 (*Pseudomonas fluorescens* DSM 4358) and group 2 (*Pseudomonas fluorescens* DSM 50090). PCA model based upon the training sets (colored filled circles) and validation sets (colored empty circles). The ellipses (or ellipsoids) depict the 95% Prediction Interval for each class.

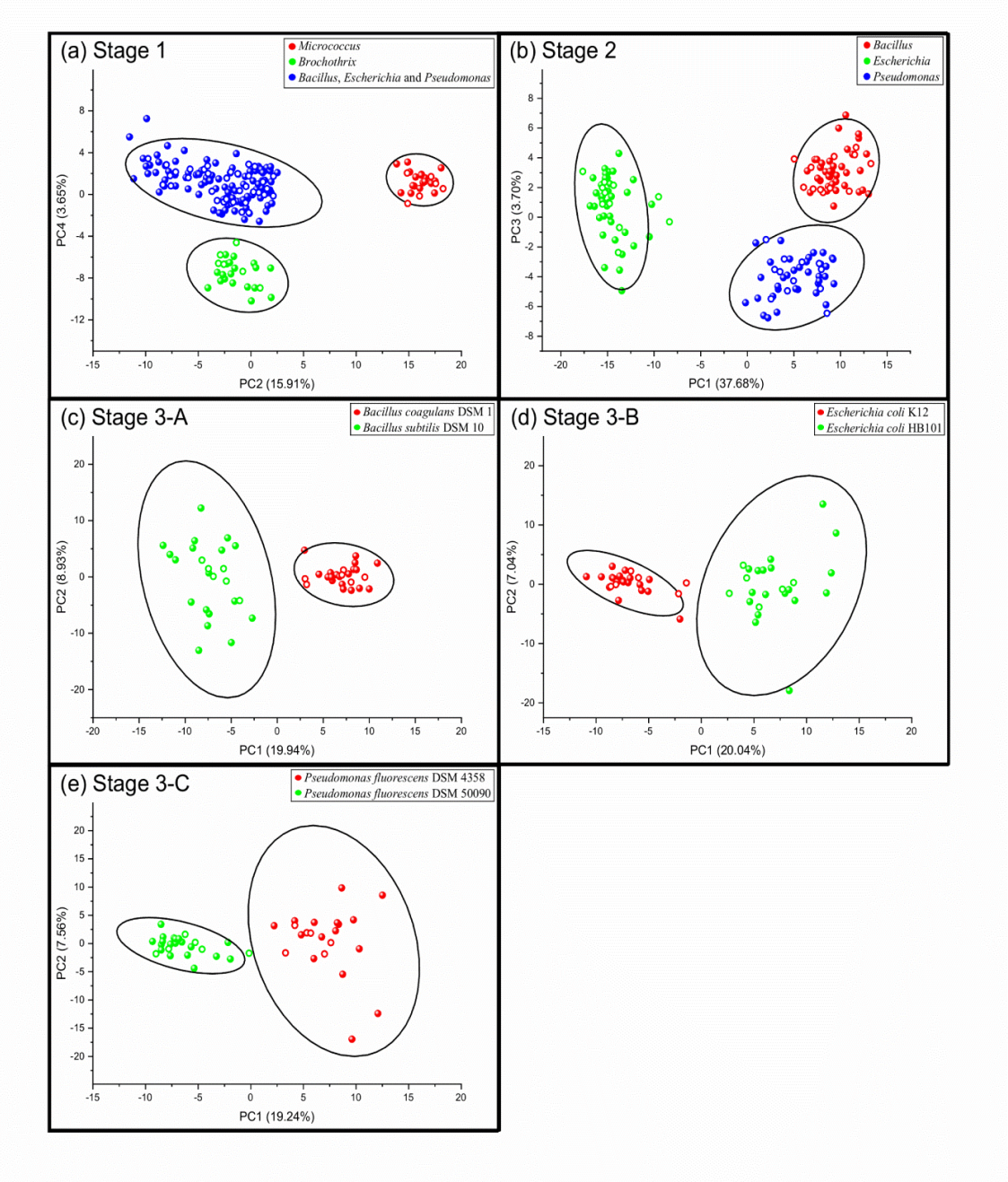

Figure 2.4: Stages and scores of PCA for bacterial spectra collected by the Portable Fiber-Optic system: (a) Stage 1, discrimination of bacterial genera to three groups; group 1 (*Micrococcus*), group 2 (*Brochothrix*) and group 3 (*Bacillus*, *Escherichia* and *Pseudomonas*). (b) Stage 2, discrimination of bacterial genera from group 3 in stage 1 into three groups; group 1 (*Bacillus*), group 2 (*Escherichia*) and group 3 (*Pseudomonas*). (c) Stage 3-A, discrimination of *Bacillus* subspecies from group 1 in stage 2 into two groups; group 1 (*Bacillus coagulans*) and group 2 (*Bacillus subtilis*). (d) Stage 3-B, discrimination of *Escherichia* strains from group 2 in stage 2 into two groups; group 1 (*Escherichia coli* K12) and group 2 (*Escherichia coli* HB101). (e) Stage 3-C, discrimination of *Pseudomonas* strains from group 3 in stage 2 into two groups; group 1 (*Pseudomonas fluorescens* DSM 4358) and group 2 (*Pseudomonas fluorescens* DSM 50090). PCA model based upon the training sets (colored filled circles) and validation sets (colored empty circles). The ellipses depict the 95% Prediction Interval for each class.

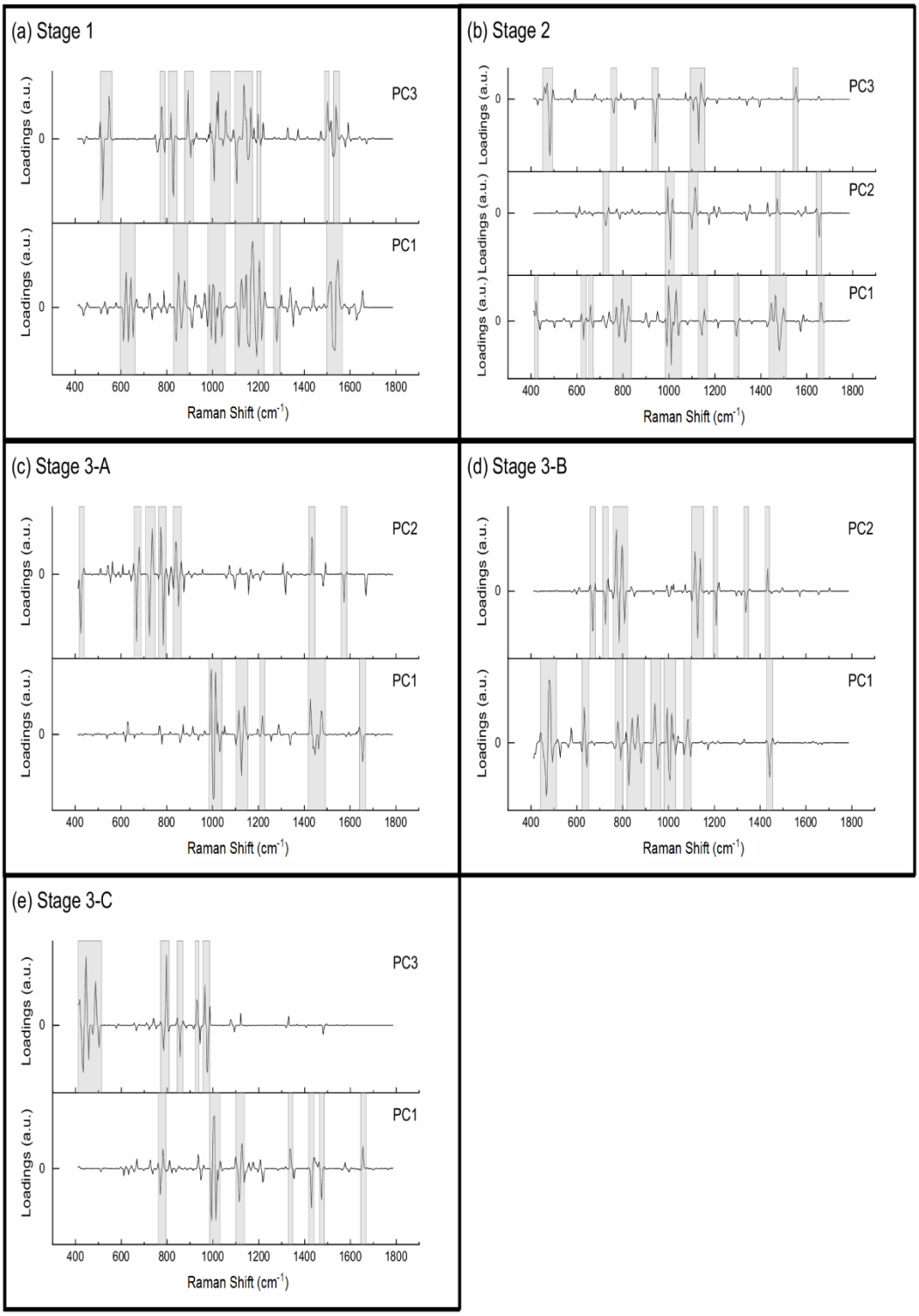

Figure 2.5: Stages and loadings of PCA for bacterial spectra collected by the Microscope system: (a) Stage 1, PC1 and PC3. (b) Stage 2, PC1, PC2 and PC3. (c) Stage 3-A, PC1 and PC2. (d) Stage 3-B, PC1 and PC2. (e) Stage 3-C, PC1 and PC3. For clarity; bands with significant contributions are marked by gray bars. The loading values were raised to the power of 5 to enable better visualization in loading curves.

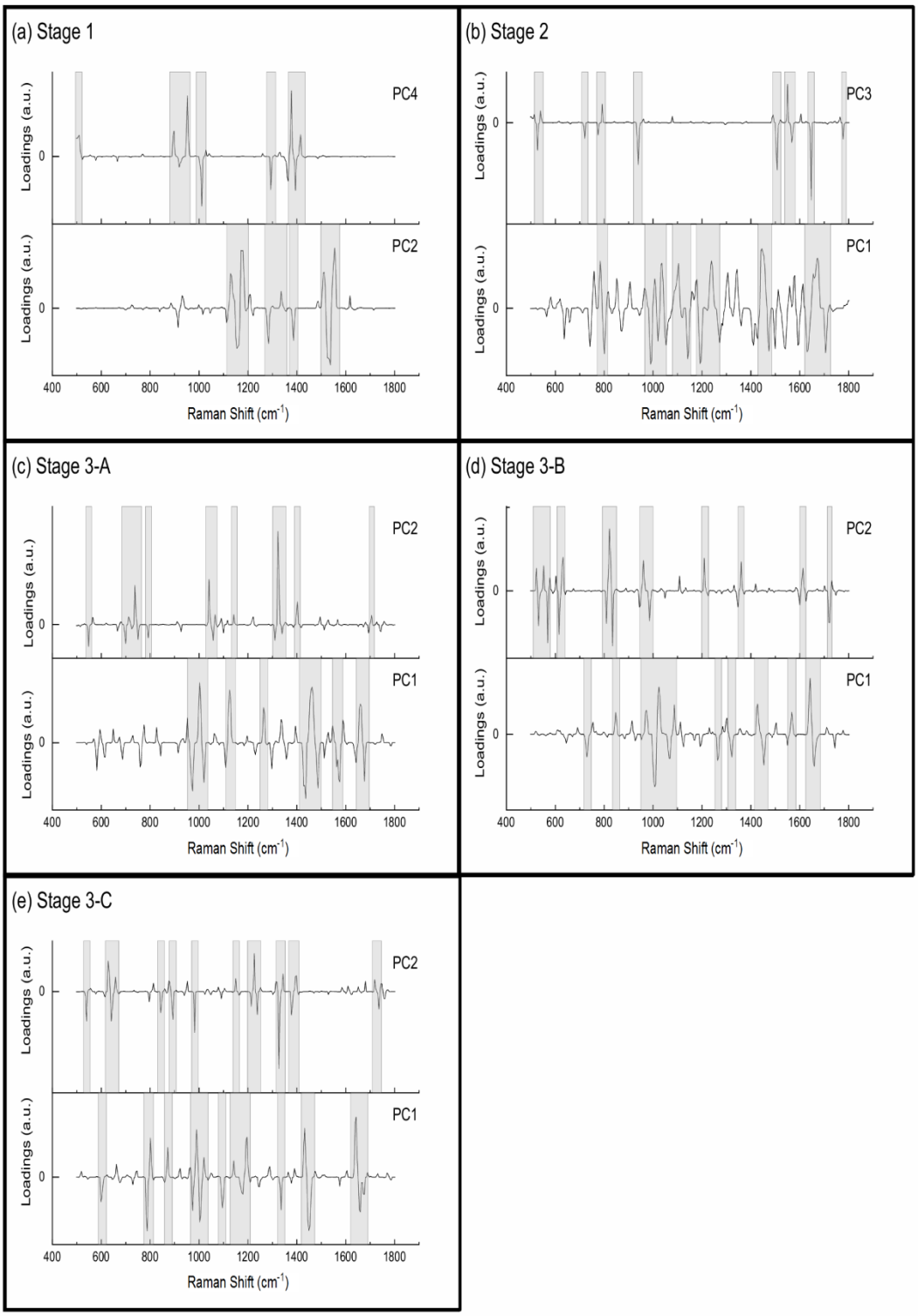

Figure 2.6: Stages and loadings of PCA for bacterial spectra collected by the Portable Fiber-Optic system: (a) Stage 1, PC2 and PC4. (b) Stage 2, PC1 and PC3. (c) Stage 3-A, PC1 and PC2. (d) Stage 3-B, PC1 and PC2. (e) Stage 3-C, PC1 and PC2. For clarity; bands with significant contributions are marked by gray bars. The loading values were raised to the power of 5 to enable better visualization in loading curves.

2.3.2.2 Support Vector Machines

Confusion matrices were used to evaluate the performance of the SVM-models for each Raman system in terms of sensitivity, specificity and accuracy as formulated below:

$$\text{Sensitivity (\%)} = \frac{\text{TP}}{\text{TP+FN}} \times 100 \quad (2.1)$$

$$\text{Specificity (\%)} = \frac{\text{TN}}{\text{TN+FP}} \times 100 \quad (2.2)$$

$$\text{Accuracy (\%)} = \frac{\text{TP+TN}}{\text{TP+FP+TN+FN}} \times 100 \quad (2.3)$$

Where TP (True Positive) and TN (True Negative) were the number of spectra of bacterial strains whose class was correctly predicted while FP (False Positive) and FN (False Negative) were the number of spectra of bacterial strains whose class was falsely predicted [150, 175].

2.3.2.2.1 Microscope System

In accordance with the two-dimensional PCA score plots, the SVM-model was initially restricted to the first two principal components (PC1 and PC2), which explain 72.67% of the total variance. Table 6.7 in the Appendix summarizes the classification results. The overall accuracy of the bacterial strains was 97.33% from 655 spectra. However, the sensitivity varied among strains used in the study. The highest rate was given for *M. lute* (100%; 87/87), *B. ther* (100%; 86/86) and *E. coli* K12 (100%; 87/87) while the lowest rate was reported for *B. subt* (66.67%; 44/66). The validation results have been summarized in Table 6.8 in the Appendix. Thus, the overall accuracy of the bacterial strains was 97.64% from 212 spectra. The highest sensitivity rate was reported for *M. lute* (100%; 28/28), *B. ther* (100%; 28/28) and *E. coli* K12 (100%; 28/28) while the lowest rate was reported for *B. subt* (71.43%; 15/21). For better separation, the number of principal components available to the SVM-model was gradually increased. Consequently, an improvement in classification and validation efficiency was observed, as shown in Table 2.3. The sensitivity, specificity and accuracy reached 100% for classification and validation data when using the first eight PC's.

Table 2.3: Overall percentage of sensitivity (Sens. [%]), specificity (Spec. [%]) and accuracy (Acc. [%]) of the classification (75%; 655 Spectra) and validation (25%; 212 Spectra) results of the bacterial strains collected by the Microscope system via MC-SVM using 2, 4, 6, 8 and 10 PCs.

		Classification, 655 Spectra			**Validation, 212 Spectra**		
No. of PC used	**% of cumulative variance explained**	**Sens. [%]**	**Spec. [%]**	**Acc. [%]**	**Sens. [%]**	**Spec. [%]**	**Acc. [%]**
2 PCs	72.67	88.45	98.48	97.33	89.80	98.66	97.64
4 PCs	84.02	98.33	99.79	99.62	97.40	99.67	99.41
6 PCs	86.56	99.85	99.98	99.96	99.55	99.93	99.88
8 PCs	88.14	100.00	100.00	100.00	100.00	100.00	100.00
10 PCs	89.07	100.00	100.00	100.00	100.00	100.00	100.00

2.3.2.2.2 Portable Fiber-Optic System

In accordance with the two-dimensional PCA score plots, the SVM-model was initially restricted to the first two principal components (PC1 and PC2), which explain 76.25% of the total variance. Table 6.9 in the Appendix summarizes the classification results. The overall accuracy of the bacterial strains was 96.26% from 147 spectra. However, the sensitivity varied among strains used in the study. The highest rate was given for *M. lute* (100%; 19/19) and *E. coli* HB101 (100%; 18/18) while the lowest rate was reported for *P. fluo* 5 (63.16%; 12/19). The validation results are summarized in Table 6.10 in the Appendix. The overall accuracy of the bacterial strains was 93.23% from 48 spectra. The highest sensitivity rate was reported for *M. lute* (100%; 6/6), *E. coli* K12 (100%; 6/6) and *E. coli* HB101 (100%; 6/6) while the lowest rate was reported for *B. coag* (33.33%; 2/6). For better separation, the number of principal components available to the SVM-model was gradually increased. Consequently, an improvement in classification and validation efficiency was observed, as shown in Table 2.4. The sensitivity, specificity and accuracy reached 100% for classification and validation data when using the first eight or ten PC's, respectively.

Table 2.4: Overall percentage of sensitivity (Sens. [%]), specificity (Spec. [%]) and accuracy (Acc. [%]) of the classification (75%; 147 Spectra) and validation (25%; 48 Spectra) results of the bacterial strains collected by the Portable Fiber-Optic system via MC-SVM using 2, 4, 6, 8 and 10 PCs.

		Classification, 147 Spectra			**Validation, 48 Spectra**		
No. of PC used	**% of cumulative variance explained**	**Sens. [%]**	**Spec. [%]**	**Acc. [%]**	**Sens. [%]**	**Spec. [%]**	**Acc. [%]**
2 PCs	76.25	85.22	97.86	96.26	72.92	96.13	93.23
4 PCs	81.95	98.56	99.81	99.66	85.42	97.92	96.35
6 PCs	84.52	99.34	99.90	99.83	95.83	99.40	98.96
8 PCs	86.19	100.00	100.00	100.00	97.92	99.70	99.48
10 PCs	87.54	100.00	100.00	100.00	100.00	100.00	100.00

2.3.2.2.3 Comparison between Both Systems

In both systems, 10 PCs (or less) were needed to reach 100% sensitivity, specificity and accuracy for each bacterial strain investigated in this study when classifying and identifying data. These results reflect the strong discriminative power of the developed SVM model and the high performance, as well as the suitability of the pre-processing method used. Furthermore, the results show that the broader bands due to the low resolution spectrometer and the relatively high fluorescence backgrounds in the Portable Fiber-Optic system do not adversely affect the discriminative power of the developed SVM model.

2.4 Conclusion

Discrimination and classification of eight important strains of meat spoilage microorganisms were successfully carried out using two dispersive Raman spectrometers (Microscope and Portable Fiber-Optic systems) which have different characteristics such as the detector, the spectral resolution, the laser spot size and the laser power. The ability of both systems to discriminate and classify bacterial strains were evaluated and compared. For both systems, PCA and MC-SVM were successfully applied to develop discrimination and classification systems. An accurate discrimination and classification of bacteria down to the strain level was successfully accomplished. The spectral features and differences among the species on which the discrimination was made were clarified through the loadings profiles. Moreover, the results show that the broader bands due to the low-resolution spectrometer and the relatively high fluorescence backgrounds in the Portable Fiber-Optic Raman system do

not adversely affect the discriminative power of the developed models. The results also reflect the high performance and suitability of the pre-processing method used in this study. Compared to traditional microbial analytical methods, Raman spectroscopy has proven to be a faster, non-destructive, noncontact and objective method. However, more samples of microorganism (different strains of the same species, phylogenetically similar bacteria) have to be tested by the models to make sure that the developed models are effective and to investigate scenarios in which the models may fail the discrimination.

2.5 Authors Contribution Statement

This chapter is adapted from the research article "S. Jaafreh, O. Valler, J. Kreyenschmidt, K. Günther, P. Kaul, In vitro discrimination and classification of Microbial Flora of Poultry using two dispersive Raman spectrometers (microscope and Portable Fiber-Optic systems) in tandem with chemometric analysis, *Talanta*. 202 (2019) 411–425. doi:10.1016/j.talanta.2019.04.082". For this research article; the following paragraphs specify the individual contributions of each author.

Author 1; S. Jaafreh: Conceptualization, conceived and designed the experiments, performed the experiments, analysis and interpretation of data, performed the PCA calculations, analysed the results which formed from PCA and SVM calculations, writing (original draft preparation), writing (review and editing), designed the figures, literature review.

Author 2; O. Valler: Performed the SVM calculations, writing (review and editing).

Author 3; Prof. Dr. J. Kreyenschmidt: Writing (review and editing), supervision.

Author 4; Prof. Dr. K. Günther: Writing (review and editing), supervision.

Author 5; Prof. Dr. P. Kaul: Writing (review and editing), supervision.

3 Rapid Poultry Spoilage Evaluation Using Portable Fiber-Optic Raman Spectrometer

This chapter is adapted from: S. Jaafreh, R. Breuch, K. Günther, J. Kreyenschmidt, P. Kaul, Rapid Poultry Spoilage Evaluation Using Portable Fiber-Optic Raman Spectrometer, *Food Anal. Methods*. 11 (2018) 2320–2328. doi:10.1007/s12161-018-1223-0.

3.1 Introduction

Muscle foods, including poultry and red meat, are rich sources of protein, essential amino acids, and a wide variety of micronutrients essential for human nutrition and health [1–3]. Fresh meat is a highly perishable product [6, 176, 177] because of microbial growth and their metabolism [93, 178]. Traditionally, evaluating the spoilage process of fresh meat has focused on evaluating the presence of microorganisms [179] by detection and enumeration using time-consuming traditional microbial analyses [12]. As the microbial load and composition of microflora are important parameters in determining the quality loss and shelf life of meat [180, 181], it is necessary to develop rapid objective methods to detect microbiological spoilage [32].

In recent years, several detection methods have been developed including Gas Chromatography-Mass Spectrometry [10, 182], Proton Transfer Reaction-Mass Spectrometer [183, 184], and Polymerase Chain Reaction [185]. But these technologies are usually expensive and destructive and require a sample pretreatment and highly-skilled personnel. Furthermore, they are time-consuming. Further difficulties lie in the fact that there is presently no consensus as to what indicators are representative of the early signs of incipient spoilage of meat. In addition, the changes in the technology of meat preservation (e.g. vacuum, modified atmosphere, packaging materials, etc.) make it more difficult to evaluate the spoilage objectively [34]. Therefore, demand remains high for the development of effective, rapid, simple, non-destructive, and inexpensive sensing technologies for detecting microbial contamination on meat [14–16].

A promising way to overcome the current difficulties is to apply non-destructive vibrational spectroscopic methods and techniques such as Fourier transform infrared (FT-IR) and Raman spectroscopy. The basic concept underlying these methods states that, as bacteria grow on meat, they utilize nutrients and produce by-products that cause spoilage. The

quantification of these metabolites represents a fingerprint characteristic of any biochemical substance and thus provides information about the type and the rate of spoilage [186]. Infrared (IR) spectroscopy supplies information on the conformational structure of polypeptides and proteins, particularly on protein secondary structure, whereas the Raman spectroscopy offers structural information about both secondary protein structure and the modifications in the local environments of amino acid residues, which are related to the protein tertiary structure [187]. However, in contrast to the IR absorption method, water does not disturb the Raman measurements in the fingerprint range [188, 189] because the water bending mode has a weak Raman signal. This is an important precondition for measuring meat, which possesses a high water content of about 75% [190]. FT-IR and Raman spectral data provide copious information, requiring an advanced data analysis approach. This has been achieved through the integration of modern analytical platforms with computational and chemometric techniques [191].

In tandem with chemometrics, the vibrational spectra have been used for real-time freshness evaluation of beef meat [192], pork meat [193], and chicken breast [194] using FT-IR spectroscopy and of pork meat [31–33] using Raman spectroscopy. The suitability of both methods to predict meat spoilage was studied by Argyri *et al.* [34], who used several computing and machine learning methods to develop prediction models of microbiological loads based on different biological measurements as well as on FT-IR and Raman spectra obtained from minced beef samples stored under different packaging conditions. They highlighted FT-IR and Raman spectroscopy as methods for the rapid and accurate assessment of meat spoilage. Another comparison of both methods was presented by Zając *et al.* [195]. They used attenuated total reflectance FT-IR and FT-Raman techniques to study the time-dependent changes of chicken stored in air at 22 °C for 10 days. The analysis of the results was based on the deconvolution of the chosen IR and Raman contours into Lorentzian components and the comparison of their integral intensities for the pairs of the bands corresponding to the specific vibrations of protein frameworks and the products of their decomposition. Although their results show that such an approach allows detection of the biochemical changes occurring in the meat as a result of its bacterial and chemical spoilage, using FT-Raman requires longer acquisition times and higher laser powers to increase the Raman signal [196, 197], which can often lead to sample damage and destruction by heating [32, 197, 198]. In addition, FT-Raman instruments are typically large and expensive with integral interferometers, which are sensitive to mechanical vibration [197]. Resultingly, FT-Raman spectroscopy does not easily lend itself to on-line applications [197, 199].

In recent years, poultry meat consumption has risen dramatically and its production is expected to grow [4, 35], which has significantly increased poultry's commercial value [14]. However, research on and investigations into fast methods for precisely predicting bacterial loads in poultry meat are rare even though they are urgently needed for efficient management in the poultry industry [36, 37]. As meat freshness is important to consumers, the meat industry and retailers, the purpose of the present study was to investigate the feasibility of a portable fiber-optic Raman spectrometer in conjunction with chemometric analysis for monitoring the spoilage process of poultry fillets through the evaluation of their freshness quality. Raman system used in this work was specifically chosen due to its relatively low cost, portability, non-destructiveness, rapidity, the use of a laser in the near-infrared region and the simplicity in coupling it with optical fibers.

For the work, commercial boneless skinless chicken breast fillets were purchased from a local store, and their storage time-dependent Raman spectra were measured in the laboratory daily for 21 days starting from the date of purchase. The results obtained from the Raman spectra combined with chemometric analysis provided information about the quality and the remaining shelf life. These results were similar to that inferred from the product label on the packages of poultry fillets. This finding indicates that this method could be used to classify samples with unknown storage time, which could lead to an evaluation of the total viable count on the surface of poultry fillets.

3.2 Material and Methods

3.2.1 Sample Preparation

Commercially packed fresh boneless skinless chicken breast fillets with the same storage life (9 days), and batch number (i.e. the same production date and the same expiry date) were ordered and purchased from a local store in a total of 42 packages. Each package weighed 600 g, with two fillets in each package. The fillets were packed under modified atmosphere (O_2 = 68%, CO_2 = 26% and N_2 = 6%). Approximately 10 minutes after purchasing, the packages were stored in a fridge at 4 °C (recommended storing conditions) during the course of the study (21 consecutive days). The measurements started on the day the chicken breast fillets packages were delivered to and purchased from the retailer. On each day of the experiment, two packages of chicken breast fillets chosen at random were opened and

their Raman spectra were measured. The measured fillets samples were disposed later on the same day of measurement. All the spectral measurements were done directly on the fillet surface without any pre-preparation of the fillet such as removal of fat or connective tissues, inoculation with bacteria, washing, or mincing.

3.2.2 Raman System

The Raman system used to collect Raman spectra consists of four components. The first component was a QE Pro-Raman spectrometer (Ocean Optics, Netherlands), which is a scientific-grade spectrometer with a small footprint, lightweight, and fiber optic-based. It is preconfigured for 785 nm Raman excitation, using a 600 lines/mm grating, and 50 µm entrance slit. The wavelength range was from 784 to 1135 nm with a resolution of around 13 cm^{-1}. At the heart of the QE Pro-Raman is a Hamamatsu scientific grade detector (back-thinned, thermoelectrically cooled, and 1044 x 64 element charge-coupled device array) with a high quantum efficiency up to 90%, and a high signal-to-noise ratio (> 1000:1). The cooled detector enables low-light-level detection and long integration times with virtually no spectral distortion. The second component was a Turnkey Raman laser of 785 nm excitation wavelength (Ocean Optics, Netherlands), which is a diode laser with an adjustable output power (> 350 mW). The third component was an RPB785 fiber-optic probe (Ocean Optics, Netherlands), which is a Raman probe for 785 nm excitation wavelength. The fiber probe configuration consists of a permanently-aligned combination of two single fibers (105 µm excitation fiber and a 200 µm collection fiber) with filtering and steering micro-optics (Numerical Aperture = 0.22), in a rugged polyurethane jacket. One fiber is coupled to the laser and the other to the spectrometer. The probe default working distance is 7.5 mm with a spot size about 155 µm. The probe length and diameter are 107 mm and 12.7 mm respectively, and the fiber length is 1.5 m. The fourth component was a computer running OceanView version 1.4.1 software (Ocean Optics, Netherlands), which provides full control of the QE Pro-Raman spectrometer. The spectrometer is connected to the computer via a USB port.

3.2.3 Raman Measurements

Raman spectra were collected with constant measurement parameters as follows: laser power of 250 mW at the sample, the distance between the sample and the laser fiber-optic

probe 7.5 mm with a laser spot size of around 155 µm, and with an integration time of 10 seconds. Three scans were used to obtain an average in each collected spectrum (i.e. three replicate scans were averaged for each collected spectrum). To reduce the noise, the detector temperature was set to -10 °C by the spectrometer's thermoelectric cooler. To eliminate ambient light from Raman spectra as well as to protect from reflected or scattered laser light during acquisition, all Raman measurements were taken inside a dark enclosure. The laser source is safety class 3B and was handled in accordance with national safety regulations. Raman spectra were acquired using OceanView software. The dark spectrum subtraction was performed during the spectral acquisition. For each fillet, five spectra from different positions were collected. During the measurements, the positions of fat were avoided. The fillets samples were homogenous, and there were no or weak spectral variations within the sample. Overall, 20 spectra were collected on every measurement day (i.e. 5 spectra × 4 fillets), with a total of 420 spectra during the 21 measurement days.

3.2.4 Spectral Processing and Chemometrics

3.2.4.1 Data Processing

For the 420 collected spectra, the pre-processing consisted of a cut-off to reduce the spectral variables to 269 variables, which corresponds to the wavenumber region from 450 cm^{-1} to 1750 cm^{-1} (fingerprint region). Then, spectra with cosmic spike(s) [200, 201] were searched for by visual inspection, and they were then eliminated from further analysis [159]. Next, the spectra containing signals of adipose tissue [202] or adipose tissue with meat were identified using the carbonyl stretching vibration of the ester and the methylene twisting vibration [203, 204] and then eliminated from further analysis. Thus, around 4% of the spectra were identified containing spikes and (or) adipose tissue (or adipose tissue with meat) and removed from the data set. After that, the average spectrum for each day of measurement was calculated and used in the analysis. The average spectra were then smoothed based on the Savitzky-Golay algorithm; the number of smoothing points was five with a second-order polynomial. Finally, the average spectra were normalized to the intensity of the phenylalanine (Phe) peak at 1006 cm^{-1}. The intensity and location of the Phe band are not sensitive to the protein conformation and can therefore be used for normalizing the Raman spectra [205–207].

3.2.4.2 Principal Components Analysis

PCA, which is built on the assumption that variation implies information, is a generally used method for feature extraction and qualitative analysis of samples. Briefly, PCA linearly transforms the original data (Raman spectra in this work) into new orthogonal variables called principal components (PCs). There are as many PCs extracted from the data matrix as there are original variables (Raman wavenumbers in this work). Each PC accounts for a consecutive decrease in the amount of data variance, which results in the compression of significant data into just a few PC variables. The first few PCs contains the maximum feature information, which could be used to observe the distribution of samples and identify their differences. Each data object has a score value on each PC, and each original variable is associated with a loadings value on each PC. The loadings profiles indicate the wavenumber variables in which the higher absolute values of the loadings significantly contribute to the discrimination of the objects described. Correlated variables will have loadings values with the same sign (either positive or negative), while loadings values with opposite signs represent anti-correlated variables. Once uncovered, PCs may be represented by scatter plots in an Euclidean plane, and the correlation structure among the variables may be inspected through loading plots. As a result, the spectra can be grouped into clusters and the extent to which these clusters correspond to classes of the sample can be determined [208, 209]. In this way, PCA was applied on pre-processed Raman spectra with a spectral region from 450 to 1750 cm^{-1} (269 variables) for the daily average spectra during 21 days.

3.2.4.3 Agglomerative Hierarchical Cluster Analysis

Hierarchical Cluster Analysis (HCA) is an algorithmic approach that aims to construct a hierarchy of clusters, and it is one of the most popular clustering methods used in the literature. HCA is a procedure for transforming a proximity matrix into a nested partition, which can be graphically represented by a tree, called a dendrogram. HCA is mainly classified into agglomerative methods (bottom-up methods) and divisive methods (top-down methods), based on how the hierarchical dendrogram is formed. Agglomerative Hierarchical Cluster Analysis (AHCA) methods are dominant in the hierarchical clustering family. In this method, clusters are consecutively formed from objects. Initially, this type of procedure starts with each object representing an individual cluster. These clusters are then sequentially merged according to their similarity. First, the two most similar clusters are merged to form a new cluster at the bottom of the hierarchy. In the next step, another pair of clusters is merged

and linked to a higher level of the hierarchy, and so on. This allows a hierarchy of clusters to be established from the bottom up and a dendrogram is formed [210, 211]. Here; AHCA of the first five principal components (i.e. PC1, PC2, PC3, PC4, and PC5) was carried out with cosine similarity measure and Ward linkage algorithm.

3.2.4.4 Software

All mathematical and statistical analyses were performed using OriginPro 2018 software (OriginLab Corporation, United States).

3.3 Results and Discussion

Storage time-dependent Raman spectra with the labels of the Raman bands of poultry fillets in the range 450–1750 cm^{-1} are presented in Figure 3.1. For clarity, the spectra are offset and only 6 spectra of days 1, 2, 9, 10, 20 and 21 are displayed.

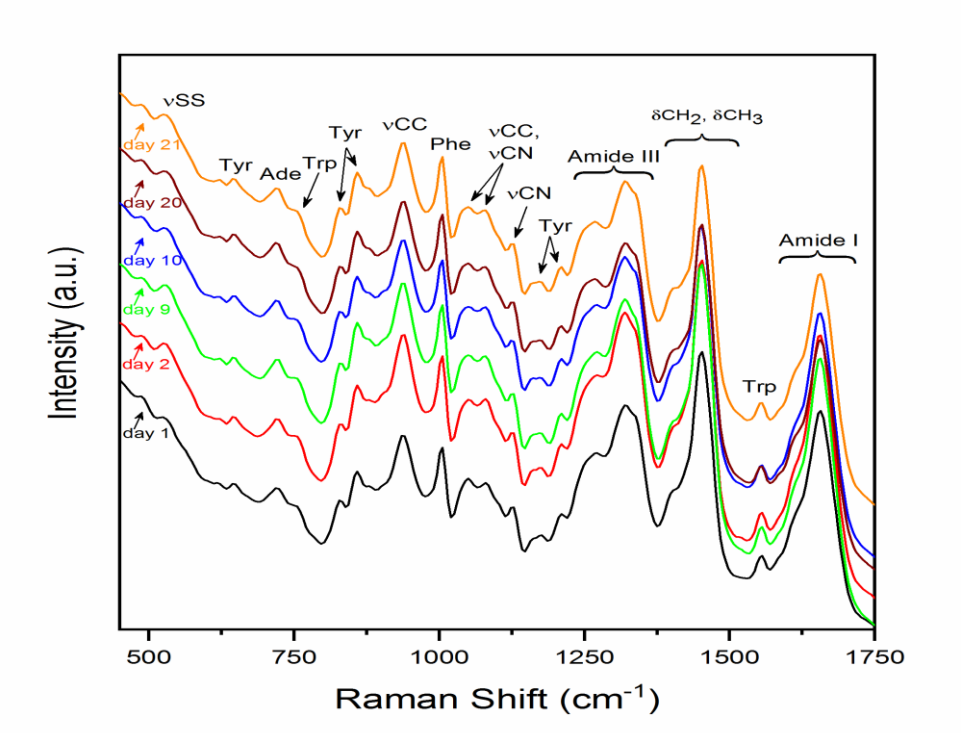

Figure 3.1: Selected Raman spectra of poultry fillets at different times of storage at 4 °C in a modified atmosphere package. The spectra are offset for clarity.

As shown in Figure 3.1, poultry fillets samples show a typical protein spectrum where Raman bands of amide I at 1657 cm^{-1}, amide III at 1319 and 1272 cm^{-1} and C-C stretch (νCC)

at 935 cm^{-1} can be observed [161, 212]. In addition, the strong CH_n bending modes (δCH_2, δCH_3) at 1453 cm^{-1} as well as the vibrations attributed to the aromatic amino acids Phe at 1006 cm^{-1}, tyrosine (Tyr) at 1211, 1177, 859, 828 and 644 cm^{-1} and tryptophan (Trp) at 1556 and 755 cm^{-1} were clearly identified [40, 161]. Further, characteristic bands of residues and of the protein backbone (C-C stretch (νCC) and C-N stretch (νCN)) at 1080 and 1050 cm^{-1} along with C-N stretch (νCN) at 1129 cm^{-1} were notable [212]. Moreover, vibrations attributed to the nucleobase adenine (Ade) at 719 cm^{-1} and S-S stretching vibration (νSS) at 525 cm^{-1} were recognizable [161]. In line with the storage time, the Raman spectra generally kept their basic structure, but all major Raman signals gradually changed. Visual examinations of these changes are difficult. To determine more detailed information about the complex spectral changes of the storage time-dependent samples, the PCA multivariate statistical tool was applied on pre-processed Raman spectra.

Preliminary to the PCA, it is necessary to apply pre-processing to the collected spectra. The pre-processing step of data analysis removes unwanted variation such as instrumental and experimental artifacts. This removal is crucial to obtain robust and accurate quantitative information from Raman spectra [125, 127, 157]. Since there is no single standard method for pre-processing Raman spectra [39], and the choice of pre-processing steps and the order in which they are conducted has been shown to have a major impact on the outcomes of spectral analysis [70, 213], several pre-processing steps with different orders were applied to the raw Raman spectra. The optimal result was achieved using the method described in Section 3.2.4.1.

A common challenge in Raman analysis of meat and other biological samples is the background fluorescence problem, which can limit or prohibit the relatively weaker Raman signal and thus make the detection of useful spectra difficult [70, 171, 212, 214]. For meat, the major absorption in the visible and near-infrared region is caused by the heme pigments of myoglobin as well as by water [31, 32, 190]. Fluorescence background is usually removed in the pre-processing step by computational methods, which are most often based on polynomial fitting, wavelet transform, and derivatives. However, these methods have major limitations e.g. the optimal choices of key parameters depends on the user's experience, the data processing can be time-consuming, the resulting spectrum could be distorted, as in the derivative method, and may contain artifacts especially in weak Raman signals [171]. Due to the use of near-infrared excitation laser at 785 nm [155, 157, 190, 198, 215] and to the myoglobin content being low in poultry compared to other kinds of meat [216, 217], the collected spectra were less susceptible to interference by fluorescence, as shown from the

gently sloping background in Figure 3.1. As a consequence, fluorescence background removal was omitted from the pre-processing step.

In the PCA results, PC1 and PC2 were found to carry most of the spectral variations between poultry samples, with PC1 describing 87.4% of variance and PC2 describing 11.7%. All remaining PCs explained less than 1% of variance. Figure 3.2(a) depicts a plot of the scored Raman data for the first two principal components (PC1, PC2), which revealed a separation of the samples according to their freshness. A distinction of spectra was found between the 9th (storage life; 9 days) and 10th day. The results show that the poultry samples can be grouped into three quality classes: fresh (1st day until the 3rd day), semi-fresh (4th day until the 9th day) and spoiled (10th day until the 21st day). These classes (fresh, semi-fresh, and spoiled) were based on and similar to the information inferred from the product label on the packages of poultry fillets (i.e. the days remaining until the expiry date and the quality classes). The scores in the fresh class have a positive sign in PC1 and a negative sign in PC2, except for the 2nd day, which has a positive sign with respect to PC2. In the semi-fresh class, the scores show a negative sign in PC1 and a positive sign in PC2, except for the 5th day, which has a positive sign with respect to PC1. In the spoiled class, the scored Raman data have a negative sign in PC1 and PC2, except for the 11th, 12th and 19th days, which have a positive sign with respect to PC2. PC1 could also be used to separate poultry samples according to storage time in an almost correct order from the 1st day until the 9th day. Similar groupings were obtained from the results of the AHCA of the first five principal components, as shown in the dendrogram (Figure 3.2(b)). These groups were, Group 1 (fresh; 1st day until the 3rd day), Group 2 (semi-fresh; 4th day until the 9th day), and Group 3 (spoiled; 10th day until the 21st day).

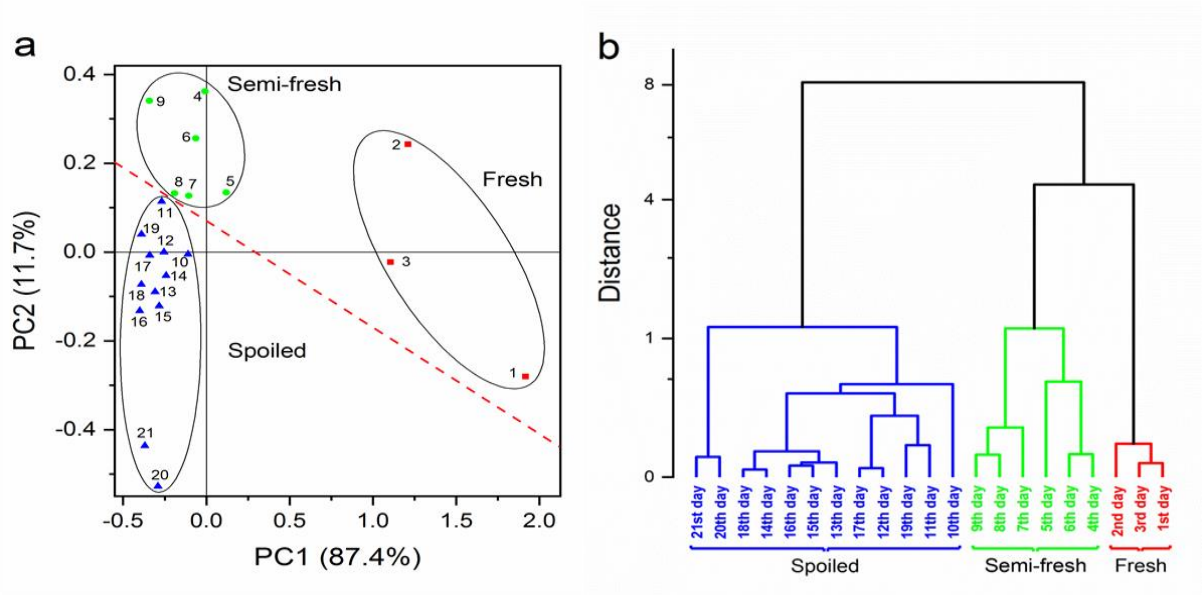

Figure 3.2: Classification of Raman spectra of poultry fillets samples using chemometric methods: (a) PCA. Scores of PCA of the Raman data plotted for PC1 and PC2. The poultry samples can be grouped into three quality classes; fresh (1st day until the 3rd day), semi-fresh (4th day until the 9th day), and spoiled (10th day until the 21st day). The dashed line indicates the distinction of spectra, separating spoiled from unspoiled poultry fillets samples with respect to the storage life (9 days). Ellipses and dashed line are only drawn as guides to the eye. (b) AHCA of the first five principal components. The poultry samples were grouped to three quality classes; Group 1 (fresh; 1st day until the 3rd day), Group 2 (semi-fresh; 4th day until the 9th day), and Group 3 (spoiled; 10th day until the 21st day). The dendrogram is based on the Ward's amalgamation method; distance measure: cosine similarity.

To analyse the spectral changes in the Raman data that were responsible for the separation found in the PCA, plots of PC1 and PC2 loadings are displayed in Figure 3.3. With no or only slight changes in peaks' positions with respect to the first day of measurements, the main contributions for PC1 were from the amide I band at 1657 cm^{-1}, a CH bending vibration at 1457 cm^{-1}, and amide III bands at 1315 and 1268 cm^{-1}. These bands are correlated with a positive sign of loadings. Significant contributions arise for PC2 from the amide I band at 1653 cm^{-1}, a CH bending vibration at 1453 cm^{-1}, and amide III bands at 1319 and 1277 cm^{-1}. These bands are correlated with a positive sign of loadings. PC2 also revealed major contributions from other correlated bands but with a negative sign of loadings represented by Tyr bands at 859, 833 and 650 cm^{-1}, Trp band at 755 cm^{-1}, Ade band at 724 cm^{-1}, and S-S stretching vibration at 531 cm^{-1}.

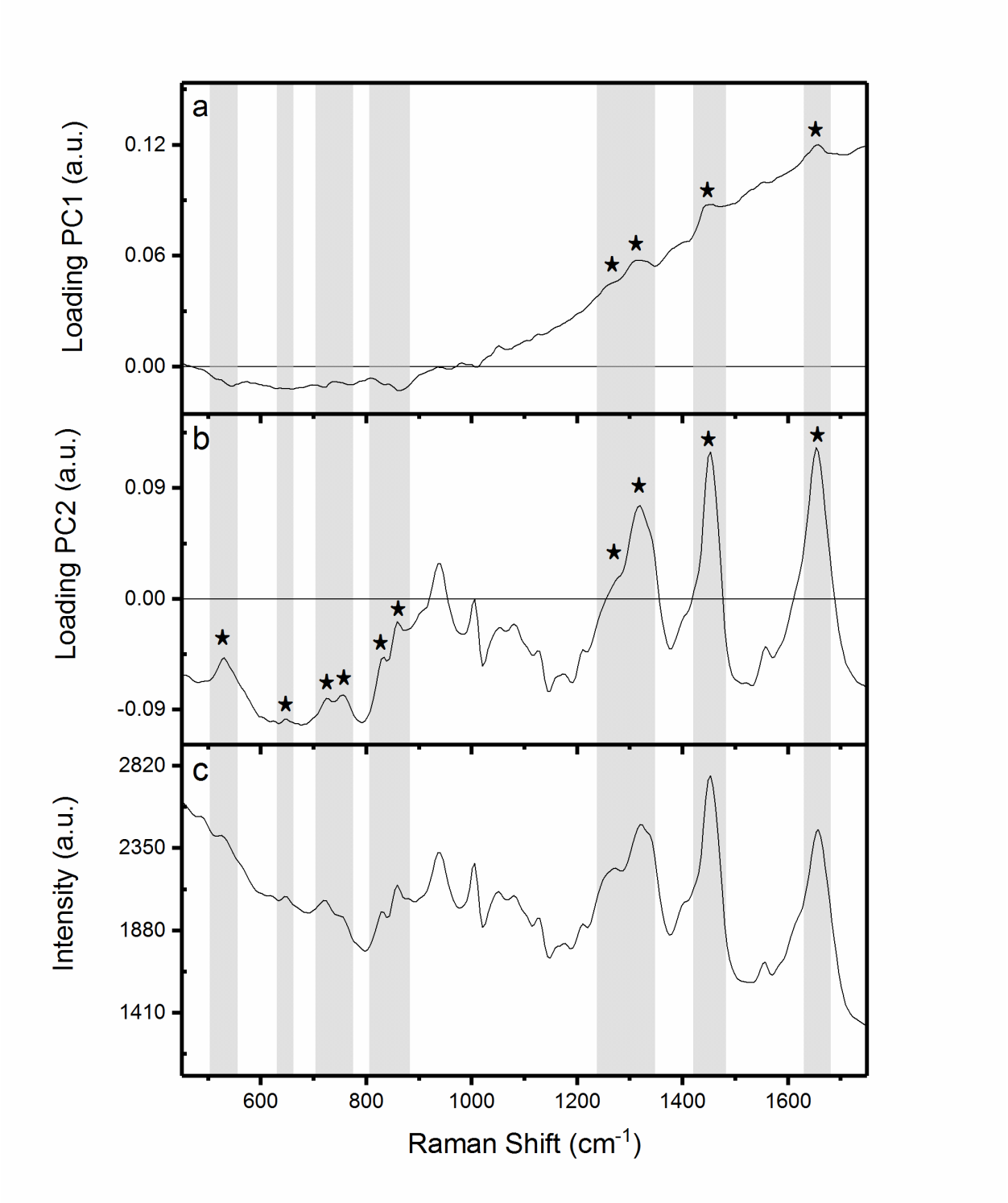

Figure 3.3: Loadings of the PCA of the Raman data plotted for PC1 (a) and PC2 (b). For clarity and comparison; bands with significant contributions are marked by asterisks and compared with the Raman spectrum for the first day of measurements (c) by gray bars.

To correlate bands intensity with loading values, the relation between the storage time and the intensity of one of the significant contributing bands from the loading values, such as amide I band at 1657 cm^{-1}, have to be investigated. The amide I band is considered to be an indicator of the overall concentration of proteins [205]. Figure 3.4 shows an inverse

relationship between the storage time of the poultry fillets and the intensity ratio of the Raman bands at 1657 cm^{-1} and 1006 cm^{-1} (the Phe peak at 1006 cm^{-1} was assumed to be constant and was used for normalization). Thus, the intensity of all correlated bands with the amide I band at 1657 cm^{-1} will decrease with time while the anti-correlated bands will increase. Hence, the loadings from PC1 and (or) PC2 show a decrease in the intensity of the bands at 1657 cm^{-1}, 1319 cm^{-1}, and 1272 cm^{-1}. These bands can be assigned to the amide I and III modes of α-helical proteins, which are known to decrease during storage [32, 190, 195, 205]. Furthermore, a decrease in the intensity of the band at 1453 cm^{-1} was observed. This band can be assigned to the CH_2 and CH_3 bending vibration. The decrease in the intensity of this band may result from hydrophobic interactions around the aliphatic residues [205, 218–220]. Moreover, an increase in Tyr bands at 859 cm^{-1}, 828 cm^{-1} and 644 cm^{-1}, and the Trp band at 755 cm^{-1} were shown. This increase may result from extra free amino acids which were formed during storage due to autolysis of meat and an increase in microbial growth [221]. The result also shows an increase in S-S stretching vibration at 525 cm^{-1}. The disulfide band may increase during storage due to oxidation of the amino acid residues cysteine and methionine [222, 223]. In addition, an increase in the Ade band at 719 cm^{-1} was observed.

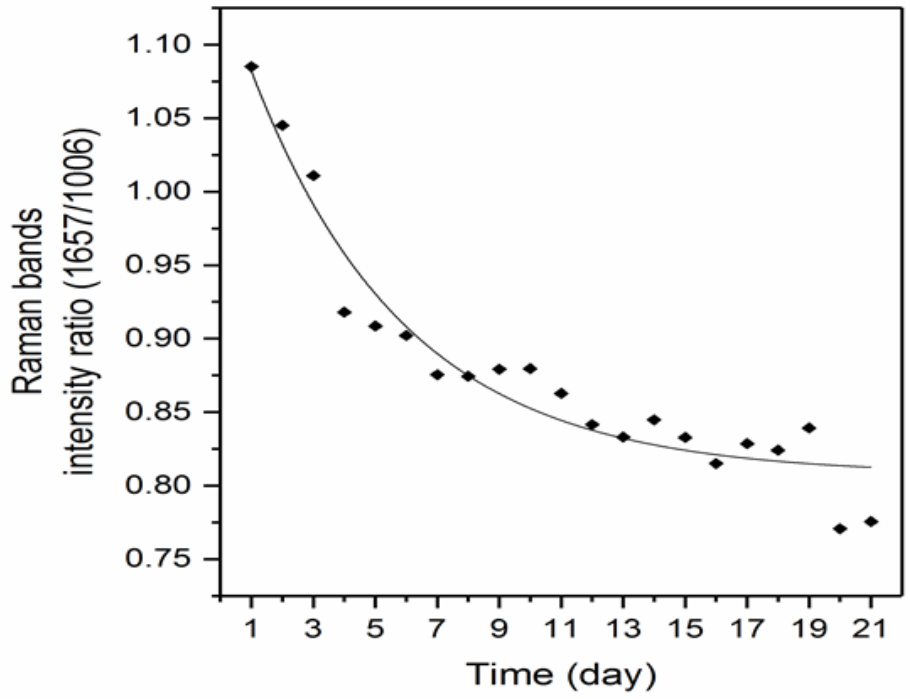

Figure 3.4: The relation between the storage time of poultry meat and the intensity ratio of the Raman bands at 1657 cm^{-1} and 1006 cm^{-1}. For clarity, a solid line was added to show that the intensity ratio decreases with storage time.

To count the effect of smoothing on spectral data, the data was pre-processed without the smoothing step, and then PCA was performed on the new pre-processed data. The new PCA scores and loadings were almost the same as those obtained when the smoothing step was included. This suggests that the adjacent peaks are positively correlated and smoothing the spectrum does not destroy their information content, which means that it is possible to reduce the resolution of the Raman spectral measurement without affecting accuracy [39].

3.4 Conclusion

The Raman spectra could be used in tandem with chemometric analysis (PCA and AHCA) to successfully group poultry fillets into three quality classes: fresh, semi-fresh, and spoiled. From the PCA results, a conclusion can be drawn on the poultry meat spoilage mechanism: The protein content of the meat decreases during spoilage, which is clearly seen from the lowering of the intensities of the amide I and amide III vibrational bands as well as from the growing amount of free amino acids from an increase in the intensity of Tyr and Trp bands. Furthermore, the growing amounts of free amino acids during storage are considered as an indicator of microbial growth. Moreover, the oxidation of amino acid residues was observed from the increase in the intensity of the S-S stretching vibrational band. Additionally, the hydrophobic interaction around the aliphatic residues was observed through a decrease in the intensity of the CH_2 and CH_3 bending vibrational band.

In conclusion, the Raman spectra collected by the portable fiber-optic Raman spectrometer in conjunction with chemometric analysis are able to monitor the spoilage process of poultry fillets at different storage days through the evaluation of poultry fillets freshness quality. This method is considered to be a simple and fast method for predicting bacterial loads in poultry, which could make off-line (or even on-line) applications possible in the poultry industry. However, further investigations along with microbial and sensory analysis are required to determine if it is possible to use this method to calculate the real shelf life of a product.

3.5 Authors Contribution Statement

This chapter is adapted from the research article "S. Jaafreh, R. Breuch, K. Günther, J. Kreyenschmidt, P. Kaul, **Rapid Poultry Spoilage Evaluation Using Portable Fiber-Optic Raman Spectrometer**, *Food Anal. Methods*. 11 (2018) 2320–2328. doi:10.1007/s12161-018-

1223-0 ". For this research article; the following paragraphs specify the individual contributions of each author.

Author 1; S. Jaafreh: Conceptualization, conceived and designed the experiments, performed the experiments, analysis and interpretation of data, performed PCA and AHCA calculations, analysed the results which formed from PCA and AHCA calculations, writing (original draft preparation), writing (review and editing), designed the figures, literature review.

Author 2; R. Breuch: Designing a computer program which helps in data averaging, writing (review and editing).

Author 3; Prof. Dr. K. Günther: Writing (review and editing), supervision.

Author 4; Prof. Dr. J. Kreyenschmidt: Writing (review and editing), supervision.

Author 5; Prof. Dr. P. Kaul: Writing (review and editing), supervision.

4 Investigation of the Influence of Different Production Systems on the Quality and Shelf Life of Poultry Meat Using a Portable Fiber-Optic Raman Spectrometer

This chapter is adapted from: S. Jaafreh, M. Hebel, J. Kreyenschmidt, K. Günther, P. Kaul, Investigation of the Influence of Different Production Systems on the Quality and Shelf Life of Poultry Meat Using Portable Fiber-Optic Raman Spectrometer, *In preparation*.

4.1 Introduction

Muscle foods, including poultry and red meat, are rich sources of protein, essential amino acids, and a wide variety of micronutrients essential for human nutrition and health [1–3, 105]. In recent years, global production and consumption of poultry meat has risen dramatically and per capita consumption is expected to grow [4, 35, 41, 105]. This has significantly increased poultry's commercial value [14, 105].

Poultry production underwent a remarkable development of intensification to meet the growing consumption and consumer demands. As a consequence of intense selection processes, poultry breeding lines were modified for shorter generation times, higher meat content and enhanced animal performance. With the selection for growth velocity, an increase of health issues and muscle failures of the animals emerged [224]. Animal health issues were combated by increased application of antibiotics in industrial animal production, which leads to the proliferation of microorganisms with antibiotic resistance with humongous impact on human health [224, 225]. In the context of these problems, the sustainability of poultry production is discussed growingly, and consumer knowledge is growing for animal health and welfare issues [224, 226, 227]. The rising demand for extensive production systems that are watchful for animal welfare led to the establishment of high-quality meat lines, a growing organic sector and local certified products [224, 228].

In Germany, the meat market reached the saturation point. Thus, meat quality as well as animal welfare and sustainability have an increasing impact on the purchase decision of the consumer. Accordingly, a production system was developed focusing on enhanced animal welfare, antibiotics-free, corn-based fattening and a slow-growing breed [224]. The use of more sustainable systems, such as corn-fed poultry lines, may increase consumer acceptance and the willingness-to-pay higher prices. Nevertheless, any modification of the production

system may also lead to differences in the nutritional parameters, meat quality and the shelf life of the final product [224]. Even though the production-specific factors (e.g. breeding, diet and stress) are known to affect meat quality; the effect of different husbandry systems on the development of quality parameters and shelf life has barely been investigated [224].

From a consumer and industry perspective, high safety, quality and long shelf life times are the most important criteria for meat and meat products [9]. In addition, the demand for extensive production systems that are watchful for animal welfare is rising [224]. The quality can be described as the measure of traits that are sought and valued by the consumer. The meat quality is a wide term and covers a variety of characteristics and can be defined in various ways from palatability to technological aspects to safety. The properties used to define the quality of meat can be divided into four groups of parameters; animal nutrition (e.g.: protein content, composition of fatty acids and mineral content), hygiene and toxicological (e.g.: microbiological status and heavy metal content), meat processing (e.g.: shear force value, pH value, drip loss and specific water content) and sensory parameters (e.g.: texture, color, juiciness, odor, taste, marbling and structure) which have the highest influence on the consumers' purchase decision [87–89]. The microbial spoilage regarded as the main cause of quality deterioration in meat, and it is causes pH change, off odors, slime formation, structural components degradation and appearance change [91–93].

The efficient assessment of meat quality is one of new challenges brought by the recent development in meat industry and the increase in public demand for high-quality meat [229]. Control procedures must be carried out on meat to keep the quality standards as close as possible to the preference of the target consumer and to keep competitive in the market. Therefore, various techniques such as chemical methods, mechanical measurement, sensory analysis and screening methods have been used to provide information about meat quality [2, 230]. However, most of the traditional techniques are costly, tedious, destructive and time-consuming, which cannot meet the requirements of the modern meat industry. Consequently, these techniques are unsuitable for on-line or at-line applications. Therefore, there is a demand for rapid, non-invasive and cheap alternatives for meat quality assessment and assurance [2, 89, 230–232].

The disadvantages of traditional methods for food quality evaluations can be overcome using Raman spectroscopy [231]. Raman spectroscopy has several advantages over other methodologies as it is a non-destructive, non-invasive, relatively inexpensive compared to other methods, rapid and being a label-free method. Furthermore, it requires simple up to

no sample preparation. Moreover, the presence of microorganisms or DNA in the laboratory environment is not a concern in Raman spectroscopy. Additionally, strains of the spoilage and pathogenic microorganisms can be identified extremely accurately [24, 121, 123, 124]. These attractive characteristics have made Raman spectroscopic techniques a powerful analytical tool for food quality evaluation [231].

Several research groups have investigated various methods for meat quality evaluation and the rapid detection of microbiological spoilage on different kinds of meat [31, 32, 233–237]. However, research on and investigations into fast methods, such as Raman spectroscopy, for evaluating the quality and predicting the bacterial loads in poultry meat are rare even though they are urgently needed for efficient management in the poultry industry [36, 37, 105]. Thus, the focus of this study was to investigate the ability of Raman spectroscopy in the revealing of the nutritional value and muscle characteristics, comparison and differentiation of two different industrial production lines (alternative and conventional) of a German poultry producer. Furthermore, the study aimed to investigate the ability of Raman spectroscopy in classifying of poultry fillets in each production line according to their storage time and their microbial load. Raman measurements were conducted directly on fillets surfaces parallel with nutritional and quality parameters and microbiological analyses.

4.2 Material and Methods

4.2.1 Study design

This study investigates the ability of Raman spectroscopy on the characterization of conventional and alternative industrial production lines of a German poultry producer. For the alternative production line, the producer recently changed breeds for a new slow-growing race showing optimized muscle growth within the prolonged production time. The characteristics of both production lines are provided in Table 4.1.

Table 4.1: Characteristics of conventional and alternative production lines.

Characteristics	Production line	
	Conventional	**Alternative**
Birds race	Ross 308	Ranger Classic
Stocking rate	39 kg/m^2	32 kg/m^2
Birds diet	Grain-based diet	Contained more than 50% corn
Antibiotic medication	Administered when required	No antibiotic medication
Birds slaughter age	30–35 days	42–45 days

All animals were slaughtered and processed at the same day and in the same industrial slaughterhouse. The breast fillets were transported under temperature-controlled conditions to the laboratory of the University of Bonn. A total of 80 fillets were investigated in two repeated storage trials. After packaging aerobically in polypropylene trays with snap-on lids, the samples were stored in high-precision low-temperature incubators (Sanyo Mir 154-PE, Sanyo Electric Co., Ora-Gun, Gunma, Japan) at 4 °C for 240 h. The investigations were conducted at five repeated investigation times (measurement days) during storage. For each investigation time, a total of 4 alternative and 4 conventional fillets were investigated. The first Raman measurements and microbial analyses of the poultry fillets started 24 h after slaughtering. This timestamp was set to zero for the experiment. The second, third, fourth and fifth investigation times started at 72, 120, 168 and 240 h of the experiment, respectively.

For each fillet, a standardized surface of meat tissue (5 cm^2) was defined with a sterile circular frame of radius 2.24 cm. For each fillet, the Raman measurements and the microbial analyses were measured for the same standardized surface. First, the Raman measurements were conducted and then the same surface was extracted aseptically and used for the microbial analyses.

4.2.2 Raman spectrometer and acquisition parameters

The Raman system used to collect Raman spectra was portable fiber-optic Raman system (QE Pro-Raman system) [105]. QE Pro-Raman system consists of four components: a QE Pro-Raman spectrometer, a Turnkey Raman laser of 785 nm excitation wavelength, an

RPB785 fiber-optic probe and a computer running OceanView version 1.4.1 software. All four components are from Ocean Optics (Ocean Optics, Netherlands).

Raman spectra were collected with constant measurement parameters as follows: laser power of 250 mW at the sample, the distance between the sample and the laser fiber-optic probe was around 7.5 mm with a laser spot size of about 155 µm, and with an integration time of 10 seconds (s). The average of five scans was used in each collected spectrum (i.e. five replicates scans were averaged for each collected spectrum). To reduce the noise, the detector temperature was set to -10 °C by the spectrometer's thermoelectric cooler. To eliminate ambient light from Raman spectra as well as to protect from reflected or scattered laser light during acquisition, all Raman measurements were taken inside a dark enclosure. The dark spectrum subtraction was performed during the spectral acquisition. Raman spectra were acquired using OceanView software (Ocean Optics, Netherlands). Inside the 5 cm^2 standardized surface of each fillet, five to eight Raman spectra were collected from random positions chosen manually. In this manner, Raman spectra collected from each production line were ~25 spectra on every measurement day and with a total of ~124 spectra during the measurement days (more details are provided in Table 4.2). During the measurements, the positions of fat were avoided. No further sample treatments were required. All of the Raman spectra were collected in a sterile environment and under ambient conditions.

Table 4.2: Number of spectra collected for each production line. Spectra containing cosmic spike(s), very high fluorescence background and signals of adipose tissue or adipose tissue with meat are not included in this table.

Measurement time (h)	**Conventional production line**		**Alternative production line**	
	1st storage trial	**2nd storage trial**	**1st storage trial**	**2nd storage trial**
0	22	23	21	23
72	24	24	28	24
120	24	27	24	27
168	24	24	24	25
240	23	28	29	28
Total	117	126	126	127

4.2.3 Microbiological analyses

For microbial investigations, the standardized surface of each fillet (i.e. the area of 5 cm^2 where the Raman measurements were conducted) was extracted aseptically using a sterile punch and a scalpel. The samples were transferred to a sterile, filtered stomacher bag. The ninefold amount of saline peptone diluent (0.85% NaCl with 0.1% peptone Saline tablets, Oxoid BR0053G, Cambridge, United Kingdom) was added with an accuracy of 0.1 g for the first dilution step. The samples were mixed with a Stomacher 400 (Kleinfeld Labortechnik, Gehrden, Germany) for 60 s. Tenfold dilutions of the homogenate were prepared in saline peptone diluents. The total viable count (TVC) was determined by the pour plate technique on Plate Count Agar (Merck, Darmstadt, Germany), and the results were recorded in $\log_{10}$ (colony-forming units (cfu)/ cm^2). The plates were incubated at 30 °C for 72 h.

4.2.4 Raman data evaluation

In this section, all calculations were performed using OriginPro 2019 software (OriginLab Corporation, United States).

4.2.4.1 Data pre-processing

For the collected spectra, the pre-processing consisted of a cut-off to reduce the spectral variables to 253 variables, which corresponds to the wavenumber region from 498 cm^{-1} to 1722 cm^{-1} (fingerprint region). Then, spectra with cosmic spike(s) [200, 201] and the spectra with a very high fluorescence background were searched for by visual inspection, and they were then eliminated from further analysis. Next, the spectra containing signals of adipose tissue [202] or adipose tissue with meat were identified using the carbonyl stretching vibration of the ester and the methylene twisting vibration [203, 204] and then eliminated from further analysis. After that, the spectra were smoothed based on the Savitzky-Golay algorithm; the number of smoothing points was nine with a second-order polynomial. The rest of the pre-processing steps were varied according to the use of the constructed model. For the models which constructed to characterize and discriminate samples from different poultry meat production systems; the area under curve for each spectrum was normalized to one, and then the second-order derivative was calculated for each spectrum. For the models which constructed to classify poultry fillets according to their storage time and their microbial load; the spectra were normalized to the intensity of the phenylalanine (Phe) peak at 1001 cm^{-1}. The

intensity and location of the Phe band are not sensitive to the protein conformation and can therefore be used for normalizing the Raman spectra [205–207].

The 1st storage trial was used as training set to build models to characterize and discriminate samples from different poultry meat production systems and to classify poultry fillets according to their storage time and their microbial load. The 2nd storage trial was used as the testing set to validate the presented pre-processing method and to test the models for their robustness.

4.2.4.2 Chemometric techniques

Chemometric techniques can be defined as the chemical discipline that uses mathematical, statistical and other methods to design or select optimal measurement procedures and experiments, and to provide maximum relevant chemical information by analysing chemical data [131, 132]. In this study, unsupervised chemometric methods Principal Components Analysis (PCA) and Agglomerative Hierarchical Cluster Analysis (AHCA) [41, 76], and a supervised chemometric method Canonical Discriminant Analysis (CDA) [191] were used to analyse the collected Raman data.

4.2.4.2.1 Principal components analysis

PCA, which is built on the assumption that variation implies information, is an unsupervised classification method (i.e., it makes no a priori assumptions about the data set) used to reduce the dimensionality as well as to investigate and visualize the grouping of different samples into different clusters. Briefly, PCA linearly transforms the original data (Raman spectra in this work) into new orthogonal variables called principal components (PCs). Potentially, there are as many PCs extracted from the data matrix as there are original variables (Raman wavenumbers in this work). Each PC accounts for a consecutive decrease in the amount of data variance, which results in the compression of significant data into just a few PC variables. The first PCs explain the largest amount of variance observed in the features, which can be used to identify the samples' differences. Each data object has a score value on each PC, and each original variable is associated with a loadings value on each PC. The loadings profiles indicate the wavenumber variables in which the higher absolute values of the loadings significantly contribute to the discrimination of the objects described. Once

uncovered, PCs may be represented by scatter plots in an Euclidean plane, and the correlation structure among the variables may be inspected through loading plots [41, 76, 105, 144, 145].

PCA was applied on pre-processed Raman spectral data of the 1st storage trial (training set). Subsequently, pre-processed Raman spectral data of the 2nd storage trial (testing set) were rotated into the PCA space of the training data by the respective PCA loadings. Before performing the PCA calculation, the standard normal variate [41, 146] was calculated for the training and testing data sets. The standard normal variate was calculated separately for each set of data.

4.2.4.2.2 Canonical discriminant analysis

Canonical discriminant analysis (CDA) is a multivariate statistical technique acting in a supervised manner. The supervised methods start with a number of objects whose group membership is known (sometimes called the training objects), and use these objects to find a rule for allocating a new object of unknown group to the correct group [191, 238–241]. CDA can identify differences among groups of objects and improve understanding the relationships among the variables measured within those groups. CDA finds linear functions of quantitative variables that maximally separate two or more groups of objects (i.e. maximizes variation between the groups of objects) while keeping variation within-groups as small as possible (i.e. minimizing within-group variation of the original variables). This approach distinguishes several uncorrelated canonical variables (CVs). CVs are linear combinations of the original variables that best separate the means of groups of observations relative to within-group variation. The maximum number of CVs is equal to the number of variables or one less than the number of groups, whichever is smaller. The first CV, CV1, yields the maximum possible variation between groups with respect to within-group variation (maximum ratio between groups and within-group variances), providing the most overall discrimination between groups. CV2 provides the group differences which are not displayed by CV1, with the condition of no correlation between CV1 and CV2. Similarly, CV3 is not correlated with CV1 and CV2; it provides the group differences which are not displayed by CV1 and CV2, and so on. The absence of correlation means that each CV extracts a unique dimension of information from the data set. In performing CDA, the aim is that the first few CVs will account for almost all differences between groups. Plotting the values of these CVs (canonical scores) enables a simple graphical representation that reveals relationships existing between groups. These plots may also be used to assign a new observation with unknown grouping to

an existing group. The canonical scores of the new object are calculated for the first few CVs and its position plotted. The new object is assigned to the group whose mean is closest to its position. Sometimes (though not as a general rule) the PC scores are analysed with CDA [13, 132, 238, 240–242].

There are two types of discriminant analysis; linear discriminant analysis (LDA) and quadratic discriminant analysis (QDA). LDA is a conventional classifier used to determine linear decision boundaries between classes, and it assumes equality of covariance matrix for all of the classes. The most popular extension of LDA is the QDA, which is more flexible than LDA in the sense that it does assume different covariance matrices for all the classes. The decision boundaries determine in QDA are quadratic curves (nonlinear). To decide whether LDA or QDA should be applied to a given problem; a preliminary test of equality of covariance matrices is often used in discriminant analysis [243–246].

In this work, the equality test of covariance matrices of the training data showed that the covariance matrices are not equivalent. Hence, CDA with a quadratic discriminant function was applied. CDA was performed based on the first few PCs generated from PCA of the pre-processed Raman spectral data of the training set. Thereafter, the prediction potential of the trained CDA model was checked using the testing set. More details on CDA models and the number of PCs used are mentioned in Section 4.3 Results and Discussion.

4.2.4.2.3 Agglomerative hierarchical cluster analysis

Hierarchical Cluster Analysis (HCA) is an algorithmic approach that aims to construct a hierarchy of clusters, and it is one of the most popular clustering methods used in the literature. HCA is a procedure for transforming a proximity matrix into a nested partition, which can be graphically represented by a tree, called a dendrogram. HCA is mainly classified into agglomerative methods (bottom-up methods) and divisive methods (top-down methods), based on how the hierarchical dendrogram is formed. Agglomerative Hierarchical Cluster Analysis (AHCA) methods are dominant in the hierarchical clustering family. In this method, clusters are consecutively formed from objects. Initially, this type of procedure starts with each object representing an individual cluster. These clusters are then sequentially merged according to their similarity. First, the two most similar clusters are merged to form a new cluster at the bottom of the hierarchy. In the next step, another pair of clusters is merged and linked to a higher level of the hierarchy, and so on. This allows a hierarchy of clusters to be established from the bottom-up and a dendrogram is formed [105, 210, 211]. Here; AHCA

of the first two principal components (i.e. PC1 and PC2) was carried out with Euclidean distance and Ward linkage algorithm [247].

4.3 Results and Discussion

4.3.1 Raman measurements and analysis

For the five investigation times (0, 72, 120, 168 and 240 h of the experiment), Raman spectra of fillets samples were collected from conventional and alternative production lines. Figures 4.1(a) and (b) show the storage time-dependent Raman spectra of fillets samples collected from conventional and alternative production lines, respectively. For each production line, each spectrum in Figures 4.1(a) and (b) represents the average of all Raman spectra of fillets collected in each investigation time. As shown in Figures 4.1(a) and (b), the Raman spectra of samples collected from both production lines share similar characteristic peaks. The peak observed at 1657 cm^{-1} could be attributed to the Amide I band, C=C and C=O stretching vibrations [41, 105, 122, 160, 161, 212, 248]. Another recognizable band at 1614 cm^{-1} is assigned to vibrations attributed to the aromatic amino acids Phenylalanine (Phe), Tyrosine (Tyr) and Tryptophan (Trp); and to COO^- asymmetric vibration of carbohydrates [41, 161, 165–168, 212, 249]. The Trp vibration and C=C stretching vibration were also observed at 1556 cm^{-1} [41, 105]. An additional band can be seen at 1525 cm^{-1}; it could be attributed to C=C stretching, carotene and carotenoids vibration [22, 41, 169]. Another important peak at 1453 cm^{-1} corresponding to a CH_n deformation vibration (δCH_2, δCH_3 and δCH_2CH_3) originates from the CH bindings in lipids, collagen, proteins and carbohydrates was recognizable [41, 105, 161, 212]. The COO^- symmetric stretching vibration of carbohydrates was also observed at 1403 cm^{-1} [41, 164, 167, 168]. Further, vibrations attributed to Amide III at 1324 and 1272 cm^{-1} were notable [105, 161, 212]. Furthermore, the peaks at 1211, 1167, 864, 828 and 650 cm^{-1} corresponds to the Tyr vibration were recognizable [40, 105, 161]. The stretching vibrations of C–C (νCC) and C–N (νCN) were also observed at 1124, 1080 and 1050 cm^{-1} [41, 105, 212]. In addition, the vibration attributed to Phe and Phe (collagen assignment) at 1001 cm^{-1} was observed [40, 41, 105, 161, 212]. Another notable band at 940 cm^{-1} could be attributed to the C–C stretching and C–O–C glycos bond vibration of carbohydrates [41, 105, 161, 212]. Moreover, vibrations attributed to Trp at 761 cm^{-1}, the nucleobase Adenine (Ade) at 719 cm^{-1} and S–S stretching vibration (νSS) at 531 cm^{-1} were recognizable [40, 41, 105, 161].

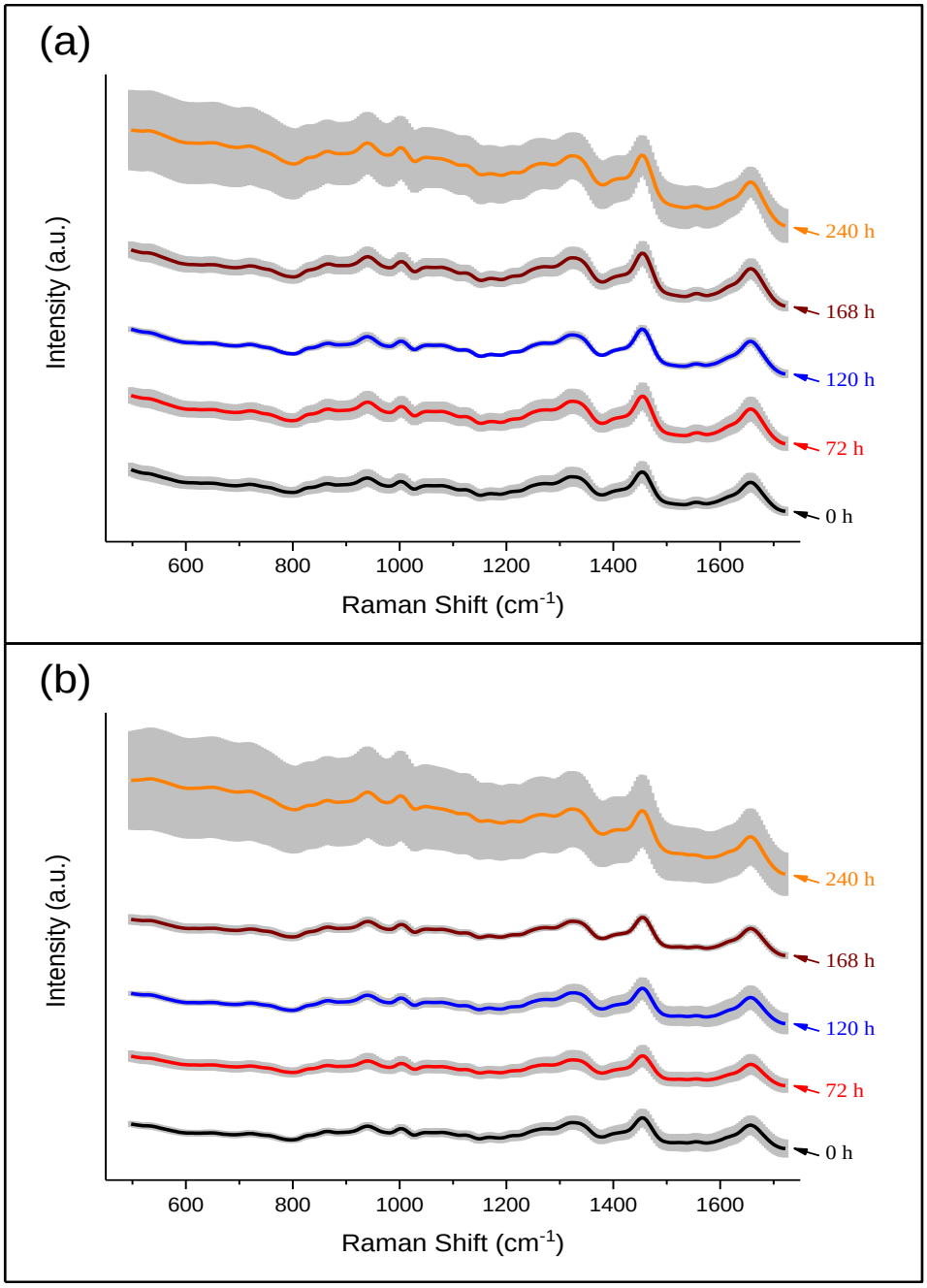

Figure 4.1: Mean Raman spectra of fillets samples collected from (a) conventional and (b) alternative production lines at different times of storage. The standard deviation is depicted as gray corona of all analysed fillets samples at different times of storage. The spectra are stacked for clarity.

The spectral features were found to be consistent with those in the literature as described before. Nonetheless, most signals are a superposition of bands from several compounds of molecular constituents (e.g., DNA, proteins, lipids, etc.), as the entirety of biochemical compounds contributes to the Raman spectrum [23, 41]. In line with the storage time, the Raman spectra generally kept their basic structure, but all major Raman signals gradually changed. Single visual discrimination between samples from both production lines

and the examinations of the changes during storage time for samples from each production line are difficult. To characterize and discriminate samples from different poultry meat production systems and to determine more detailed information about the complex spectral changes of the storage time-dependent samples from each production line; multivariate statistical methods were applied on pre-processed Raman spectra.

Even though Raman scattered light can provide a molecular structural signature (fingerprint information) and quantitatively reflects the chemical composition of biological samples; the Raman spectrum contains other contributions that influence the Raman signal and thereby obscure the desirable information (e.g.: fluorescence background, substrate background, cosmic spikes, Gaussian noise, CCD background noise, varying in sampling geometries). Pre-processing the raw data helps eliminate unwanted variation such as instrumental and experimental artifacts, enhances Raman spectral features and allows more reproducible data for qualitative and quantitative analysis [41, 59, 70, 105, 125–128, 157]. The background fluorescence, which can limit or prohibit the relatively weaker Raman signal and thus make the detection of useful spectra difficult, is a common challenge in Raman analysis of meat and other biological samples [70, 105, 171, 212, 214]. Fluorescence background is usually removed in the pre-processing step by computational methods. However, these methods have major limitations, for instance, the data processing can be time-consuming, the resulting spectrum could be distorted and may contain artifacts especially in weak Raman signals [105, 171]. Due to the use of near-infrared excitation laser at 785 nm [105, 155, 157, 190, 198, 215] and to the myoglobin content (cause major absorption in the visible and near-infrared region) being low in poultry compared to other kinds of meat [105, 216, 217]; the collected spectra were less susceptible to interference by fluorescence, as shown from the gently sloping background in Figures 4.1(a) and (b). As a consequence, fluorescence background removal was omitted from the pre-processing step. Since there is no single standard method for pre-processing Raman spectra, and the choice of pre-processing steps and the order in which they are conducted has been shown to have a major impact on the outcomes of spectral analysis [105]; the pre-processing steps applied in this work to the raw Raman spectra achieved the optimal results (see Section 4.2.4.1 Data pre-processing).

4.3.2 Chemometric techniques and constructed models

Since biological samples are heterogeneous mixtures of different biomolecules; their Raman spectra have a complex structure. They have numerous peaks in a broad band. Only

slight spectral differences are visible if Raman spectra of different biological states are measured and compared. A manual differentiating and rating of these slight changes are not possible or practical. Consequently, the use of chemometrics techniques is required [45, 128].

To characterize and discriminate different poultry meat production systems and to classify poultry fillets according to their storage time and their microbial load, chemometric techniques were applied to the pre-processed Raman spectral data. These techniques enhance the sensitivity of Raman spectroscopy, which are capable of distinguishing subtle spectral differences between classes. Furthermore, chemometric techniques make biological diagnostics more objective since little to no human intervention is required. In addition, chemometrics dramatically speed up biological diagnostic procedures, making it possible to deal with large-size Raman spectral datasets within an acceptable time [21, 143].

4.3.2.1 Characterization and discrimination of samples from different production systems

To avoid the effects of the growth of microorganisms and the changes in poultry fillets during storage on the characterization and discrimination of samples from different production systems; the training and testing data sets used in the calculations of the following subsections represent only the 1st investigation time (0 h of the experiment; 24 h after slaughter).

4.3.2.1.1 PCA model

The characterization and discrimination of fillets samples from different poultry meat production systems (see Tables 4.1 and 4.2) were successfully accomplished using PCA model. The training data points (pre-processed Raman spectral data of the 1st storage trial) were used to build the PCA model while the testing data points (pre-processed Raman spectral data of the 2nd storage trial) were used to validate the presented pre-processing method and to test the model for its robustness.

In the PCA results, PC1 and PC2 were found to carry most of the spectral variations between poultry samples, with PC1 describing 19.67% of variance and PC2 describing 8.18%. Figure 4.2 depicts a plot of the scored training data points (solid circles) for the first two principal components (PC1, PC2), which revealed a separation of the samples according to their production system. The results show that the poultry samples can be grouped into two

classes: conventional and alternative poultry meat production systems. Subsequently, testing data points were rotated into the PCA space of the training data by the respective PCA loadings. Figure 4.2, empty circles, shows that all testing data points have been assigned to the correct cluster.

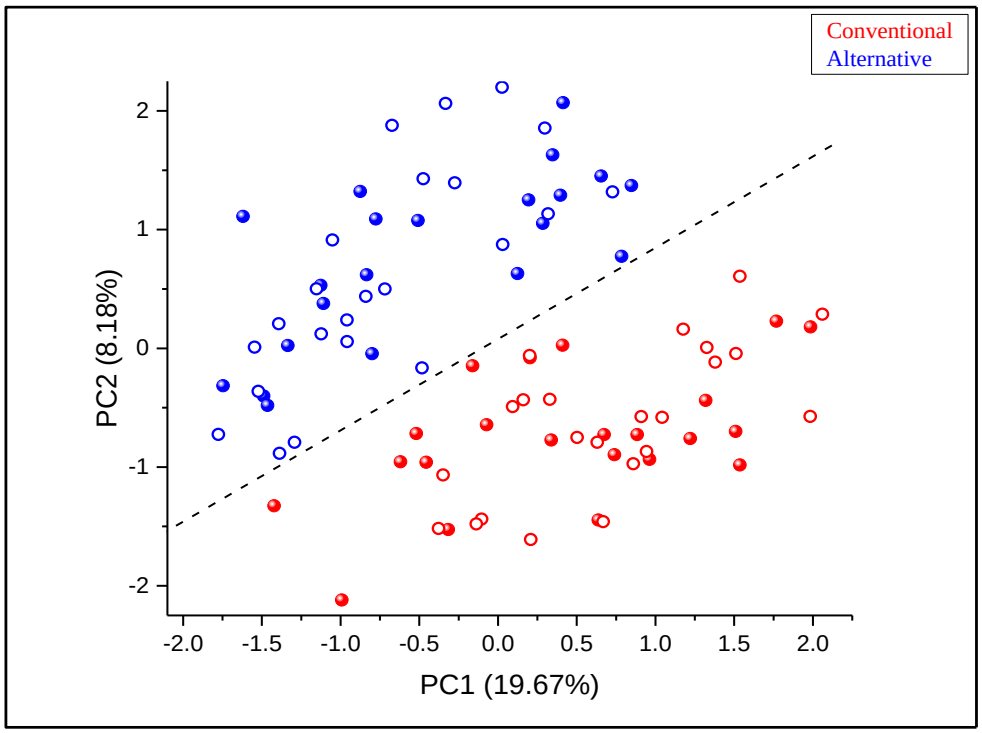

Figure 4.2: Scores of PCA model of the pre-processed Raman spectral data plotted for PC1 and PC2. The fillets samples from different poultry meat production systems can be grouped into two classes; conventional (red circles) and alternative (blue circles). The dashed line indicates the distinction of spectra, separating conventional from alternative poultry fillets samples. Solid and empty circles represent the training and testing data points, respectively. Dashed line is only drawn as guides to the eye. The training and testing data sets uesd in this calculations represent only the 1st investigation time.

To investigate the origin of the separation of the scores plot, the loading plots were analysed. The loadings values are plotted in Figures 4.3(a) and (b) for PC1 and PC2, respectively. The loadings profiles show that the main contributions for PC1 were from the peaks: 1657 cm^{-1} (Amide I band, C=C and C=O stretching vibrations [41, 105, 122, 160, 161, 212, 248]), 1453 cm^{-1} (δCH_n [41, 105, 161, 212]) and 1001 cm^{-1} (Phe vibration and collagen [40, 41, 105, 161, 212]). These peaks are correlated with a positive sign of loadings. While for PC2, the significant contributions arise from the peaks: 1525 cm^{-1} (C=C stretching, carotene and carotenoids vibration [22, 41, 169]) and 1167 cm^{-1} (Tyr vibration [40, 105, 161]). These peaks are correlated with a negative sign of loadings. PC2 also revealed major contributions

from other correlated peak at 1556 cm^{-1} (Trp vibration and C=C stretching vibration [41, 105]) but it correlated with a positive sign of loading.

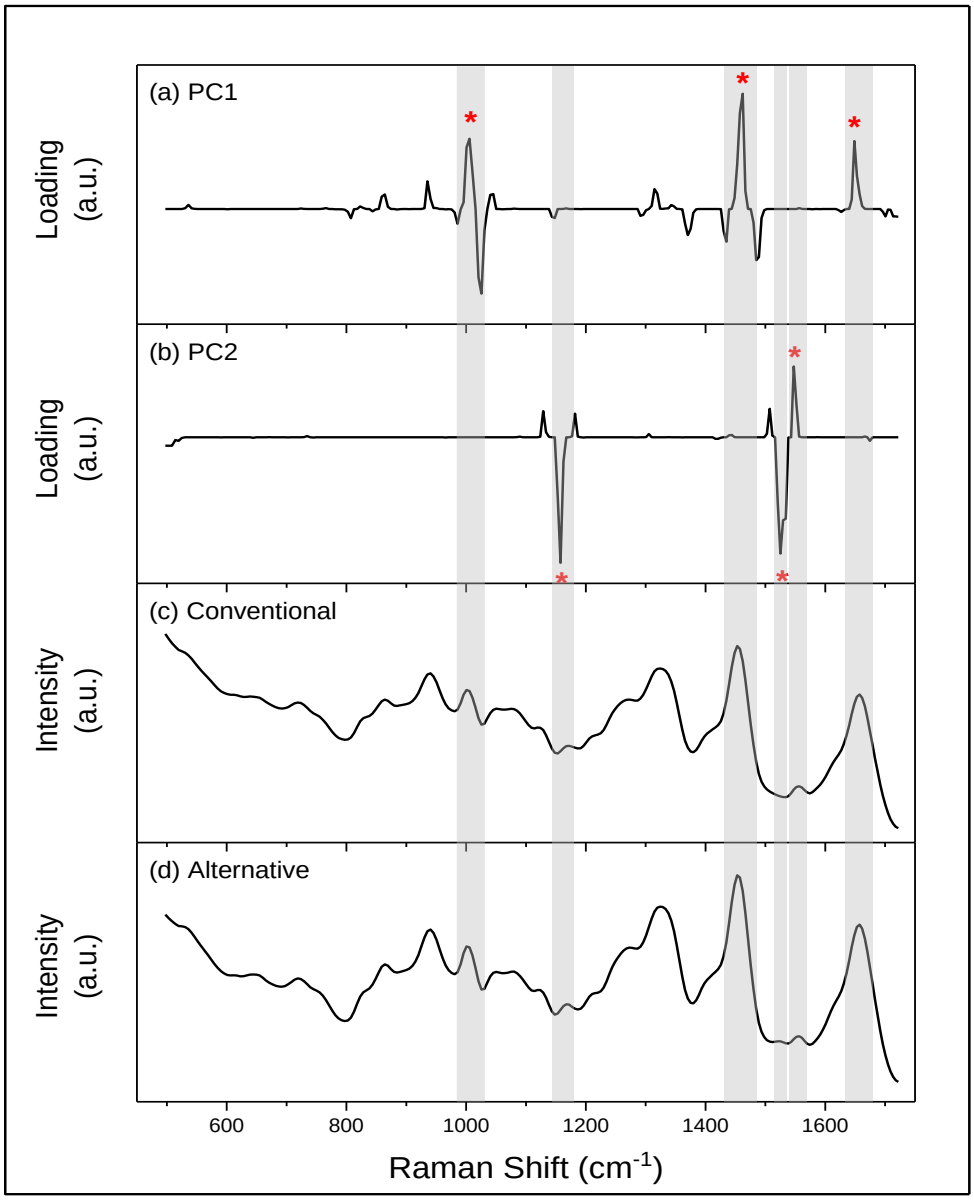

Figure 4.3: Loadings of the PCA of the training data points (shown as the second derivative of spectra) plotted for PC1 (a) and PC2 (b). For clarity and comparison; bands with significant contributions are marked by asterisks and compared with the Raman spectrum for the conventional (c) and alternative production lines (d) by gray bars. For each production line, Raman spectrum represents the average of all Raman spectra of fillets collected in the 1st investigation time. The loading values were raised to the power of 9 to enable better visualization in loading curves.

To investigate more about these peaks; the average area under each peak for the fillets samples from each production system was calculated and compared. First, the smoothed 43 Raman spectra (conventional: 22 spectra; alternative: 21 spectra) collected from the fillets

samples in the 1st investigation time (see Table 4.2) were cut to intervales (bands) related to these peaks (see Table 4.3). After that, the intensity values for each band were background corrected in such a way that the smallest intensity value was set to zero. Next, the area under each curve was calculated for each Raman spectrum. Finally, the average area under each curve was calculated for each production system.

Table 4.3 provides the average area under each peak for each production system. The results show that the alternative production line showed higher values of average area under peak for all peaks except the peak at 1556 cm^{-1}. The higher values at 1657, 1453, 1167 and 1001 cm^{-1} indicate that the alternative production line has higher collagen and protein content. Additionally, the alternative production line has a higher carbohydrates content indicated by the higher value of the average area under peak at 1453 cm^{-1}. These results were consistent with the analysis of nutrients in the alternative and conventional production lines [224]. The alternative production line also shows a higher value of the average area under peak at 1525 cm^{-1}. This indicates that the alternative production line has higher carotenoids content. Carotenoids are present in ingredients of feed for poultry [250]. They are compounds that are synthesized naturally by higher plants. Poultry reared on high forage rations pass a portion of the ingested carotenoids into the muscle [251]. The high carotenoids content in alternative production line could be due to their diet system which contained more than 50% corn (corn contains significant amounts of carotenoids [252]). The high carotenoids content in alternative production line may also account for the color difference between both production lines, with the alternative production line displaying more yellowish fillets.

Table 4.3: Average area under peak for the fillets samples from each production system.

Raman shift (cm^{-1}) at the highest absolute loading values			Average area under peak		Area ratio (Alternative to Conventional)
PC	Peak	Band	Conventional	Alternative	
1	1453	1434-1485	19038.04 ± 3641.50	23607.34 ± 2679.58	1.24 ± 0.38
	1001	985-1031	4466.07 ± 947.25	5933.36 ± 760.76	1.33 ± 0.45
	1657	1635-1679	7019.97 ± 1556.60	8885.73 ± 1093.37	1.27 ± 0.44
2	1525	1516-1538	114.68 ± 49.86	209.47 ± 97.90	1.83 ± 1.65
	1556	1538-1570	1010.91 ± 241.59	897.76 ± 155.74	0.89 ± 0.37
	1167	1143-1173	532.49 ± 113.18	830.50 ± 177.18	1.56 ± 0.66

4.3.2.1.2 CDA model

The classification of poultry fillets according to their production systems (see Table 4.2) was successfully accomplished using CDA model. The 1st storage trial (training set) was used to build the model using the cross-validation method and the 2nd storage trial (testing set) was used to validate the constructed model. In the cross-validation method, which is a data resampling method to assess the generalization ability of predictive models, the training data divides into several disjointed parts. Each part is selected in turn as the testing data, whereas the remaining parts are used as the training data. The CDA model built on the training data is then applied to predict the class labels of testing data. This process is repeated until all parts have been masked once. Then the prediction error rates across all blinded tests are combined to give an overall performance estimate [191, 253–255]. Here, CDA was performed based on the first few PCs generated from PCA of the pre-processed Raman spectral data of the training set (1st storage trial: 1st investigation time; 43 Raman spectra).To select the optimal number of PCs for model construction, a CDA of the classification between the two production systems was performed for different numbers of PCs from one to 20. The maximum PCs number used was 20 because computational problems will arise if the corresponding number of variables (here: PCs) is higher than the number of samples in the smallest group (here: alternative production line; 21 Raman spectra) [241]. Thus, the usage of a higher number of PCs for the analysis was avoided. The model with the lowest cross-validation error rate from the training data set will perform best on the testing data and avoids underfitting and overfitting [256, 257]. As can be seen in Figure 4.4; the first two PCs give the minimum error rate (0.00%), where all samples were correctly classified (see Table 4.4; confusion matrix). Therefore; the first two PCs has been selected for model construction. Subsequently, the performance of the constructed CDA model was checked using the testing set (pre-processed Raman spectral data of the 2nd storage trial: 1st investigation time; 46 spectra). First, the testing data points were rotated into the PCA space of the training data (pre-processed Raman spectral data of the 1st storage trial: 1st investigation time; 43 spectra) which used to build the CDA model by the respective PCA loadings. After that, the new PCs resulted from the testing data points were converted to new scores in the space of the training data set using the loadings obtained from the CDA model. Subsequently, the performance of the CDA model was checked. Here, CDA classification error rate was 0.00%. As can be seen in the confusion matrix (see Table 4.5), all samples were correctly classified. Since there is only one canonical variable, canonical score plot can’t be shown.

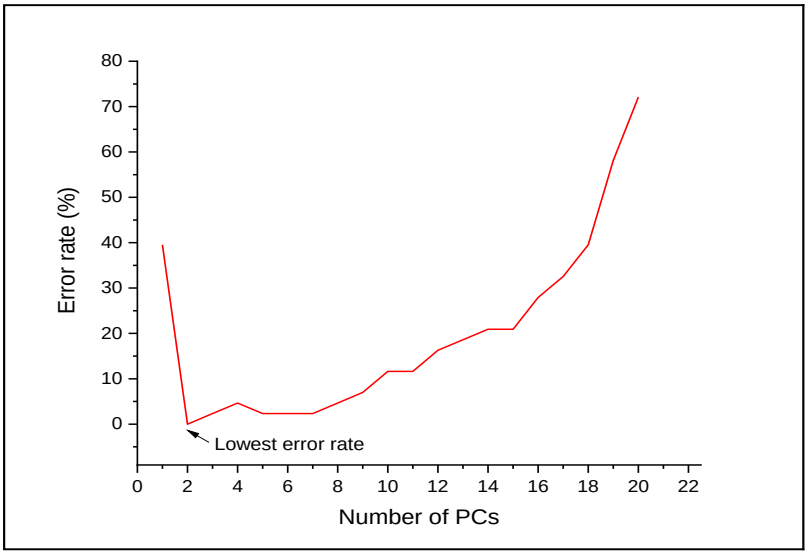

Figure 4.4: The CDA cross-validation error rate over the number of PCs for the conventional and the alternative production lines (training set: 1st storage trial; 1st investigation time).

Table 4.4: Cross-validation confusion matrix by CDA for the conventional and the alternative production lines (training set: 1st storage trial; 1st investigation time). Rows represent the true class and the columns the assigned class.

Groups: Production lines and their size	**Predicted Groups**	
	Conventional	**Alternative**
Conventional; 22	22	0
Alternative; 21	0	21

Table 4.5: Validation confusion matrix by CDA for the conventional and the alternative production lines (testing set: 2nd storage trial; 1st investigation time). Rows represent the true class and the columns the assigned class.

Groups: Production lines and their size	**Predicted Groups**	
	Conventional	**Alternative**
Conventional; 23	23	0
Alternative; 23	0	23

4.3.2.1.3 AHCA model

Similar groupings were obtained from the results of the AHCA. The poultry samples were grouped into two classes: class 1 (conventional production line) and class 2 (alternative

production line). Figures 4.5(a) and (b) show the AHCA dendrograms of the first two principal components for training and testing data sets, respectively. Prior to performing AHCA, the testing data set was rotated into the PCA space of the training data by the respective PCA loadings.

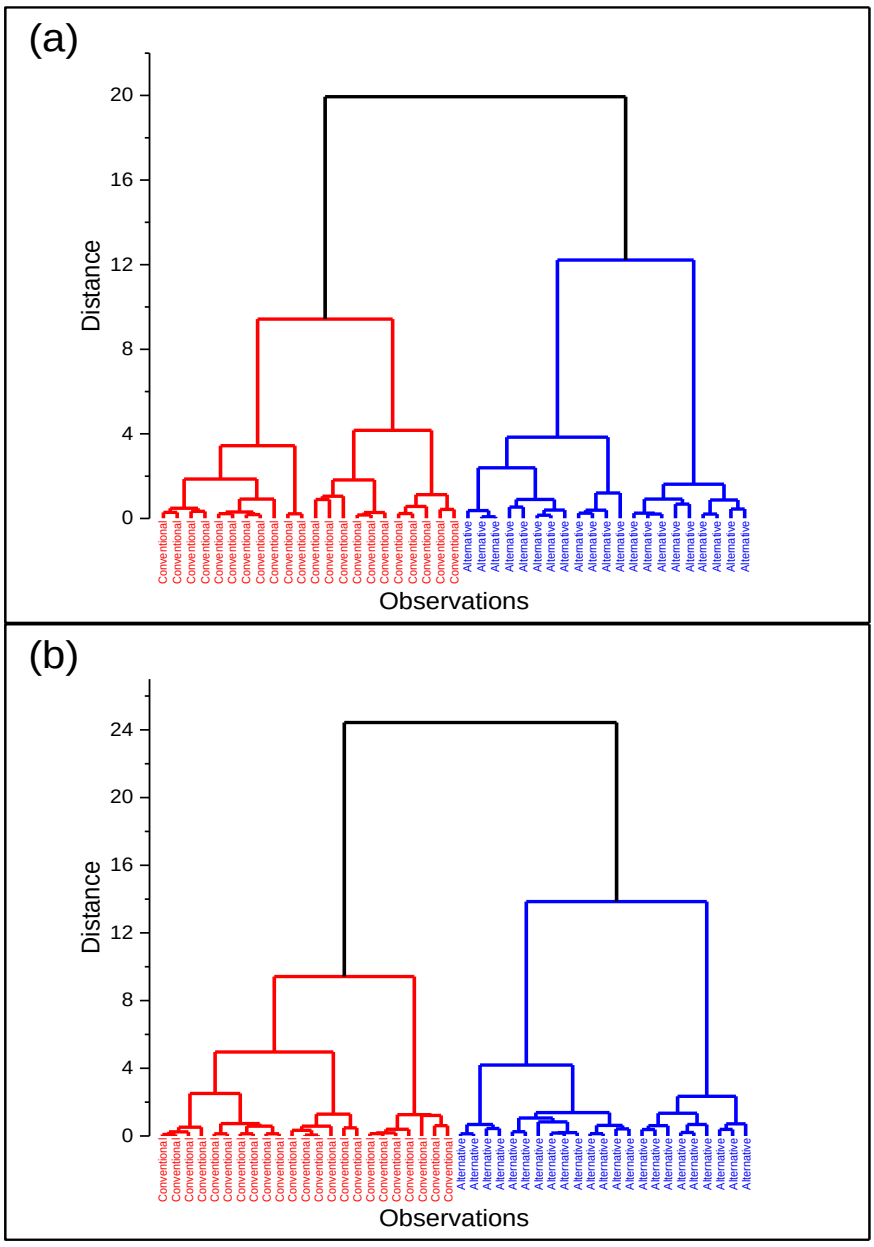

Figure 4.5: AHCA of the first two PCs of (a) training data set and (b) testing data set. The poultry samples were grouped into two classes: class 1 (conventional; red lines) and class 2 (alternative; blue lines). The dendrograms are based on the Ward's amalgamation method; the distance measure was Euclidean.

4.3.2.2 Classifying poultry fillets according to their storage time and their microbial load

To identify the classification potential of poultry fillets according to their storage time and their microbial load; CDA was applied for each production line. CDA calculation was performed on each production line separately to avoid the effect of the different characteristics between the two production lines on the classification ability. The 1st storage trial (training set) was used to build the models using the cross-validation method and the 2nd storage trial (testing set) was used to validate the constructed models.

4.3.2.2.1 Storage time

For the conventional production line, CDA was performed based on the first few PCs generated from PCA of the pre-processed Raman spectral data of the training set (1st storage trial: five investigation times; 117 Raman spectra). To select the optimal number of PCs for model construction, a CDA of the classification between the five investigation times was performed for different numbers of PCs from one to 21. As can be seen in Figure 6.2 in the Appendix; the first 10 PCs give the minimum error rate (22.22%), where 26 samples were not correctly classified (see Table 6.11 in the Appendix). Therefore; the first 10 PCs has been selected for model construction. The results of the CDA model using four CVs are depicted in scatter matrix plot in Figure 6.3 in the Appendix, with CV1, CV2, CV3 and CV4 describing 64.61%, 27.77%, 5.62% and 2.00% of variance, respectively. The score diagram based on the first two CVs (see Figure 4.6) revealed that the group means are clearly separated. Subsequently, the performance of the constructed CDA model was checked using the testing set (pre-processed Raman spectral data of the 2nd storage trial: five investigation times; 126 Raman spectra). First, the testing data points were rotated into the PCA space of the training data (pre-processed Raman spectral data of the 1st storage trial: five investigation times; 117 Raman spectra) which used to build the CDA model by the respective PCA loadings. After that, the new PCs resulted from the testing data points were converted to new scores in the space of the training data set using the loadings obtained from the CDA model (see Figure 4.7). Here, CDA classification error rate was 42.06%. As can be seen in the confusion matrix (see Table 6.12 in the Appendix), 53 samples were not correctly classified.

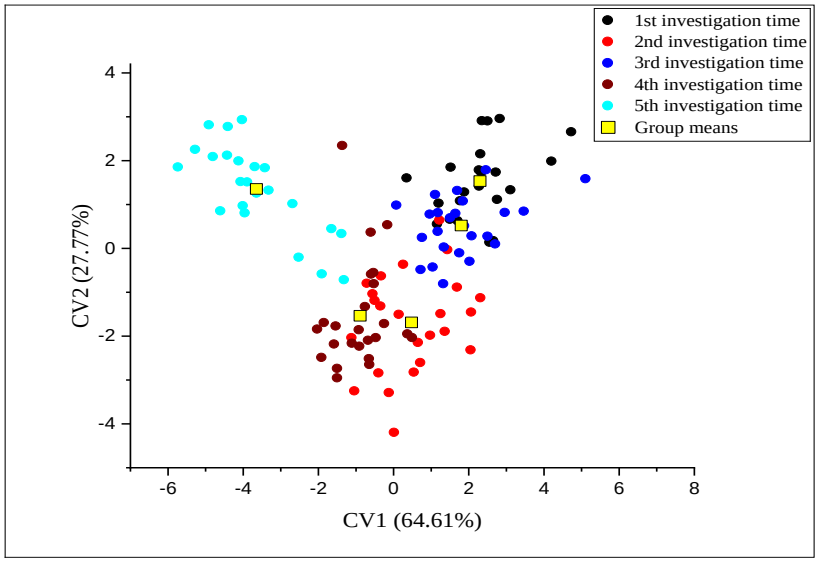

Figure 4.6: Score diagram based on the first two CVs of the first 10 PCs derived from the pre-processed Raman spectra of the training data set (1st storage trial) for the five investigation times of the conventional production line.

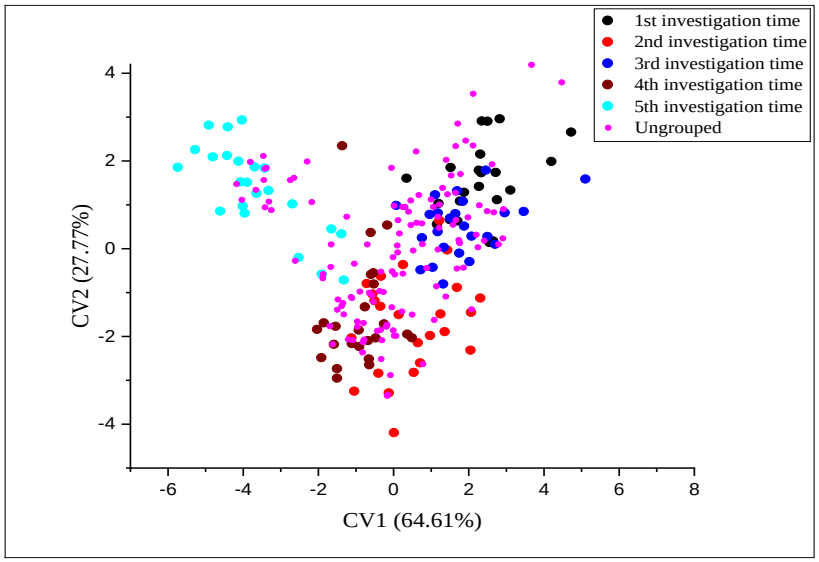

Figure 4.7: Score diagram based on the first two CVs of the first 10 PCs derived from the pre-processed Raman spectra of the training data set (1st storage trial) including the testing set (2nd storage trial) for the five investigation times of the conventional production line.

For the alternative production line, the calculations were carried out in the same way as in the conventional production line where CDA was performed based on the first few PCs generated from PCA of the pre-processed Raman spectral data of the training set (1st storage trial: five investigation times; 126 Raman spectra). The first 14 PCs give the minimum error

rate (15.87%), where 20 samples were not correctly classified (see in the Appendix Figure 6.4 and Table 6.13). Therefore; the first 14 PCs has been selected for model construction. The results of the CDA model using four CVs are depicted in scatter matrix plot in Figure 6.5 in the Appendix, with CV1, CV2, CV3 and CV4 describing 77.98%, 14.02%, 6.88% and 1.12% of variance, respectively. The score diagram based on the first two CVs (see Figure 4.8) revealed that the group means are clearly separated. Subsequently, the performance of the constructed CDA model was checked using the testing set (pre-processed Raman spectral data of the 2nd storage trial: five investigation times; 127 Raman spectra). Here, CDA classification error rate was 62.99%, where 80 samples were not correctly classified (see Figure 4.9, and in the Appendix Table 6.14).

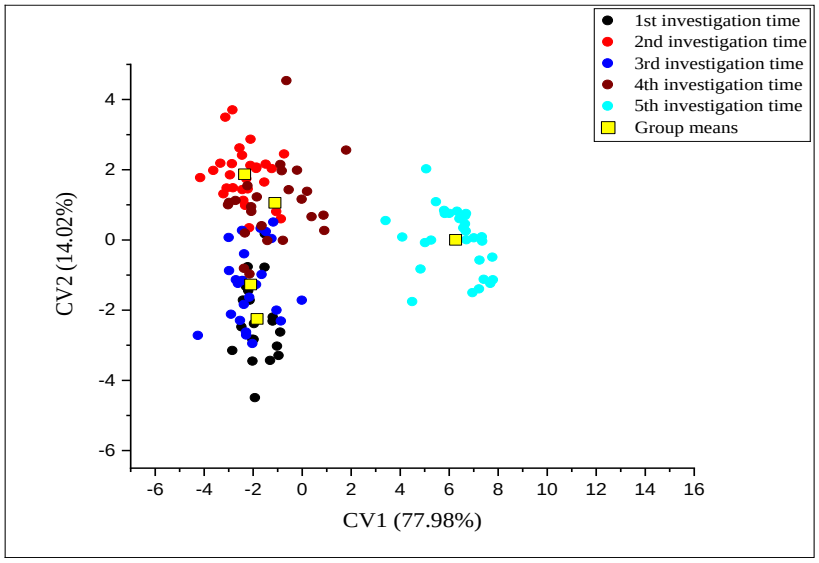

Figure 4.8: Score diagram based on the first two CVs of the first 14 PCs derived from the pre-processed Raman spectra of the training data set (1st storage trial) for the five investigation times of the alternative production line.

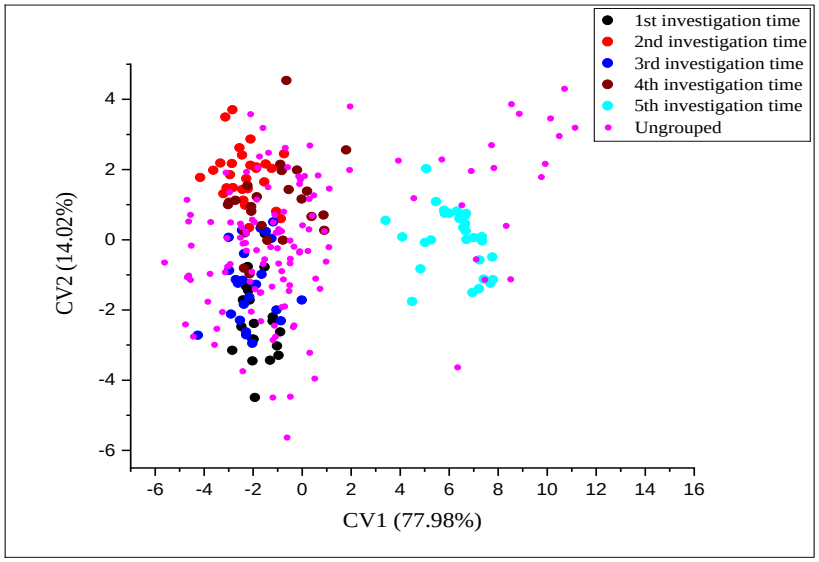

Figure 4.9: Score diagram based on the first two CVs of the first 14 PCs derived from the pre-processed Raman spectra of the training data set (1st storage trial) including the testing set (2nd storage trial) for the five investigation times of the alternative production line.

The results for both production lines are summarized in Table 4.6. For both production lines, the CDA models showed a good ability to classify poultry fillets according to their storage time by the cross-validation method (error rate: 22.22% and 15.87% for conventional and alternative, respectively). However, the CDA models showed a poor ability to classify poultry fillets when tested with testing sets (error rate: 42.06% and 62.99% for conventional and alternative, respectively). The high error rates for both production lines could be correlated to the high variations of the bacterial load between the two storage trials for each production line (see Figure 4.10). The microbial spoilage regarded as the main cause of quality deterioration in meat, and it is causes pH change, off odors, slime formation, structural components degradation and appearance change [91–93]. Accordingly, high variations of the bacterial load among different trials will affect the classification potential of the constructed models. To minimize these variations, thus minimizing the error rate, CDA was applied for each production line to identify the classification potential of poultry fillets according to their microbial load.

Table 4.6: The error rates for the conventional and the alternative production lines, and the number of PCs used to build each CDA model. The classification of poultry fillets was according to their storage time.

Production line	Number of PCs	Error rate (%)	
		Cross-validation (training set)	Independent validation data (testing set)
Conventional	10	22.22	42.06
Alternative	14	15.87	62.99

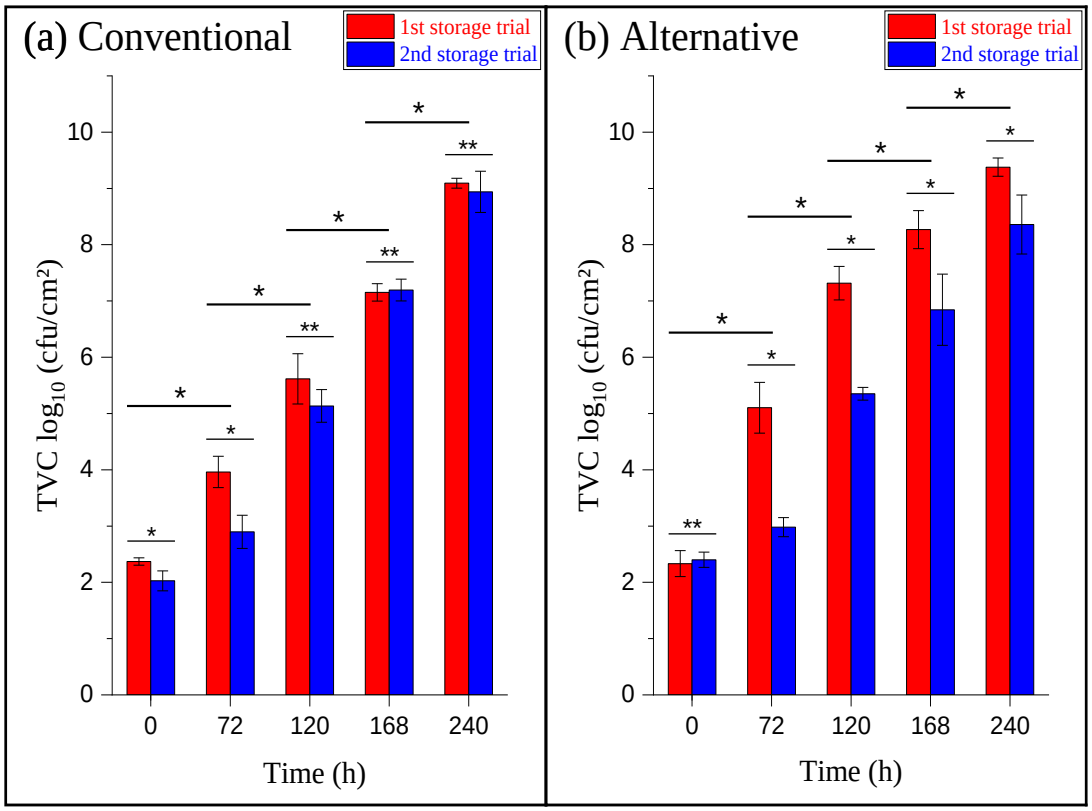

Figure 4.10: Average of TVC per investigation time of the fillets samples from (a) the conventional and (b) the alternative production lines. Red and blue bars represent the 1st and the 2nd storage trials, respectively. The error bars indicate standard deviations within each investigation time. * represent P value < 0.05, and ** represent P value > 0.05. P values were obtained by the *t* test (two-sample assuming unequal variances).

4.3.2.2.2 Microbial load

The bacterial load variations were minimized by grouping the data according to their TVC (see Figure 4.11). The data were grouped into 3 quality classes: Fresh (TVC < 4.8), Semi-fresh (4.8 ≤ TVC < 7.5) and Spoiled (7.5 ≤ TVC). The chicken fillet considered spoiled for both production lines when TVC reached a level of 7.5 $\log_{10}$ cfu/cm^2 [224].

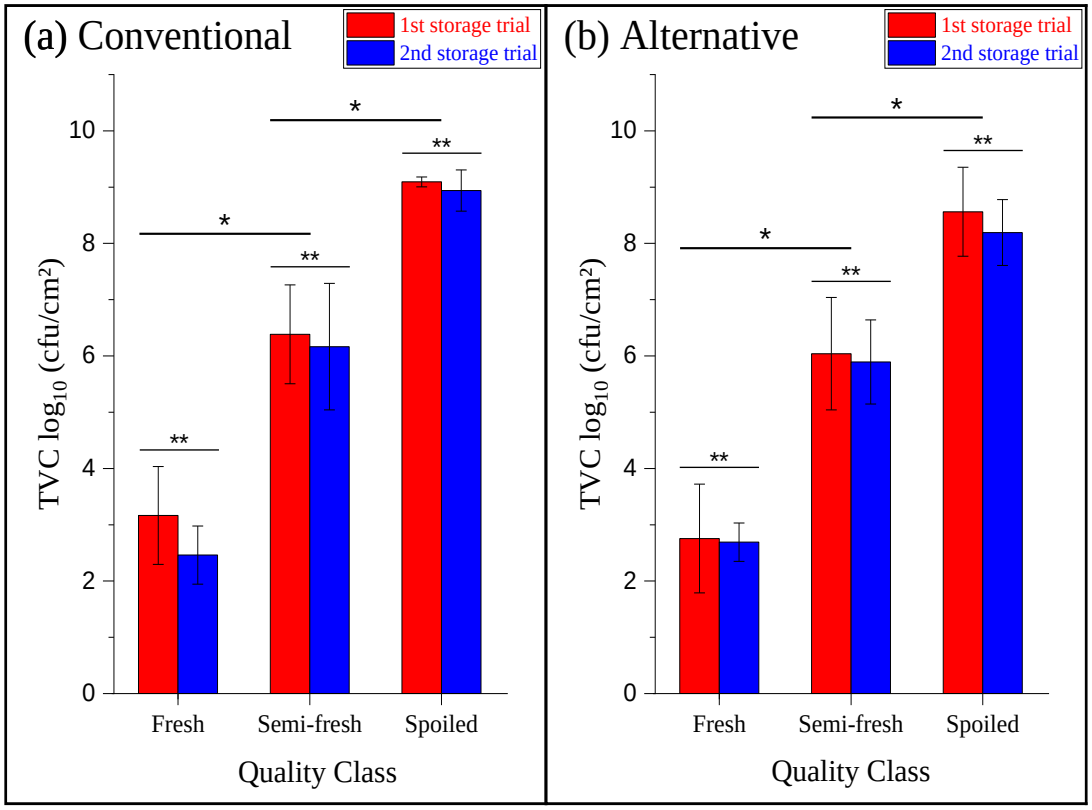

Figure 4.11: Average of TVC per quality class of the fillets samples from (a) the conventional and (b) the alternative production lines. Red and blue bars represent the 1st and the 2nd storage trials, respectively. The error bars indicate standard deviations within each quality class. * represent P value < 0.05, and ** represent P value > 0.05. P values were obtained by the *t* test (two-sample assuming unequal variances).

For both production lines, the calculations were carried out in the same way as in subsection 4.3.2.2.1 Storage time, where CDA was performed based on the first few PCs generated from PCA of the training set. The number of PCs that give the minimum error rate was selected for model construction. After that, the performance of the constructed CDA model was checked using the testing set.

For the conventional production line, the first 9 PCs give the minimum error rate (23.93%), where 28 samples were not correctly classified (see in the Appendix Figure 6.6 and Table 6.15). The results of the CDA model using the two CVs are depicted in the score

diagram (see Figure 4.12), with CV1 and CV2, describing 93.55% and 6.45% of variance, respectively. The score diagram revealed that the group means are clearly separated. The classification error rate of the constructed CDA model using the testing set was 24.60%, where 31 samples were not correctly classified (see Figure 4.13, and in the Appendix Table 6.16).

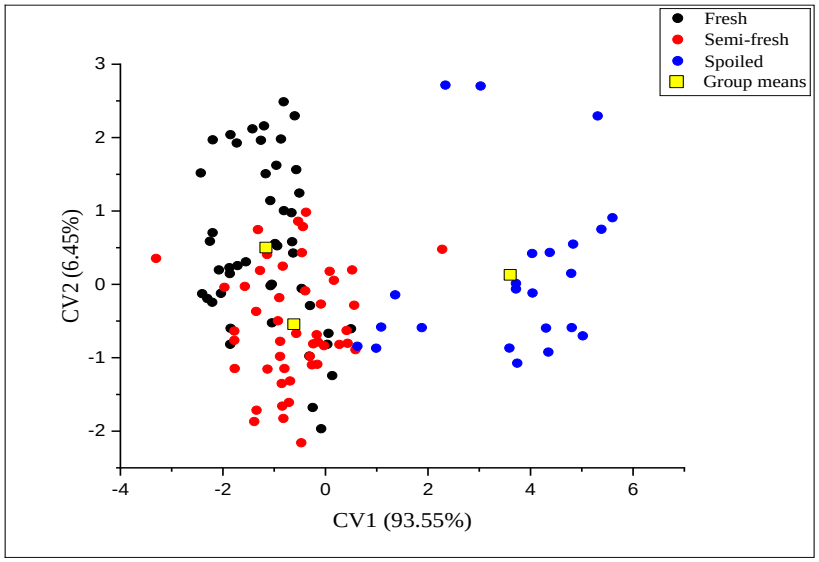

Figure 4.12: Score diagram based on the two CVs of the first 9 PCs derived from the pre-processed Raman spectra of the training data set (1st storage trial) for the three quality classes of the conventional production line.

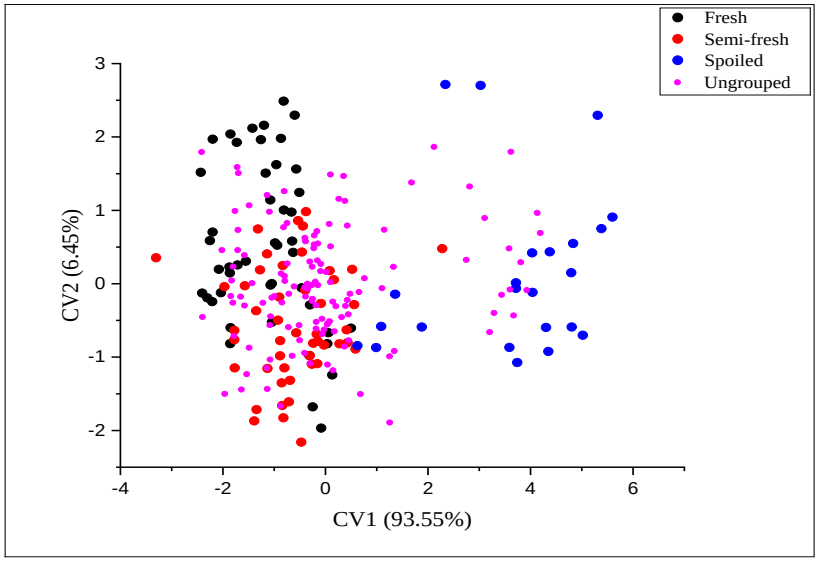

Figure 4.13: Score diagram based on the two CVs of the first 9 PCs derived from the pre-processed Raman spectra of the training data set (1st storage trial) including the testing set (2nd storage trial) for the three quality classes of the conventional production line.

For the alternative production line, the first 10 PCs give the minimum error rate (14.29%), where 18 samples were not correctly classified (see in the Appendix Figure 6.7 and Table 6.17). The results of the CDA model using the two CVs are depicted in the score diagram (see Figure 4.14), with CV1 and CV2, describing 73.70% and 26.30% of variance, respectively. The score diagram revealed that the group means are clearly separated. The classification error rate of the constructed CDA model using the testing set was 54.33%, where 69 samples were not correctly classified (see Figure 4.15, and in the Appendix Table 6.18).

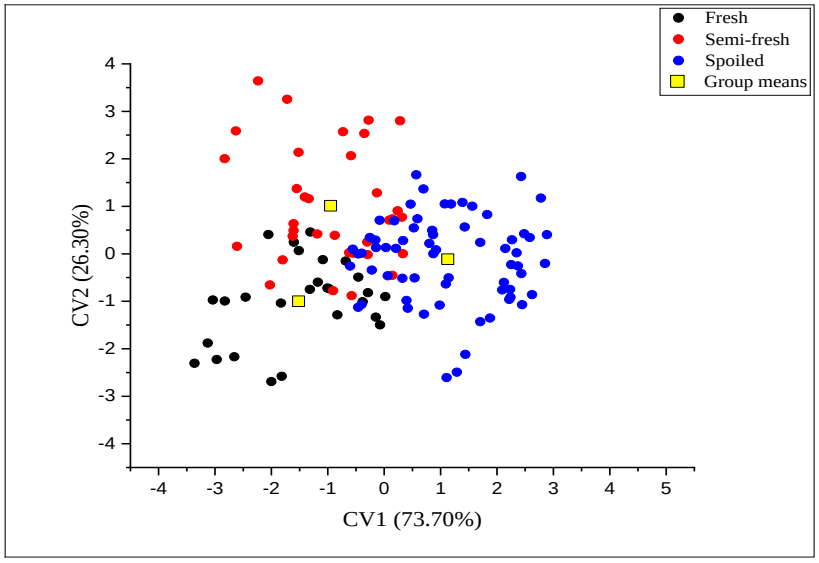

Figure 4.14: Score diagram based on the two CVs of the first 10 PCs derived from the pre-processed Raman spectra of the training data set (1st storage trial) for the three quality classes of the alternative production line.

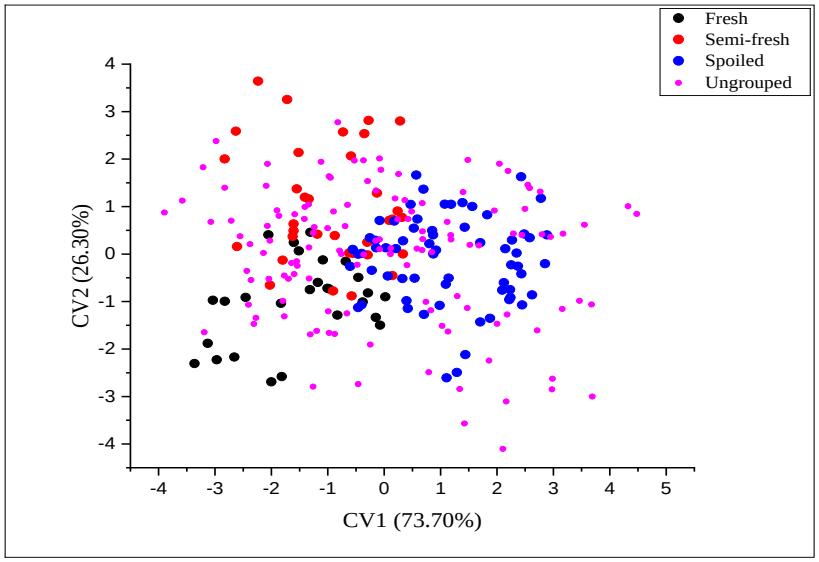

Figure 4.15: Score diagram based on the two CVs of the first 10 PCs derived from the pre-processed Raman spectra of the training data set (1st storage trial) including the testing set (2nd storage trial) for the three quality classes of the alternative production line.

The results for both production lines are summarized in Table 4.7. For both production lines, the CDA models showed a good ability to classify poultry fillets according to their microbial load by the cross-validation method (error rate: 23.93% and 14.29% for conventional and alternative, respectively). These results are very close to the results obtained when the classification was based on the storage time (error rate: 22.22% and 15.87% for conventional and alternative, respectively). When the CDA models tested with testing sets, only conventional production line showed a good ability to classify poultry fillets (error rate: 24.60%). However; error rates for both production lines were smaller than the one obtained when the classification was based on the storage time as can be seen in Table 4.8.

The high error rate for alternative production line (54.33%) reflects that the microbial load is not the only factor that has an impact on the collected Raman spectra from the two storage trials. Since fillets of the alternative line had significantly higher protein and lower water and intramuscular fat content in comparison to the conventional production line (different production systems can have a significant influence on biochemical composition, nutritional value, and physicochemical characteristics of poultry meat) [224], and taking into account that the lipid oxidation and autolytic enzymatic spoilage are also considered one of the main mechanisms for meat spoilage after slaughtering and during processing and storage [93]; high variations from different storage trials will appear in the collected Raman spectra which will affect the classification ability. To take these factors into consideration, thus minimizing the error rate, a trial repetition with a higher sample size is desired.

Table 4.7: The error rates for the conventional and the alternative production lines, and the number of PCs used to build each CDA model. The classification of poultry fillets was according to their microbial load.

Production line	Number of PCs	Error rate (%)	
		Cross-validation (training set)	Independent validation data (testing set)
Conventional	9	23.93	24.60
Alternative	10	14.29	54.33

Table 4.8: Error rates for testing data for the conventional and the alternative production lines. The classification of poultry fillets was according to their storage time and their microbial load.

Predicted Group	Error rate (%); Testing data	
	Production line	
	Conventional	Alternative
Storage time	42.06	62.99
Microbial load	24.60	54.33

4.4 Conclusion

The characterization and discrimination of fillets samples from different poultry meat production systems (conventional and alternative) and different storage trials were successfully accomplished using PCA, CDA and AHCA models. The 1st storage trial (training set: 1st investigation time; 0 h) was used to build the models and the 2nd storage trial (testing set: 1st investigation time; 0 h) was used to validate these models. The results show that the poultry samples can be grouped into two classes: conventional and alternative poultry meat production systems. The models were validated using testing data points (2nd storage trial) and all have been successfully assigned to the correct cluster. The origin of the separation in PCA model was investigated by analysing the loading plots. The results show that the alternative production line has higher collagen, protein and carbohydrates content than the conventional production line. These results were consistent with the analysis of nutrients in the alternative and conventional production lines. The alternative production line also shows a higher carotenoids content which may account for the color difference between both production lines, with the alternative production line displaying more yellowish fillets.

Further, CDA models were constructed for each production line to classify poultry fillets according to their storage time (five investigation times) and their microbial load (three quality classes). The 1st storage trial (training set) was used to build the models and the 2nd storage trial (testing set) was used to validate these models. For both production lines, the constructed CDA models showed good ability to classify poultry fillets according to their storage time with error rates less than 25.00%. However, the constructed CDA models showed poor classification ability when tested with 2nd storage trial (error rate: 42.06% and 62.99% for conventional and alternative, respectively). The high error rates could be correlated to the high variations of the bacterial load between the two storage trials for each production line. To minimize these variations, the data were regrouped according to their microbial load to three quality classes (fresh, semi-fresh and spoiled). For the conventional production line, the constructed CDA model showed good ability to classify poultry fillets according to their microbial load. The error rates were 23.93% and 24.60% for training and testing set, respectively. This indicates that the variations between the two storage trials are not high. For the alternative production line, different results were obtained. Even though the constructed CDA model showed a good ability to classify poultry fillets according to their microbial load (error rate: 14.29%), it failed to classify poultry fillets when tested with the 2nd storage trial (error rate: 54.33%). This indicates that the variations between the two storage trials are too high and that the microbial load is not the only factor that has an impact on the collected Raman spectra from the two storage trials. Since fillets of the alternative line had significantly higher protein and lower water and intramuscular fat content in comparison to the conventional production line, and taking into account that the lipid oxidation and autolytic enzymatic spoilage are also considered one of the main mechanisms for meat spoilage; high variations from different storage trials will appear in the collected Raman spectra which will affect the classification ability. To take these factors into consideration, thus minimizing the error rate, and to confirm our findings; a trial repetition with a higher sample size is desired.

In conclusion, the Raman spectra collected by the portable fiber-optic Raman spectrometer in conjunction with chemometric analysis are able to characterize and discriminate samples from different poultry meat production systems. Compared to traditional methods (microbiological and nutrients analysis), Raman spectroscopy has proven to be a faster, non-destructive, noncontact and objective method. Raman spectroscopy could make off-line (or even on-line) applications possible in the poultry industry. However, further investigations with a higher sample size are required to confirm the findings.

4.5 Authors Contribution Statement

This chapter is adapted from the research article "S. Jaafreh, M. Hebel, J. Kreyenschmidt, K. Günther, P. Kaul, Investigation of the Influence of Different Production Systems on the Quality and Shelf Life of Poultry Meat Using a Portable Fiber-Optic Raman Spectrometer, *In preparation*.". For this research article; the following paragraphs specify the individual contributions of each author.

Author 1; S. Jaafreh: Performed the experiments, analysis and interpretation of data, performed PCA, AHCA and CDA calculations, analysed the results which formed from PCA, AHCA and CDA calculations, writing (original draft preparation), writing (review and editing), designed the figures, literature review.

Author 2; M. Hebel: Performed the microbiological analysis, writing (review and editing).

Author 3; Prof. Dr. J. Kreyenschmidt: Conceptualization and designed the experiments, writing (review and editing), supervision.

Author 4; Prof. Dr. K. Günther: Writing (review and editing), supervision.

Author 5; Prof. Dr. P. Kaul: Writing (review and editing), supervision.

5 General Conclusion

The production and consumption of poultry meat which is rich sources of protein, essential amino acids and a wide variety of micronutrients essential for human nutrition and health; has risen dramatically in recent years leading to a significant increase in its commercial value. However, fresh poultry meat ranks among the highly perishable food due to its nutritional composition, which transforms it into a susceptible product for the growth of spoilage microorganisms. Therefore, the production of high quality and safe meat poultry products with a long shelf life is one of the meat industry's major tasks. Currently, the spoilage microorganisms are determined by culture and colony counting methods which are laborious and time-consuming. This is inconvenient in modern food industrial applications. As meat freshness is important to consumers, the meat industry and retailers, a high demand, therefore, remains for the development of effective, rapid, simple, non-destructive and inexpensive sensing technologies for detecting microbial contamination on meat. Several methods such as Raman spectroscopy have been developed to achieve fast and reliable bacterial identification. Raman spectroscopy has several advantages over other methodologies as it is a non-destructive, non-invasive, relatively inexpensive compared to other methods, rapid and being a label-free method. Furthermore, it requires simple up to no sample preparation. Moreover, the presence of microorganisms or DNA in the laboratory environment is not a concern in Raman spectroscopy. Additionally, strains can be identified extremely accurately.

Although much research has employed Raman spectroscopy in identifying clinically relevant bacteria, less has been done with food-related bacteria. Several research groups have investigated various methods for the rapid detection of microbiological spoilage on different kinds of meat. However, research on and investigations into fast methods for precisely predicting bacterial loads in poultry meat are rare even though they are urgently needed for efficient management in the poultry industry.

Therefore, the main objective of this thesis was to investigate the feasibility of Raman spectroscopy in conjunction with chemometric methods for the characterization and analysis of quality and shelf life of poultry meat. Therefore, five research questions were proposed.

The first three research questions were focused on (a) determining the ability of two dispersive Raman spectrometers with different characteristics (microscope and portable fiber-optic systems) to characterize, discriminate and classify important strains of meat spoilage

microorganisms commonly found in poultry meat; (b) investigating the effect of the used Raman systems accuracy on the accurate discriminating and classifying of bacteria down to the strain level; and (c) identifying the Raman spectral features and differences on which the discrimination is made. For that, eight important strains of meat spoilage microorganisms were cultivated and their Raman spectra were collected using two dispersive Raman spectrometers with different characteristics (conventional and microscope). From each bacterial strain, a small amount of the biomass was placed on a disinfected stainless steel slide and was used for the Raman measurements. The measurements were conduct directly from a stainless steel slide without the need for any pretreatments steps. After the pre-processing step for the data collected by each system; chemometric methods were applied to develop discrimination and classification models. The obtained results from both systems were compared. An accurate discrimination and classification of bacteria down to the strain level was successfully accomplished for both systems. The constructed models were certified using validation data sets which were successfully assigned to the correct bacterial genera and even to the right strain. The spectral features and differences among the species on which the discrimination was based were clarified. The results reflect the strong discriminative power and the high performance of the developed models, the suitability of the used pre-processing method and that the low accuracy of the portable fiber-optic Raman system does not adversely affect the discriminative power of the developed models.

The fourth research question aimed at investigation the ability of Raman spectroscopy to monitor the spoilage process of poultry fillets through the evaluation of their freshness quality. For that, commercially packed fresh boneless skinless chicken breast fillets with the same storage life (9 days) were purchased and their storage time-dependent Raman spectra were collected by the portable fiber-optic Raman spectrometer. The measurements started on the day the chicken breast fillets packages were delivered to and purchased from the retailer. The Raman spectra were collected on a daily basis up to day 21. On each day of the experiment, two packages of chicken breast fillets chosen at random were opened and their Raman spectra were measured. The measured fillets samples were disposed later on the same day of measurement. All the spectral measurements were done directly on the fillet surface without any pre-preparation of the fillet such as removal of fat or connective tissues, inoculation with bacteria, washing, or mincing. After the pre-processing step, the complex spectra were analysed using chemometric methods (PCA and AHCA).

The constructed PCA model was successfully able to group the samples into three quality classes according to their freshness: fresh, semi-fresh, and spoiled. These classes were

based on and similar to the information inferred from the product label on the packages of poultry fillets. Similar groupings were also obtained from the AHCA of the first five PCs. From the PCA results, a conclusion can be drawn on the poultry meat spoilage mechanism: The protein content of the meat decreases during spoilage, which was clearly seen from the lowering of the intensities of the amide I and amide III vibrational bands as well as from the growing amount of free amino acids from an increase in the intensity of Tyr and Trp bands. Furthermore, the growing amounts of free amino acids during storage are considered as an indicator of microbial growth. Moreover, the oxidation of amino acid residues was observed from the increase in the intensity of the S-S stretching vibrational band. Additionally, the hydrophobic interaction around the aliphatic residues was observed through a decrease in the intensity of the CH_2 and CH_3 bending vibrational band.

The results obtained from the Raman spectra combined with chemometric analysis provided information about the quality and the remaining shelf life. This finding indicates that this method could be used to classify samples with unknown storage time, which could lead to an evaluation of the total viable count on the surface of poultry fillets. The results also show that the portable fiber-optic Raman spectrometer can be used as a reliable and fast method for real-time freshness evaluation of poultry during storage.

The final research question was focused on determining the ability of Raman spectroscopy to investigate the influence of different production systems on the quality and shelf life of poultry meat. For that, fillets samples from different poultry meat production lines (conventional and alternative) were purchased from a German poultry producer. The birds race were Ross 308 for conventional and Ranger Classic for alternative, and the birds diet were grain-based for conventional and contained more than 50% corn for alternative. All birds were slaughtered and processed the same day and in the same industrial slaughterhouse, and transported under temperature-controlled conditions to the laboratory of the University of Bonn. The samples were aerobically packaged and stored in incubators at 4 °C. The investigations were conducted at five repeated investigation times during storage started at 0 h of the experiment (24 h after slaughter). The 2nd, 3rd, 4th and 5th investigation times started at 72, 120, 168 and 240 h of the experiment, respectively. For each investigation time, a total of 4 conventional and 4 alternative fillets were investigated. Raman measurements were conducted directly on fillets surfaces parallel with microbiological and nutrients analysis. A total of 80 fillets were investigated in two repeated storage trials. After the pre-processing step for the collected Raman spectra, the characterization and discrimination of fillets samples

from different poultry meat production systems were successfully accomplished using chemometric methods (PCA, CDA and AHCA).

PCA model was constructed using the 1st storage trial (1st investigation time; 0 h). The model was able to group the poultry samples according to their production line into two classes: conventional and alternative. The testing data points (2nd storage trial: 1st investigation time; 0 h) were used to validate the model and all have been successfully assigned to the correct cluster. Similar results were also obtained from the CDA and AHCA of the first two PCs. The origin of the separation in PCA model was investigated by analysing the loading plots. The results show that the alternative production line has higher collagen, protein and carbohydrates content than the conventional. These results were consistent with the analysis of nutrients in both production lines. The alternative production line also shows a higher carotenoids content which may account for the color difference between both production lines, with the alternative production line displaying more yellowish fillets.

Further, CDA models were constructed for each production line to classify poultry fillets according to their storage time (five investigation times) and their microbial load (three quality classes). The 1st storage trial (training set) was used to build the models and the 2nd storage trial (testing set) was used to validate these models. For both production lines, the constructed CDA models showed good ability to classify poultry fillets according to their storage time with error rates less than 25.00%. However, the constructed CDA models showed poor classification ability when tested with 2nd storage trial (error rate: 42.06% and 62.99% for conventional and alternative, respectively). The high error rates could be correlated to the high variations of the bacterial load between the two storage trials for each production line. To minimize these variations, the data were regrouped according to their microbial load to three quality classes (fresh, semi-fresh and spoiled). For the conventional production line, the constructed CDA model showed good ability to classify poultry fillets according to their microbial load. The error rates were 23.93% and 24.60% for training and testing set, respectively. This indicates that the variations between the two storage trials are not high. For the alternative production line, different results were obtained. Even though the constructed CDA model showed a good ability to classify poultry fillets according to their microbial load (error rate: 14.29%), it failed to classify poultry fillets when tested with the 2nd storage trial (error rate: 54.33%). This indicates that the variations between the two storage trials are too high and that the microbial load is not the only factor that has an impact on the collected Raman spectra from the two storage trials. Since fillets of the alternative line had significantly higher protein and lower water and intramuscular fat content in comparison

to the conventional production line, and taking into account that the lipid oxidation and autolytic enzymatic spoilage are also considered one of the main mechanisms for meat spoilage; high variations from different storage trials will appear in the collected Raman spectra which will affect the classification ability. To take these factors into consideration, thus minimizing the error rate, and to confirm our findings; a trial repetition with a higher sample size is desired.

The results allow the conclusion that the Raman spectra collected by the portable fiber-optic Raman spectrometer in conjunction with chemometric analysis can be used as a reliable and fast method to characterize and discriminate samples from different poultry meat production systems.

The overall results of this thesis revealed that the Raman spectroscopy in conjunction with chemometric analysis were able to characterize and discriminate samples from different poultry meat production systems and to monitor the spoilage process of poultry fillets at different storage days through the evaluation of poultry fillets freshness quality. Moreover, the results show that the broader bands due to the low-resolution spectrometer and the relatively high fluorescence backgrounds in the portable fiber-optic Raman system do not adversely affect the discriminative power of the developed models. Further, the results also reflect the high performance and suitability of the pre-processing method used in this work. Compared to traditional methods (microbiological and nutrients analysis), Raman spectroscopy has proven to be a faster, non-destructive, noncontact and objective method. Raman spectroscopy could make off-line (or even on-line) applications possible in the poultry industry. However, to make sure that the developed models are effective, to confirm the findings and to investigate scenarios in which the models may fail the discrimination; higher sample size of microorganism (different strains of the same species, phylogenetically similar bacteria) and poultry (same and different production lines) have to be tested by the models.

6 Appendix

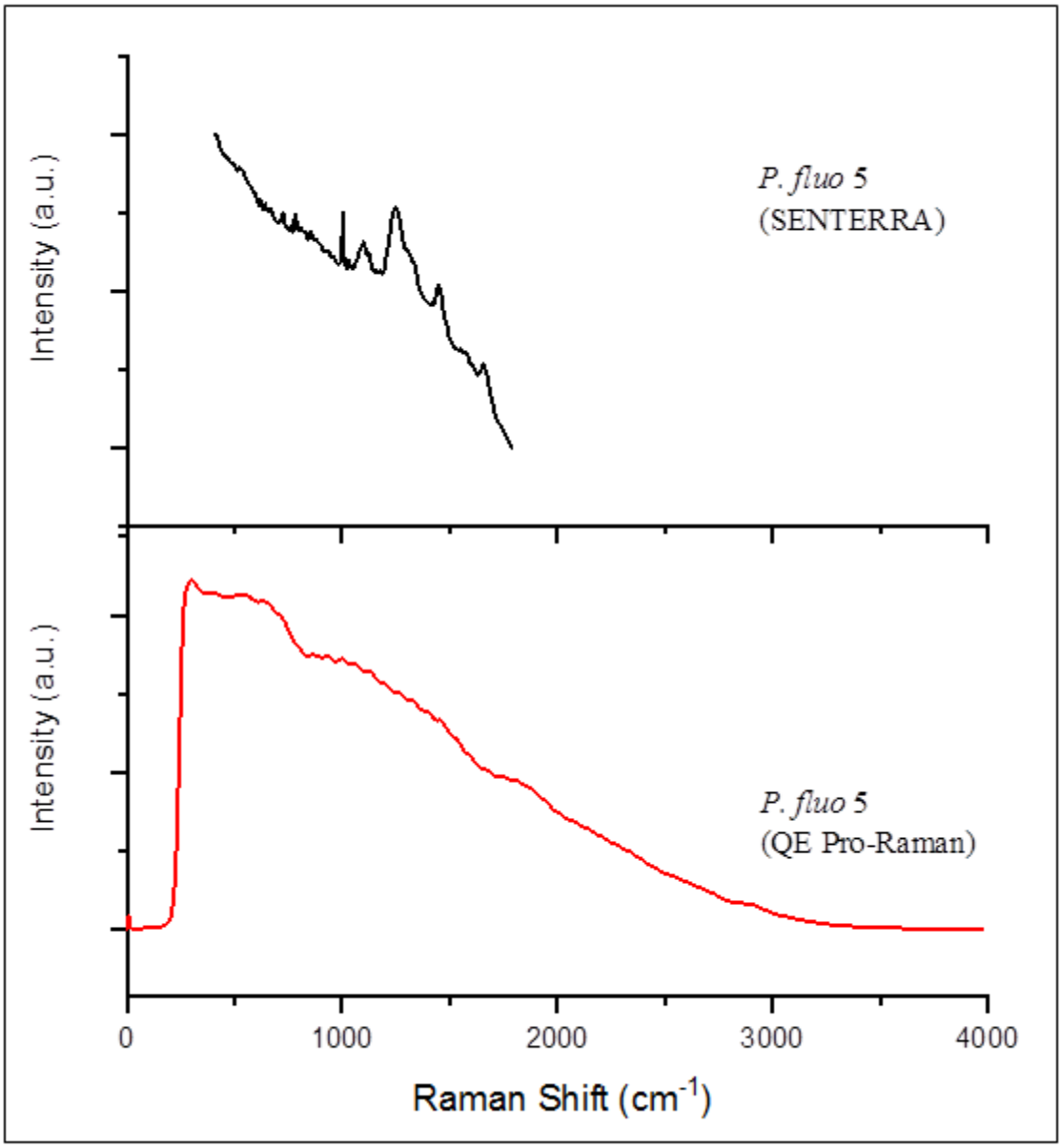

Figure 6.1: Mean of raw Raman spectra for *Pseudomonas fluorescens* DSM 50090 (*P. fluo* 5) collected by the Microscope system (SENTERRA) and the Portable Fiber-Optic system (QE Pro-Raman).

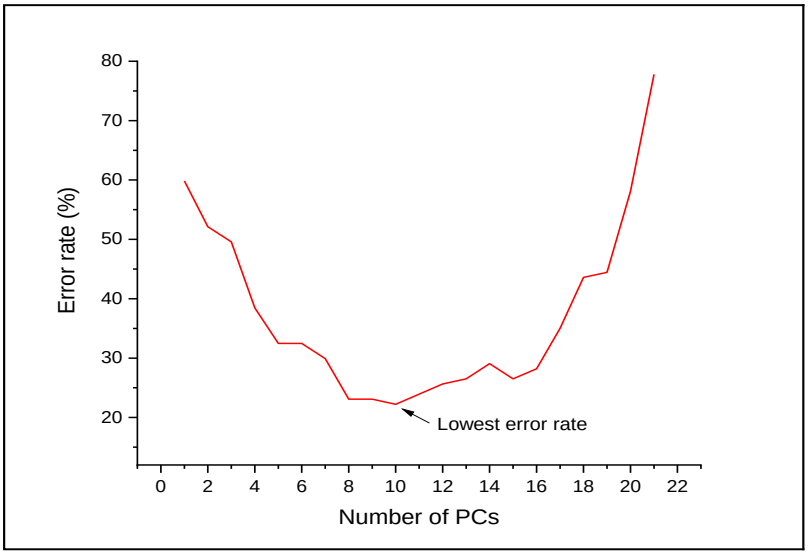

Figure 6.2: The CDA cross-validation error rate over the number of PCs for the conventional production lines (training set: 1st storage trial; five investigation times).

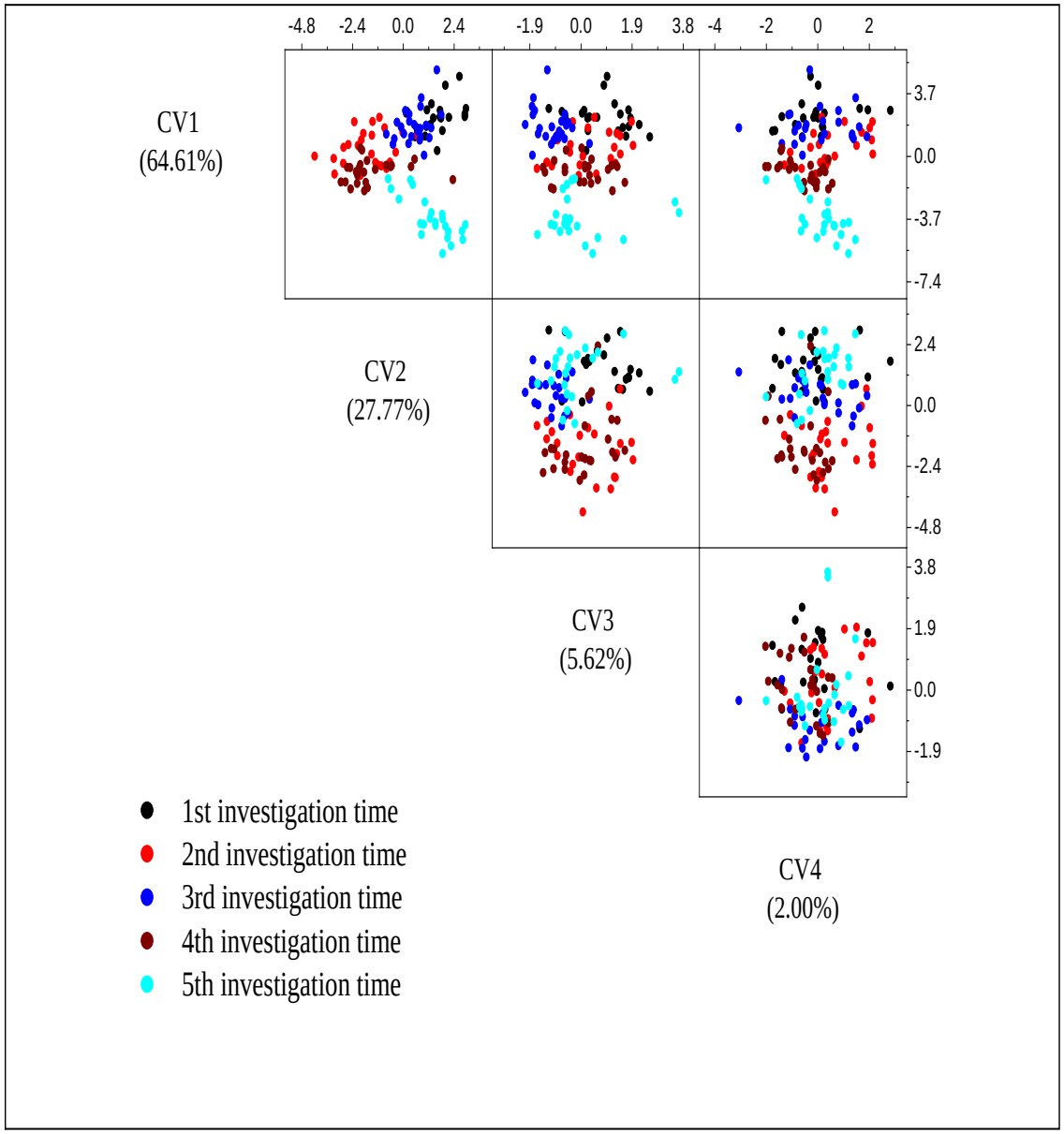

Figure 6.3: Scatter matrix plot of the score diagrams for the four CVs of the first 10 PCs derived from the pre-processed Raman spectra of the training data set (1st storage trial) for the five investigation times of the conventional production line.

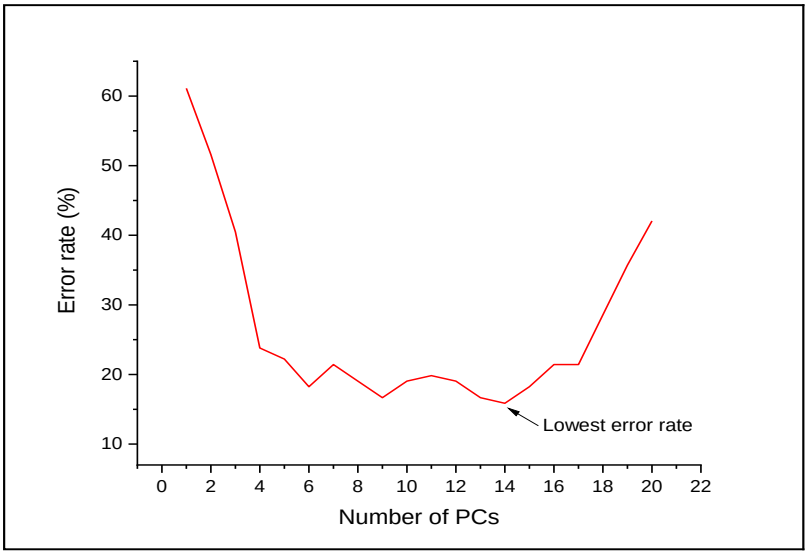

Figure 6.4: The CDA cross-validation error rate over the number of PCs for the alternative production lines (training set: 1st storage trial; five investigation times).

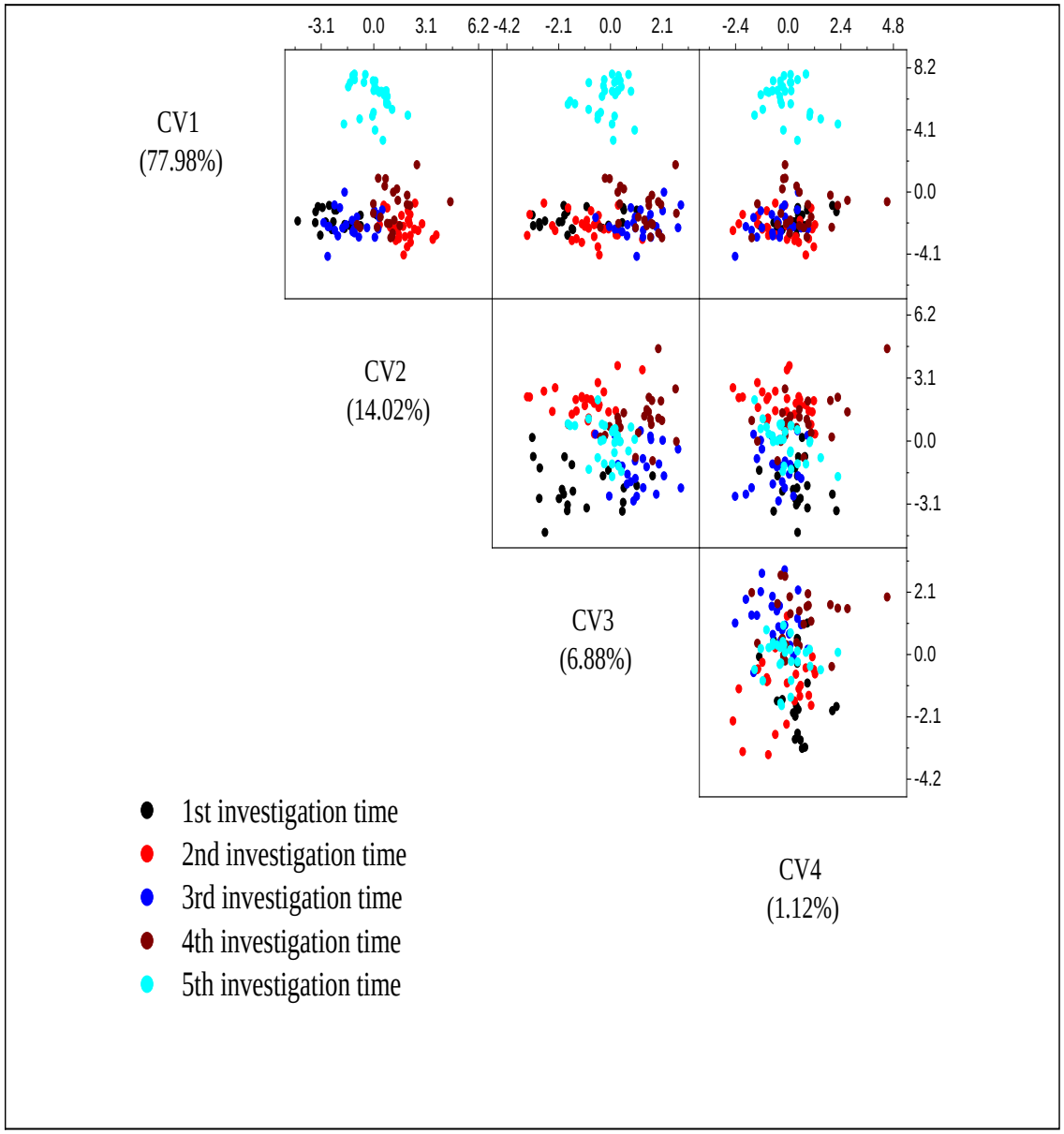

Figure 6.5: Scatter matrix plot of the score diagrams for the four CVs of the first 14 PCs derived from the pre-processed Raman spectra of the training data set (1st storage trial) for the five investigation times of the alternative production line.

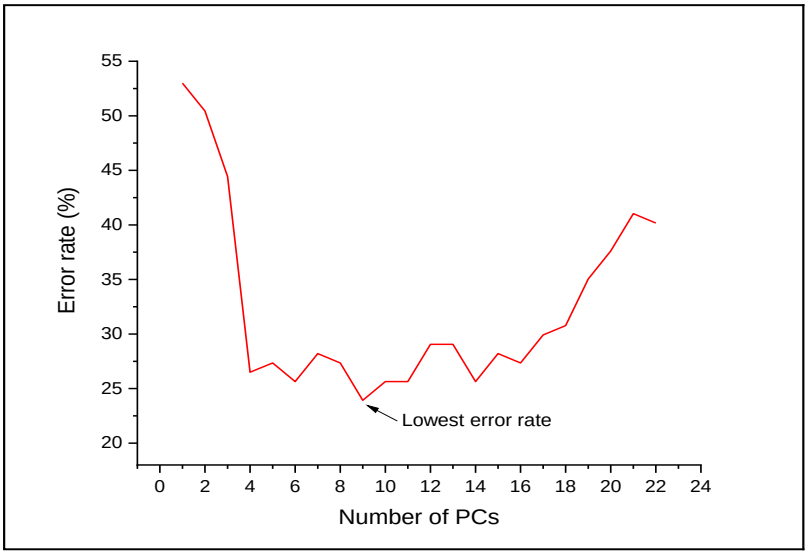

Figure 6.6: The CDA cross-validation error rate over the number of PCs for the conventional production lines (training set: 1st storage trial; three quality classes).

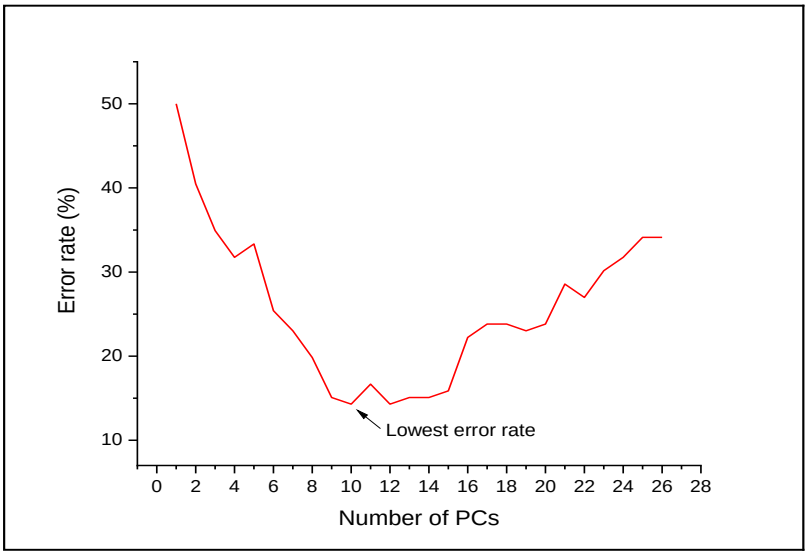

Figure 6.7: The CDA cross-validation error rate over the number of PCs for the alternative production lines (training set: 1st storage trial; three quality classes).

Table 6.1: Raman bands (cm^{-1}) observed in spectra of bacterial cells collected by the Microscope system and tentative assignment.

Frequency	Assignment	References
410-482	Carbohydrates	[119, 167, 168]
497	S–S vibration (Cysteine)	[258, 259]
521-542	S–S stretching (Cysteine), C–O–C glycosidic ring deformation	[119, 161, 167, 168, 248, 258, 260]
578	C–O–C glycosidic ring deformation, Carbohydrates	[166, 261]
599	Cytochrome c	[120]
620	Phenylalanine	[120, 161, 166]
644	Guanine, Methionine, Tyrosine	[119, 120, 161, 164, 166]
668	Cytosine, Guanine, Thymine	[120, 161, 166, 249]
725	Adenine, Glycoside	[122, 161–164]
743	Adenine, Thymine, Tryptophan	[161, 166, 259, 261]
758	Cytosine, Tryptophan, Uracil	[161, 164, 166, 167]
782	Cytosine, Guanine, Thymine, Uracil, O–P–O^- vibration (DNA), Cytochrome c	[120, 122, 158, 161, 163, 164, 166, 249]
812	C–C stretching, O–P–O stretching (RNA), Tyrosine	[161, 166, 259]
827	C–C stretching, Tyrosine (Proteins), O–P–O stretching (DNA/RNA)	[120, 166–168, 259]
854	C–C stretching, C–O–C skeletal mode of α-anomers (Polysaccharides, Pectin), Tyrosine	[120, 122, 161, 167, 259]
872-912	CH_2 stretching, C–C stretching, C–O–C 1,4-glycosidic link	[167, 168, 212, 248, 259]
935	C–C stretching, α-helix (Protein), C–O–C glycos bond (Carbohydrates)	[161, 166, 212, 249, 259]
947-968	C–C stretching, C–N stretching, Tryptophan, Valine	[163, 258, 259, 262–264]
977	C–C stretching β-sheet (Proteins), =CH bending (Lipids)	[161, 166]
1004	Phenylalanine	[24, 105, 122, 158, 160–162, 263, 264]
1031	C–C and C–O stretching (Carbohydrates), Phenylalanine	[120, 161, 166, 248, 249, 258]
1082	C–C and C–O stretching (Carbohydrates), C–N stretching, O–P–O (DNA)	[161, 164, 212, 248, 259]
1100	Carbohydrates C–C, C–O, –C–OH deformation, C–C stretching, C–O–C glycosidic link, O–P–O (DNA)	[122, 163–166, 248]
1124	=C–C= (Lipids), C–N stretching, C–C stretching, Carbohydrates, Cytochrome c	[119, 120, 122, 165–167]
1157	C–C stretching, C–N stretching, Carotene, Carotenoids	[22, 120, 160, 161, 167–169]
1175	Cytosine, Guanine, Thymine, Tyrosine, Cytochrome c	[120, 161, 166, 259]
1190	Carotene, Carotenoids	[40, 169, 212]
1250	Amide III	[122, 161–163, 262]
1337	CH deformation, Amide III, Adenine, Guanine, Tryptophan	[122, 161, 163, 164]
1388	COO^- stretching, CH_3 bending, Cytochrome c	[120, 166, 167, 265, 266]
1448	CH deformation (Lipid, Protein), CH_2 deformation, CH_2CH_3 deformation	[122, 161–164, 249]
1484	CH deformation, Adenine, Guanine, Nucleic acids	[120, 161, 258, 259]
1529	C=C stretching, Carotene, Carotenoids	[22, 24, 120, 167, 169]
1553	COO^- asymmetric (Carbohydrates), C=C stretching, Tryptophan	[161, 166–168, 212, 259]
1577	Adenine, Guanine, Exopolysaccharide-associated bands	[161, 166–168, 249]
1607	COO^- asymmetric (Carbohydrates), Phenylalanine, Tyrosine	[161, 166–168, 249]
1661	C=C stretching, C=O stretching, Amide I	[105, 122, 160, 161, 248]

Table 6.2: Raman bands (cm^{-1}) observed in spectra of bacterial cells collected by the Portable Fiber-Optic system and tentative assignment.

Frequency	Assignment	References
519-540	S–S stretching (Cysteine), C–O–C glycosidic ring deformation	[119, 161, 167, 168, 248, 258, 260]
544-578	C–O–C glycosidic ring deformation	[21, 164]
603	Cytochrome c	[120]
624	Phenylalanine	[120, 161, 166]
641-674	C–S stretching mode of Cystine, Guanine, Methionine, Thymine, Tyrosine	[119, 164, 166, 249]
700-742	Adenine, Glycoside	[122, 162–164]
780-797	Cytosine, Guanine, Thymine, Uracil, O–P–O (DNA), Cytochrome c	[120, 122, 163, 164, 166, 249]
797-822	C–C stretching, Tyrosine, Uracil, O–P–O stretching (DNA, RNA)	[161, 164–166, 259, 267]
830	C–C stretching, Ring breath Tyrosine (Proteins), O–P–O stretching (DNA/RNA)	[120, 166–168, 259]
847-919	C–C stretching (Carbohydrates), C–O–C 1,4-glycosidic link (Carbohydrates)	[167, 168, 212, 248, 259]
927-948	C–C stretching, α-helix (Protein), C–O–C glycos bond (Carbohydrates)	[161, 166, 212, 249, 259]
1003	Phenylalanine	[24, 105, 122, 158, 160–162, 263, 264]
1036	C–C and C–O stretching (Carbohydrates), Phenylalanine	[120, 161, 166, 248, 249, 258]
1049-1112	C–C stretching (Lipids, Carbohydrates), C–N stretching, C–O stretching (Carbohydrates), O–P–O^- stretching (DNA/RNA)	[119, 161, 164, 212, 248, 259]
1125-1129	C–C stretching (Carbohydrates, Proteins, Lipids), C–N stretching (Proteins), C–O stretching (Carbohydrates), C–O–C glycosidic link (Carbohydrates), Cytochrome c	[120, 158, 161, 167, 168, 212, 259, 260]
1159	C–C stretching, C–N stretching, Carotene, Carotenoids	[22, 120, 160, 161, 167–169]
1196-1209	Amide III, Hydroxyproline, Phenylalanine, Tryptophan, Tyrosine	[119, 161, 166, 167, 212, 259]
1255-1268	Amide III	[161–164, 167, 259]
1331	CH deformation, Amide III, Adenine, Guanine	[120, 164, 167, 248]
1390-1411	COO^- symmetric stretching (Carbohydrates)	[164, 167, 168]
1453-1462	CH_2 deformation (Carbohydrates, Proteins, Lipids)	[158, 164, 167, 260, 262, 267]
1529	C=C stretching, Carotene, Carotenoids	[22, 24, 120, 167, 169]
1538	NH deformation, CH deformation, C=C stretching	[119, 259]
1554	COO^- asymmetric (Carbohydrates), C=C stretching, Tryptophan	[161, 166–168, 212, 259]
1580-1592	COO^- asymmetric (Carbohydrates), Adenine, Guanine	[162, 164, 167, 168]
1605-1618	COO^- asymmetric (Carbohydrates), Phenylalanine, Tyrosine, Tryptophan	[165, 167, 168, 212]
1664	C=C stretching, C=O stretching, Amide I	[105, 122, 160, 161, 248]
1706	C=O stretching	[161, 259]
1744	C=O stretching (Carbohydrates, Lipids)	[161, 167, 168, 212, 259]

Table 6.3: Analysis of stage 2 loading plots for Microscope and Portable Fiber-Optic systems. The spectral differences among the bacterial genera were based on the Raman bands with the highest variance values. The values of Raman shift (RS) were sorted in ascending order.

Microscope		**Portable Fiber-Optic**	
PC1, PC2 and PC3; Figure 2.5(b)		**PC1 and PC3; Figure 2.6(b)**	
RS (cm^{-1})	**Observations**	**RS (cm^{-1})**	**Observations**
476	*Pseudomonas* has lowest intensity value, and it is appears slightly shifted in *Escherichia* when compared to *Bacillus* and *Pseudomonas*	. . . . .	. . . . .
. . . . .	. . . . .	531	*Escherichia* has the lowest intensity value
. . . . .	. . . . .	721	*Escherichia* has the lowest intensity value
. . . . .	. . . . .	784	*Escherichia* has highest intensity value and a slight shift in position in comparing to *Bacillus* and *Pseudomonas*
935	*Pseudomonas* has lowest intensity value	935	*Bacillus* has highest intensity value
1004	*Bacillus* has highest intensity value	1003	*Escherichia* has the highest intensity value
1031	*Bacillus* has highest intensity value	1036	Present only in *Escherichia*
1100	*Bacillus* has highest intensity value	1100	*Escherichia* has the highest intensity value and a slight shift in position in comparing to *Bacillus* and *Pseudomonas*
1124	*Bacillus* has highest intensity value	1125	*Escherichia* has the highest intensity value
. . . . .	. . . . .	1209	*Escherichia* has the lowest intensity value and a slight shift in position compared to *Bacillus* and *Pseudomonas*
. . . . .	. . . . .	1255	*Escherichia* has the highest intensity value and a slight shift in position compared to *Bacillus* and *Pseudomonas*
1448	*Bacillus* has highest intensity value	1453	*Escherichia* has the highest intensity value
1484	Absent in *Bacillus*	. . . . .	. . . . .
. . . . .	. . . . .	1538	*Escherichia* has the lowest intensity value and peak splitting compared to *Bacillus* and *Pseudomonas*
1661	*Pseudomonas* has highest intensity value	1664	*Escherichia* has the highest intensity value

Table 6.4: Analysis of stage 3-A loading plots for Microscope and Portable Fiber-Optic systems. The spectral differences among the bacterial subspecies were based on the Raman bands with the highest variance values. The values of Raman shift (RS) were sorted in ascending order.

Microscope		**Portable Fiber-Optic**	
PC1 and PC2; Figure 2.5(c)		**PC1 and PC2; Figure 2.6(c)**	
RS (cm^{-1})	**Observations**	**RS (cm^{-1})**	**Observations**
425	*B. coag* has higher intensity value	. . . . .	. . . . .
. . . . .	. . . . .	557	*B. coag* has higher intensity value
668	*B. coag* has higher intensity value	. . . . .	. . . . .
725	*B. coag* has higher intensity value	717	*B. coag* has higher intensity value
743	*B. subt* has higher intensity value	. . . . .	. . . . .
782	*B. coag* has higher intensity value	. . . . .	. . . . .
854	*B. subt* has higher intensity value	. . . . .	. . . . .
1004	*B. subt* has higher intensity value	1003	*B. subt* has higher intensity value
. . . . .	. . . . .	1062	*B. subt* has higher intensity value
1124	*B. subt* has higher intensity value	1129	*B. subt* has higher intensity value
. . . . .	. . . . .	1264	*B. subt* has higher intensity value
. . . . .	. . . . .	1331	*B. subt* has higher intensity value
. . . . .	. . . . .	1399	*B. subt* has higher intensity value
1448	*B. subt* has higher intensity value	1462	*B. subt* has higher intensity value
1577	*B. coag* has higher intensity value	. . . . .	. . . . .
. . . . .	. . . . .	1664	*B. subt* has higher intensity value

Table 6.5: Analysis of stage 3-B loading plots for Microscope and Portable Fiber-Optic systems. The spectral differences among the bacterial strains were based on the Raman bands with the highest variance values. The values of Raman shift (RS) were sorted in ascending order.

Microscope		**Portable Fiber-Optic**	
PC1 and PC2; Figure 2.5(d)		**PC1 and PC2; Figure 2.6(d)**	
RS (cm^{-1})	**Observations**	**RS (cm^{-1})**	**Observations**
455	Absent in *E. coli* K12	.....	.....
482	*E. coli* K12 has higher intensity value	.....	.....
.....	.....	519-540	*E. coli* HB101 has higher intensity value
.....	.....	573	*E. coli* K12 has the lowest intensity value and a slight shift in position compared to *E. coli* HB101
.....	.....	624	Present only in *E. coli* K12
644	*E. coli* HB101 has higher intensity value	.....	.....
668	*E. coli* HB101 has higher intensity value	.....	.....
.....	.....	725	*E. coli* HB101 has higher intensity value
782	*E. coli* K12 has higher intensity value	.....	.....
812	*E. coli* K12 has higher intensity value	813	*E. coli* HB101 has higher intensity value
827	*E. coli* HB101 has higher intensity value	830	*E. coli* HB101 has higher intensity value
854	*E. coli* K12 has higher intensity value	860	*E. coli* HB101 has higher intensity value
881	*E. coli* HB101 has higher intensity value	.....	.....
935	*E. coli* K12 has higher intensity value	.....	.....
1004	*E. coli* HB101 has higher intensity value	1003	*E. coli* HB101 has higher intensity value
.....	.....	1036	*E. coli* K12 has higher intensity value
1082	*E. coli* K12 has higher intensity value	1049-1112	*E. coli* K12 has higher intensity value
1124	*E. coli* K12 has higher intensity value	.....	.....
.....	.....	1209	*E. coli* K12 has higher intensity value
.....	.....	1255	*E. coli* K12 has higher intensity value
.....	.....	1331	*E. coli* K12 has higher intensity value
1448	*E. coli* HB101 has higher intensity value	1453	*E. coli* HB101 has higher intensity value
.....	.....	1613	*E. coli* HB101 has higher intensity value
.....	.....	1664	*E. coli* HB101 has higher intensity value
.....	.....	1744	*E. coli* HB101 has higher intensity value

Table 6.6: Analysis of stage 3-C loading plots for Microscope and Portable Fiber-Optic systems. The spectral differences among the bacterial strains were based on the Raman bands with the highest variance values. The values of Raman shift (RS) were sorted in ascending order.

Microscope		**Portable Fiber-Optic**	
PC1 and PC3; Figure 2.5(e)		**PC1 and PC2; Figure 2.6(e)**	
RS (cm^{-1})	**Observations**	**RS (cm^{-1})**	**Observations**
413-437	*P. fluo* 5 has higher intensity value	. . . . .	. . . . .
440-482	Broader and less intense for *P. fluo* 5	. . . . .	. . . . .
497	*P. fluo* 5 has higher intensity value	. . . . .	. . . . .
. . . . .	. . . . .	519-540	*P. fluo* 5 has higher intensity value
. . . . .	. . . . .	544-578	*P. fluo* 5 has higher intensity value
. . . . .	. . . . .	603	Absent in *P. fluo* 5
. . . . .	. . . . .	641-674	*P. fluo* 5 has higher intensity value
782	*P. fluo* 4 has higher intensity value	788	*P. fluo* 4 has higher intensity value and a slight shift in position compared to *P. fluo* 5
854	*P. fluo* 4 has higher intensity value	864	*P. fluo* 5 has higher intensity value
935	*P. fluo* 5 has higher intensity value	. . . . .	. . . . .
959	*P. fluo* 5 has higher intensity value	. . . . .	. . . . .
977	Absent in *P. fluo* 5	. . . . .	. . . . .
1004	*P. fluo* 5 has higher intensity value	1003	*P. fluo* 4 has higher intensity value
1124	*P. fluo* 5 has higher intensity value	. . . . .	. . . . .
. . . . .	. . . . .	1196	*P. fluo* 5 has higher intensity value
. . . . .	. . . . .	1331	*P. fluo* 4 has higher intensity value
. . . . .	. . . . .	1399	*P. fluo* 5 has higher intensity value
. . . . .	. . . . .	1462	*P. fluo* 4 has higher intensity value
1661	*P. fluo* 5 has higher intensity value	1664	*P. fluo* 4 has higher intensity value

Table 6.7: Classification results of the bacterial strains collected by the Microscope system via MC-SVM using 2 PCs. Numbers between brackets represent 75% of the spectra collected for each bacterial strain.

Classification Confusion Matrix, 2 PCs

True	Classif.								
	M. lute	***B. ther***	***B. coag***	***B. subt***	***E. coli* K12**	***E. coli* HB101**	***P. fluo* 4**	***P. fluo* 5**	
***M. lute* (87)**	87	0	0	0	0	0	0	0	
***B. ther* (86)**	0	86	0	0	0	0	0	0	
***B. coag* (74)**	0	0	59	15	0	0	0	0	
***B. subt* (66)**	0	0	22	44	0	0	0	0	
***E. coli* K12 (87)**	0	0	0	0	87	0	0	0	
***E. coli* HB101 (87)**	0	0	0	0	0	75	8	4	
***P. fluo* 4 (84)**	0	0	0	0	1	4	77	2	
***P. fluo* 5 (84)**	0	0	0	0	0	11	3	70	
Sens. [%]	100.00	100.00	79.73	66.67	100.00	86.21	91.67	83.33	Average 88.45
Spec. [%]	100.00	100.00	96.21	97.45	99.82	97.36	98.07	98.95	Average 98.48
Acc. [%]	100.00	100.00	94.35	94.35	99.85	95.88	97.25	96.95	Average 97.33

Table 6.8: Validation results of the bacterial strains collected by the Microscope system via MC-SVM using 2 PCs. Numbers between brackets represent 25% of the spectra collected for each bacterial strain.

Validation Confusion Matrix, 2 PCs

True	Identif.								
	M. lute	***B. ther***	***B. coag***	***B. subt***	***E. coli* K12**	***E. coli* HB101**	***P. fluo* 4**	***P. fluo* 5**	
***M. lute* (28)**	28	0	0	0	0	0	0	0	
***B. ther* (28)**	0	28	0	0	0	0	0	0	
***B. coag* (24)**	0	0	20	4	0	0	0	0	
***B. subt* (21)**	0	0	6	15	0	0	0	0	
***E. coli* K12 (28)**	0	0	0	0	28	0	0	0	
***E. coli* HB101 (28)**	0	0	0	0	0	26	2	0	
***P. fluo* 4 (28)**	0	0	0	0	0	3	25	0	
***P. fluo* 5 (27)**	0	0	0	0	0	5	0	22	
Sens. [%]	100.00	100.00	83.33	71.43	100.00	92.86	89.29	81.48	Average 89.80
Spec. [%]	100.00	100.00	96.81	97.91	100.00	95.65	98.91	100.00	Average 98.66
Acc. [%]	100.00	100.00	95.28	95.28	100.00	95.28	97.64	97.64	Average 97.64

Table 6.9: Classification results of the bacterial strains collected by the Portable Fiber-Optic system via MC-SVM using 2 PCs. Numbers between brackets represent 75% of the spectra collected for each bacterial strain.

Classification Confusion Matrix, 2 PCs

True	Classif. *M. lute*	*B. ther*	*B. coag*	*B. subt*	*E. coli* K12	*E. coli* HB101	*P. fluo* 4	*P. fluo* 5		
***M. lute* (19)**	19	0	0	0	0	0	0	0		
***B. ther* (19)**	0	14	0	0	2	3	0	0		
***B. coag* (19)**	0	0	16	1	0	0	0	2		
***B. subt* (18)**	0	0	1	13	0	0	1	3		
***E. coli* K12 (19)**	0	0	0	0	18	1	0	0		
***E. coli* HB101 (18)**	0	0	0	0	0	18	0	0		
***P. fluo* 4 (16)**	0	0	0	1	0	0	15	0		
***P. fluo* 5 (19)**	0	0	2	5	0	0	0	12		
Sens. [%]	100.00	73.68	84.21	72.22	94.74	100.00	93.75	63.16	Average	85.22
Spec. [%]	100.00	100.00	97.66	94.57	98.44	96.90	99.24	96.09		97.86
Acc. [%]	100.00	96.60	95.92	91.84	97.96	97.28	98.64	91.84		96.26

Table 6.10: Validation results of the bacterial strains collected by the Portable Fiber-Optic system via MC-SVM using 2 PCs. Numbers between brackets represent 25% of the spectra collected for each bacterial strain.

Validation Confusion Matrix, 2 PCs

True	Identif. *M. lute*	*B. ther*	*B. coag*	*B. subt*	*E. coli* K12	*E. coli* HB101	*P. fluo* 4	*P. fluo* 5		
***M. lute* (6)**	6	0	0	0	0	0	0	0		
***B. ther* (6)**	0	5	0	0	0	1	0	0		
***B. coag* (6)**	0	0	2	3	0	0	0	1		
***B. subt* (6)**	0	0	0	3	0	0	0	3		
***E. coli* K12 (6)**	0	0	0	0	6	0	0	0		
***E. coli* HB101 (6)**	0	0	0	0	0	6	0	0		
***P. fluo* 4 (6)**	0	0	0	2	0	0	4	0		
***P. fluo* 5 (6)**	0	0	1	1	0	0	1	3		
Sens. [%]	100.00	83.33	33.33	50.00	100.00	100.00	66.67	50.00	Average	72.92
Spec. [%]	100.00	100.00	97.62	85.71	100.00	97.62	97.62	90.48		96.13
Acc. [%]	100.00	97.92	89.58	81.25	100.00	97.92	93.75	85.42		93.23

Table 6.11: Cross-validation confusion matrix by CDA for the five investigation times of the conventional production line (training set: 1st storage trial). Rows represent the true class and the columns the assigned class.

Groups: Investigation times and their size	Predicted Groups				
	1st	2nd	3rd	4th	5th
1st; 22	17	2	1	2	0
2nd; 24	2	18	2	2	0
3rd; 24	1	3	19	1	0
4th; 24	1	6	0	17	0
5th; 23	0	0	2	1	20

Table 6.12: Validation confusion matrix by CDA for the five investigation times of the conventional production line (testing set: 2nd storage trial). Rows represent the true class and the columns the assigned class.

Groups: Investigation times and their size	Predicted Groups				
	1st	2nd	3rd	4th	5th
1st; 23	15	4	4	0	0
2nd; 24	1	9	10	4	0
3rd; 27	7	1	14	5	0
4th; 24	0	5	2	15	2
5th; 28	1	1	0	6	20

Table 6.13: Cross-validation confusion matrix by CDA for the five investigation times of the alternative production line (training set: 1st storage trial). Rows represent the true class and the columns the assigned class.

Groups: Investigation times and their size	Predicted Groups				
	1st	**2nd**	**3rd**	**4th**	**5th**
1st; 21	14	1	6	0	0
2nd; 28	2	26	0	0	0
3rd; 24	1	1	19	3	0
4th; 24	2	2	2	18	0
5th; 29	0	0	0	0	29

Table 6.14: Validation confusion matrix by CDA for the five investigation times of the alternative production line (testing set: 2nd storage trial). Rows represent the true class and the columns the assigned class.

Groups: Investigation times and their size	Predicted Groups				
	1st	**2nd**	**3rd**	**4th**	**5th**
1st; 23	5	5	6	7	0
2nd; 24	3	10	9	2	0
3rd; 27	0	8	11	8	0
4th; 25	0	18	1	6	0
5th; 28	1	1	1	10	15

Table 6.15: Cross-validation confusion matrix by CDA for the three quality classes of the conventional production line (training set: 1st storage trial). Rows represent the true class and the columns the assigned class.

Groups: Quality classes and their size	Predicted Groups		
	Fresh	**Semi-fresh**	**Spoiled**
Fresh; 46	32	14	0
Semi-fresh; 48	11	37	0
Spoiled; 23	0	3	20

Table 6.16: Validation confusion matrix by CDA for the three quality classes of the conventional production line (testing set: 2nd storage trial). Rows represent the true class and the columns the assigned class.

Groups: Quality classes and their size	Predicted Groups		
	Fresh	**Semi-fresh**	**Spoiled**
Fresh; 47	38	9	0
Semi-fresh; 51	12	38	1
Spoiled; 28	0	9	19

Table 6.17: Cross-validation confusion matrix by CDA for the three quality classes of the alternative production line (training set: 1st storage trial). Rows represent the true class and the columns the assigned class.

Groups: Quality classes and their size	Predicted Groups		
	Fresh	**Semi-fresh**	**Spoiled**
Fresh; 27	22	3	2
Semi-fresh; 34	1	27	6
Spoiled; 65	3	3	59

Table 6.18: Validation confusion matrix by CDA for the three quality classes of the alternative production line (testing set: 2nd storage trial). Rows represent the true class and the columns the assigned class.

Groups: Quality classes and their size	**Predicted Groups**		
	Fresh	**Semi-fresh**	**Spoiled**
Fresh; 47	11	17	19
Semi-fresh; 46	0	16	30
Spoiled; 34	0	3	31

7 References

[1] J. Weeranantanaphan, G. Downey, P. Allen, D.-W. Sun, A Review of near Infrared Spectroscopy in Muscle Food Analysis: 2005–2010, J. Near Infrared Spectrosc. 19 (2011) 61–104. https://doi.org/10.1255/jnirs.924.

[2] Z. Xiong, D.-W. Sun, H. Pu, W. Gao, Q. Dai, Applications of emerging imaging techniques for meat quality and safety detection and evaluation: A review, Crit. Rev. Food Sci. Nutr. 57 (2017) 755–768. https://doi.org/10.1080/10408398.2014.954282.

[3] Y.-N. Chen, D.-W. Sun, J.-H. Cheng, W.-H. Gao, Recent Advances for Rapid Identification of Chemical Information of Muscle Foods by Hyperspectral Imaging Analysis, Food Eng. Rev. 8 (2016) 336–350. https://doi.org/10.1007/s12393-016-9139-1.

[4] A.A. Argyri, O.S. Papadopoulou, A. Nisiotou, C.C. Tassou, N. Chorianopoulos, Effect of high pressure processing on the survival of Salmonella Enteritidis and shelf-life of chicken fillets, Food Microbiol. 70 (2018) 55–64. https://doi.org/10.1016/j.fm.2017.08.019.

[5] S. Noori, F. Zeynali, H. Almasi, Antimicrobial and antioxidant efficiency of nanoemulsion-based edible coating containing ginger (Zingiber officinale) essential oil and its effect on safety and quality attributes of chicken breast fillets, Food Control. 84 (2018) 312–320. https://doi.org/10.1016/j.foodcont.2017.08.015.

[6] S. Bruckner, A. Albrecht, B. Petersen, J. Kreyenschmidt, Characterization and Comparison of Spoilage Processes in Fresh Pork and Poultry, J. Food Qual. 35 (2012) 372–382. https://doi.org/10.1111/j.1745-4557.2012.00456.x.

[7] F. Leroy, A. Geyzen, M. Janssens, L. De Vuyst, P. Scholliers, Meat fermentation at the crossroads of innovation and tradition: A historical outlook, Trends Food Sci. Technol. 31 (2013) 130–137. https://doi.org/10.1016/j.tifs.2013.03.008.

[8] G.H. Zhou, X.L. Xu, Y. Liu, Preservation technologies for fresh meat – A review, Meat Sci. 86 (2010) 119–128. https://doi.org/10.1016/j.meatsci.2010.04.033.

[9] J. Kreyenschmidt, R. Ibald, Modeling shelf life using microbial indicators, in: Shelf Life Assess. Food, 2012: pp. 127–168. https://doi.org/10.1201/b11871.

[10] D. Klein, S. Maurer, U. Herbert, J. Kreyenschmidt, P. Kaul, Detection of Volatile Organic Compounds Arising from Chicken Breast Filets Under Modified Atmosphere

Packaging Using TD-GC/MS, Food Anal. Methods. 11 (2018) 88–98. https://doi.org/10.1007/s12161-017-0978-z.

[11] S. Umesha, H.M. Manukumar, Advanced molecular diagnostic techniques for detection of food-borne pathogens: Current applications and future challenges, Crit. Rev. Food Sci. Nutr. 58 (2018) 84–104. https://doi.org/10.1080/10408398.2015.1126701.

[12] J.H. Cheng, D.W. Sun, Recent Applications of Spectroscopic and Hyperspectral Imaging Techniques with Chemometric Analysis for Rapid Inspection of Microbial Spoilage in Muscle Foods, Compr. Rev. Food Sci. Food Saf. 14 (2015) 478–490. https://doi.org/10.1111/1541-4337.12141.

[13] D. Klein, R. Breuch, S. von der Mark, C. Wickleder, P. Kaul, Detection of spoilage associated bacteria using Raman-microspectroscopy combined with multivariate statistical analysis, Talanta. 196 (2019) 325–328. https://doi.org/10.1016/j.talanta.2018.12.094.

[14] D.I. Ellis, D. Broadhurst, S.J. Clarke, R. Goodacre, Rapid identification of closely related muscle foods by vibrational spectroscopy and machine learning, Analyst. 130 (2005) 1648. https://doi.org/10.1039/b511484e.

[15] Y.-Z. Feng, G. ElMasry, D.-W. Sun, A.G.M. Scannell, D. Walsh, N. Morcy, Near-infrared hyperspectral imaging and partial least squares regression for rapid and reagentless determination of Enterobacteriaceae on chicken fillets, Food Chem. 138 (2013) 1829–1836. https://doi.org/10.1016/j.foodchem.2012.11.040.

[16] P.-S. Liang, T.S. Park, J.-Y. Yoon, Rapid and reagentless detection of microbial contamination within meat utilizing a smartphone-based biosensor, Sci. Rep. 4 (2014) 5953. https://doi.org/10.1038/srep05953.

[17] M.M. Hlaing, M. Dunn, P.R. Stoddart, S.L. McArthur, Raman spectroscopic identification of single bacterial cells at different stages of their lifecycle, Vib. Spectrosc. 86 (2016) 81–89. https://doi.org/10.1016/j.vibspec.2016.06.008.

[18] A. Colniță, N. Dina, N. Leopold, D. Vodnar, D. Bogdan, S. Porav, L. David, Characterization and Discrimination of Gram-Positive Bacteria Using Raman Spectroscopy with the Aid of Principal Component Analysis, Nanomaterials. 7 (2017) 248. https://doi.org/10.3390/nano7090248.

[19] M. Ghebremedhin, R. Heitkamp, S. Yesupriya, B. Clay, N.J. Crane, Accurate and Rapid Differentiation of Acinetobacter baumannii Strains by Raman Spectroscopy: a

Comparative Study, J. Clin. Microbiol. 55 (2017) 2480–2490. https://doi.org/10.1128/jcm.01744-16.

[20] A.I.M. Athamneh, R.A. Alajlouni, R.S. Wallace, M.N. Seleem, R.S. Sengera, Phenotypic profiling of antibiotic response signatures in Escherichia coli using raman spectroscopy, Antimicrob. Agents Chemother. 58 (2014) 1302–1314. https://doi.org/10.1128/AAC.02098-13.

[21] D. Kusić, B. Kampe, P. Rösch, J. Popp, Identification of water pathogens by Raman microspectroscopy, Water Res. 48 (2014) 179–189. https://doi.org/10.1016/j.watres.2013.09.030.

[22] O.D. Ayala, C.A. Wakeman, I.J. Pence, J.A. Gaddy, J.C. Slaughter, E.P. Skaar, A. Mahadevan-Jansen, Drug-Resistant Staphylococcus aureus Strains Reveal Distinct Biochemical Features with Raman Microspectroscopy, ACS Infect. Dis. 4 (2018) 1197–1210. https://doi.org/10.1021/acsinfecdis.8b00029.

[23] U. Münchberg, P. Rösch, M. Bauer, J. Popp, Raman spectroscopic identification of single bacterial cells under antibiotic influence, Anal. Bioanal. Chem. 406 (2014) 3041–3050. https://doi.org/10.1007/s00216-014-7747-2.

[24] K. Rebrošová, M. Šiler, O. Samek, F. Růžička, S. Bernatová, V. Holá, J. Ježek, P. Zemánek, J. Sokolová, P. Petráš, Rapid identification of staphylococci by Raman spectroscopy, Sci. Rep. 7 (2017) 14846. https://doi.org/10.1038/s41598-017-13940-w.

[25] K. Rebrošová, M. Šiler, O. Samek, F. Růžička, S. Bernatová, J. Ježek, P. Zemánek, V. Holá, Differentiation between Staphylococcus aureus and Staphylococcus epidermidis strains using Raman spectroscopy, Future Microbiol. 12 (2017) 881–890. https://doi.org/10.2217/fmb-2016-0224.

[26] C.C. Lin, C.Y. Lin, C.J. Kao, C.H. Hung, High efficiency SERS detection of clinical microorganism by AgNPs-decorated filter membrane and pattern recognition techniques, Sensors Actuators B Chem. 241 (2017) 513–521. https://doi.org/10.1016/j.snb.2016.09.183.

[27] S. Stöckel, S. Meisel, B. Lorenz, S. Kloß, S. Henk, S. Dees, E. Richter, S. Andres, M. Merker, I. Labugger, P. Rösch, J. Popp, Raman spectroscopic identification of Mycobacterium tuberculosis, J. Biophotonics. 10 (2017) 727–734. https://doi.org/10.1002/jbio.201600174.

[28] S. Meisel, S. Stöckel, P. Rösch, J. Popp, Identification of meat-associated pathogens

via Raman microspectroscopy, Food Microbiol. 38 (2014) 36–43. https://doi.org/10.1016/j.fm.2013.08.007.

[29] S.B. Rodriguez, M.A. Thornton, R.J. Thornton, Discrimination of wine lactic acid bacteria by Raman spectroscopy, J. Ind. Microbiol. Biotechnol. 44 (2017) 1167–1175. https://doi.org/10.1007/s10295-017-1943-y.

[30] A. Assaf, C.B.Y. Cordella, G. Thouand, Raman spectroscopy applied to the horizontal methods ISO 6579:2002 to identify Salmonella spp. in the food industry, Anal. Bioanal. Chem. 406 (2014) 4899–4910. https://doi.org/10.1007/s00216-014-7909-2.

[31] K. Sowoidnich, H. Schmidt, M. Maiwald, B. Sumpf, H.-D. Kronfeldt, Application of Diode-Laser Raman Spectroscopy for In situ Investigation of Meat Spoilage, Food Bioprocess Technol. 3 (2010) 878–882. https://doi.org/10.1007/s11947-010-0360-2.

[32] K. Sowoidnich, H. Schmidt, H.-D. Kronfeldt, F. Schwägele, A portable 671nm Raman sensor system for rapid meat spoilage identification, Vib. Spectrosc. 62 (2012) 70–76. https://doi.org/10.1016/j.vibspec.2012.04.002.

[33] H. Al-Ebrahim, K. Sowoidnich, H. Schmidt, H.-D. Kronfeldt, Polarization Dependence of the Raman Scattering of Oriented Porcine Muscle Fibers Affected by Storage Time and Spoilage, Focus. Mod. Food Ind. 2 (2013) 9.

[34] A.A. Argyri, R.M. Jarvis, D. Wedge, Y. Xu, E.Z. Panagou, R. Goodacre, G.-J.E. Nychas, A comparison of Raman and FT-IR spectroscopy for the prediction of meat spoilage, Food Control. 29 (2013) 461–470. https://doi.org/10.1016/j.foodcont.2012.05.040.

[35] A.E. Lytou, E.Z. Panagou, G.-J.E. Nychas, Effect of different marinating conditions on the evolution of spoilage microbiota and metabolomic profile of chicken breast fillets, Food Microbiol. 66 (2017) 141–149. https://doi.org/10.1016/j.fm.2017.04.013.

[36] Y.-Z. Feng, D.-W. Sun, Determination of total viable count (TVC) in chicken breast fillets by near-infrared hyperspectral imaging and spectroscopic transforms, Talanta. 105 (2013) 244–249. https://doi.org/10.1016/j.talanta.2012.11.042.

[37] Y. Xu, F.Y.H. Kutsanedzie, H. Sun, M. Wang, Q. Chen, Z. Guo, J. Wu, Rapid Pseudomonas Species Identification from Chicken by Integrating Colorimetric Sensors with Near-Infrared Spectroscopy, Food Anal. Methods. 11 (2018) 1199–1208. https://doi.org/10.1007/s12161-017-1095-8.

[38] B. Lorenz, C. Wichmann, S. Stöckel, P. Rösch, J. Popp, Cultivation-Free Raman Spectroscopic Investigations of Bacteria, Trends Microbiol. 25 (2017) 413–424. https://doi.org/10.1016/j.tim.2017.01.002.

[39] M. de Biasio, G. McGunnigle, R. Leitner, J. Popp, P. Rösch, D. Balthasar, Identification of single bacteria using micro Raman spectroscopy, in: 2013 Seventh Int. Conf. Sens. Technol., IEEE, 2013: pp. 34–39. https://doi.org/10.1109/ICSensT.2013.6727612.

[40] J. De Gelder, K. De Gussem, P. Vandenabeele, L. Moens, Reference database of Raman spectra of biological molecules, J. Raman Spectrosc. 38 (2007) 1133–1147. https://doi.org/10.1002/jrs.1734.

[41] S. Jaafreh, O. Valler, J. Kreyenschmidt, K. Günther, P. Kaul, In vitro discrimination and classification of Microbial Flora of Poultry using two dispersive Raman spectrometers (microscope and Portable Fiber-Optic systems) in tandem with chemometric analysis, Talanta. 202 (2019) 411–425. https://doi.org/10.1016/j.talanta.2019.04.082.

[42] J. Qiu, X. Qi, X. Li, Z. Ma, Jirigalantu, Y. Tang, X. Mi, X. Zheng, R. Zhang, Bayanheshig, Development of a spatial heterodyne Raman spectrometer with echelle-mirror structure, Opt. Express. 26 (2018) 11994. https://doi.org/10.1364/OE.26.011994.

[43] E. Cordero, I. Latka, C. Matthäus, I.W. Schie, J. Popp, In-vivo Raman spectroscopy: from basics to applications, J. Biomed. Opt. 23 (2018) 1. https://doi.org/10.1117/1.JBO.23.7.071210.

[44] D.W. Shipp, F. Sinjab, I. Notingher, Raman spectroscopy: techniques and applications in the life sciences, Adv. Opt. Photonics. 9 (2017) 315. https://doi.org/10.1364/AOP.9.000315.

[45] S. Guo, T. Bocklitz, J. Popp, Optimization of Raman-spectrum baseline correction in biological application, Analyst. 141 (2016) 2396–2404. https://doi.org/10.1039/C6AN00041J.

[46] V.H. Segtnan, K.I. Hildrum, J.P. Wold, New methods for analysis of factors affecting meat eating quality, in: Improv. Sens. Nutr. Qual. Fresh Meat, Elsevier, 2009: pp. 519–538. https://doi.org/10.1533/9781845695439.4.519.

[47] Z. Xu, Z. He, Y. Song, X. Fu, M. Rommel, X. Luo, A. Hartmaier, J. Zhang, F. Fang,

Topic Review: Application of Raman Spectroscopy Characterization in Micro/Nano-Machining, Micromachines. 9 (2018) 361. https://doi.org/10.3390/mi9070361.

[48] G.S. Bumbrah, R.M. Sharma, Raman spectroscopy – Basic principle, instrumentation and selected applications for the characterization of drugs of abuse, Egypt. J. Forensic Sci. 6 (2016) 209–215. https://doi.org/10.1016/j.ejfs.2015.06.001.

[49] O.I. Olubiyi, F.-K. Lu, D. Calligaris, F.A. Jolesz, N.Y. Agar, Advances in Molecular Imaging for Surgery, in: Image-Guided Neurosurg., Elsevier, 2015: pp. 407–439. https://doi.org/10.1016/B978-0-12-800870-6.00017-0.

[50] E. Garmire, Overview of Nonlinear Optics, in: Nonlinear Opt., InTech, 2012. https://doi.org/10.5772/37416.

[51] D. Bertoldo Menezes, A. Reyer, A. Yüksel, B. Bertoldo Oliveira, M. Musso, Introduction to Terahertz Raman spectroscopy, Spectrosc. Lett. 51 (2018) 438–445. https://doi.org/10.1080/00387010.2018.1501704.

[52] M. Testa-Anta, M.A. Ramos-Docampo, M. Comesaña-Hermo, B. Rivas-Murias, V. Salgueiriño, Raman spectroscopy to unravel the magnetic properties of iron oxide nanocrystals for bio-related applications, Nanoscale Adv. 1 (2019) 2086–2103. https://doi.org/10.1039/C9NA00064J.

[53] T. Athar, Metal oxide nanopowder, in: Emerg. Nanotechnologies Manuf., Elsevier, 2015: pp. 343–401. https://doi.org/10.1016/B978-0-323-28990-0.00014-2.

[54] R. Coat, B. Gouilleux, G. Thouand, A. Assaf, A. Arhaliass, J. Legrand, A. Thierry, E. Martineau, F. Courant, P. Giraudeau, O. Gonçalves, Characterizing the Spoilage of Egg Products using Targeted and Non-targeted Approaches, in: O. Gonçalves, J. Legrand (Eds.), Alter. Ovoproducts, Elsevier, 2018: pp. 157–258. https://doi.org/10.1016/B978-1-78548-271-7.50003-1.

[55] R. Kiselev, I.W. Schie, S. Aškrabić, C. Krafft, J. Popp, Design and first applications of a flexible Raman micro-spectroscopic system for biological imaging, Biomed. Spectrosc. Imaging. 5 (2016) 115–127. https://doi.org/10.3233/BSI-160141.

[56] J. Qin, K. Chao, M.S. Kim, Introduction to Raman Chemical Imaging Technology, in: Comput. Vis. Technol. Food Qual. Eval., Elsevier, 2016: pp. 141–171. https://doi.org/10.1016/B978-0-12-802232-0.00006-2.

[57] A.A. Bunaciu, H.Y. Aboul-Enein, Ş. Fleschin, Vibrational Spectroscopy in Clinical

Analysis, Appl. Spectrosc. Rev. 50 (2015) 176–191. https://doi.org/10.1080/05704928.2014.955582.

[58] R.R. Jones, D.C. Hooper, L. Zhang, D. Wolverson, V.K. Valev, Raman Techniques: Fundamentals and Frontiers, Nanoscale Res. Lett. 14 (2019) 231. https://doi.org/10.1186/s11671-019-3039-2.

[59] G.W. Auner, S.K. Koya, C. Huang, B. Broadbent, M. Trexler, Z. Auner, A. Elias, K.C. Mehne, M.A. Brusatori, Applications of Raman spectroscopy in cancer diagnosis, Cancer Metastasis Rev. 37 (2018) 691–717. https://doi.org/10.1007/s10555-018-9770-9.

[60] J.R. Ferraro, K. Nakamoto, C.W. Brown, Basic Theory, in: J.R. Ferraro, K. Nakamoto, C.W. Brown (Eds.), Introd. Raman Spectrosc., 2nd ed., Elsevier, 2003: pp. 1–94. https://doi.org/10.1016/B978-012254105-6/50004-4.

[61] R. Ravanshad, A.K. Zadeh, A.M. Amani, S.M. Mousavi, S.A. Hashemi, A.S. Dashtaki, E. Mirzaei, B. Zare, Application of nanoparticles in cancer detection by Raman scattering based techniques, Nano Rev. Exp. 9 (2018) 1373551. https://doi.org/10.1080/20022727.2017.1373551.

[62] H. Vašková, A powerful tool for material identification : Raman spectroscopy, Int. J. Math. Model. Methods Apllied Sci. 5 (2011) 1205–1212.

[63] C. Steuwe, C.F. Kaminski, J.J. Baumberg, S. Mahajan, Surface Enhanced Coherent Anti-Stokes Raman Scattering on Nanostructured Gold Surfaces, Nano Lett. 11 (2011) 5339–5343. https://doi.org/10.1021/nl202875w.

[64] H. Félix-Rivera, S.P. Hernández-Rivera, Raman Spectroscopy Techniques for the Detection of Biological Samples in Suspensions and as Aerosol Particles: A Review, Sens. Imaging An Int. J. 13 (2012) 1–25. https://doi.org/10.1007/s11220-011-0067-0.

[65] S. Vanden-Hehir, W. Tipping, M. Lee, V. Brunton, A. Williams, A. Hulme, Raman Imaging of Nanocarriers for Drug Delivery, Nanomaterials. 9 (2019) 341. https://doi.org/10.3390/nano9030341.

[66] K.J.I. Ember, M.A. Hoeve, S.L. McAughtrie, M.S. Bergholt, B.J. Dwyer, M.M. Stevens, K. Faulds, S.J. Forbes, C.J. Campbell, Raman spectroscopy and regenerative medicine: a review, Npj Regen. Med. 2 (2017) 12. https://doi.org/10.1038/s41536-017-0014-3.

[67] I. Durickovic, Using Raman Spectroscopy for Characterization of Aqueous Media and Quantification of Species in Aqueous Solution, in: M. Stauffer (Ed.), Appl. Mol. Spectrosc. to Curr. Res. Chem. Biol. Sci., InTech, 2016. https://doi.org/10.5772/64550.

[68] M. Wahadoszamen, A. Rahaman, N.M.R. Hoque, A. I Talukder, K.M. Abedin, A.F.M.Y. Haider, Laser Raman Spectroscopy with Different Excitation Sources and Extension to Surface Enhanced Raman Spectroscopy, J. Spectrosc. 2015 (2015) 1–8. https://doi.org/10.1155/2015/895317.

[69] K.J. Kobayashi-Kirschvink, H. Nakaoka, A. Oda, K.F. Kamei, K. Nosho, H. Fukushima, Y. Kanesaki, S. Yajima, H. Masaki, K. Ohta, Y. Wakamoto, Linear Regression Links Transcriptomic Data and Cellular Raman Spectra, Cell Syst. 7 (2018) 104-117.e4. https://doi.org/10.1016/j.cels.2018.05.015.

[70] H.J. Butler, L. Ashton, B. Bird, G. Cinque, K. Curtis, J. Dorney, K. Esmonde-White, N.J. Fullwood, B. Gardner, P.L. Martin-Hirsch, M.J. Walsh, M.R. McAinsh, N. Stone, F.L. Martin, Using Raman spectroscopy to characterize biological materials, Nat. Protoc. 11 (2016) 664–687. https://doi.org/10.1038/nprot.2016.036.

[71] B. Kann, H.L. Offerhaus, M. Windbergs, C. Otto, Raman microscopy for cellular investigations — From single cell imaging to drug carrier uptake visualization, Adv. Drug Deliv. Rev. 89 (2015) 71–90. https://doi.org/10.1016/j.addr.2015.02.006.

[72] P.G. Etchegoin, E.C. Le Ru, M. Meyer, Evidence of Natural Isotopic Distribution from Single-Molecule SERS, J. Am. Chem. Soc. 131 (2009) 2713–2716. https://doi.org/10.1021/ja808934d.

[73] X. Zhu, T. Xu, Q. Lin, Y. Duan, Technical Development of Raman Spectroscopy: From Instrumental to Advanced Combined Technologies, Appl. Spectrosc. Rev. 49 (2014) 64–82. https://doi.org/10.1080/05704928.2013.798801.

[74] K. Esmonde-White, F. Esmonde-White, Raman spectroscopy in biomineralization, in: E. DiMasi, L.B. Gower (Eds.), Biominer. Sourceb. Charact. Biominer. Biomim. Mater., 1st ed., Taylor & Francis Group, 2014: p. 432.

[75] A. Merlen, J. Buijnsters, C. Pardanaud, A Guide to and Review of the Use of Multiwavelength Raman Spectroscopy for Characterizing Defective Aromatic Carbon Solids: from Graphene to Amorphous Carbons, Coatings. 7 (2017) 153. https://doi.org/10.3390/coatings7100153.

[76] J.M. Chalmers, H.G.M. Edwards, M.D. Hargreaves, eds., Infrared and Raman

Spectroscopy in Forensic Science, John Wiley & Sons, Ltd, Chichester, UK, 2012. https://doi.org/10.1002/9781119962328.

[77] T. Schmid, P. Dariz, Raman Microspectroscopic Imaging of Binder Remnants in Historical Mortars Reveals Processing Conditions, Heritage. 2 (2019) 1662–1683. https://doi.org/10.3390/heritage2020102.

[78] Bruker Optics GmbH, SENTERRA® Raman Microscope user manual, 3rd ed., 2013.

[79] A. Deneckere, B. Vekemans, L. Voorde, P. Paepe, L. Vincze, L. Moens, P. Vandenabeele, Feasibility study of the application of micro-Raman imaging as complement to micro-XRF imaging, Appl. Phys. A. 106 (2012) 363–376. https://doi.org/10.1007/s00339-011-6693-5.

[80] J. Zhang, M. Irannejad, B. Cui, Bowtie Nanoantenna with Single-Digit Nanometer Gap for Surface-Enhanced Raman Scattering (SERS), Plasmonics. 10 (2015) 831–837. https://doi.org/10.1007/s11468-014-9870-5.

[81] R. Nath, K. Baruah, S. Sarma, D.C. Roy, R. Bhuyan, M. Dutta, N. Deka, Effect in meat composition and carcass characteristics of goat feeding mixture of different medicinal leaves of north east India., J. Pharmacogn. Phytochem. 6 (2017) 211–213. http://www.phytojournal.com/archives/2017/vol6issue1/PartC/6-1-48-678.pdf.

[82] S.K. Matarneh, E.M. England, T.L. Scheffler, D.E. Gerrard, The Conversion of Muscle to Meat, in: F. Toldra´ (Ed.), Lawrie´s Meat Sci., 8th ed., Elsevier, 2017: pp. 159–185. https://doi.org/10.1016/B978-0-08-100694-8.00005-4.

[83] K. Gul, P. Singh, A.A. Wani, Safety of Meat and Poultry, in: V. Prakash, O. Martín-Belloso, L. Keener, S. Astley, S. Braun, H. McMahon, H. Lelieveld (Eds.), Regul. Saf. Tradit. Ethn. Foods, Elsevier Inc., 2016: pp. 63–77. https://doi.org/10.1016/B978-0-12-800605-4.00004-9.

[84] P.L. Greenwood, F.R. Dunshea, Biology and regulation of carcass composition, in: J.P. Kerry, D. Ledward (Eds.), Improv. Sens. Nutr. Qual. Fresh Meat, Elsevier, 2009: pp. 19–60. https://doi.org/10.1533/9781845695439.1.19.

[85] R. Tarté, Meat-Derived Protein Ingredients, in: R. Tarté (Ed.), Ingredients Meat Prod., Springer New York, New York, NY, 2009: pp. 145–171. https://doi.org/10.1007/978-0-387-71327-4_7.

[86] W.R. Frontera, J. Ochala, Skeletal Muscle: A Brief Review of Structure and Function,

Calcif. Tissue Int. 96 (2015) 183–195. https://doi.org/10.1007/s00223-014-9915-y.

[87] P.P. Purslow, Introduction, in: P.P. Purslow (Ed.), New Asp. Meat Qual., Elsevier, 2017: pp. 1–9. https://doi.org/10.1016/B978-0-08-100593-4.00001-1.

[88] J. Hartung, B. Nowak, A.C. Springorum, Animal welfare and meat quality, in: J.P. Kerry, D. Ledward (Eds.), Improv. Sens. Nutr. Qual. Fresh Meat, Elsevier, 2009: pp. 628–646. https://doi.org/10.1533/9781845695439.4.628.

[89] A.M. Mullen, New techniques for analysing raw meat quality, in: J. Kerry, J. Kerry, D. Ledward (Eds.), Meat Process., Elsevier, 2002: pp. 394–416. https://doi.org/10.1533/9781855736665.3.394.

[90] J.F. Hocquette, R. Botreau, I. Legrand, R. Polkinghorne, D.W. Pethick, M. Lherm, B. Picard, M. Doreau, E.M.C. Terlouw, Win–win strategies for high beef quality, consumer satisfaction, and farm efficiency, low environmental impacts and improved animal welfare, Anim. Prod. Sci. 54 (2014) 1537–1548. https://doi.org/10.1071/AN14210.

[91] C. Blanco, R. Bodas, L. Morán, J. Mateo, S. Andrés, F.J. Giráldez, Effect of hop (Humulus lupulus L.) inclusion in the diet for fattening lambs on animal performance, ruminal characteristics and meat quality, Food Res. Int. 108 (2018) 42–47. https://doi.org/10.1016/j.foodres.2018.03.030.

[92] A.B. Sabow, I. Zulkifli, Y.M. Goh, M.Z.A. Ab Kadir, U. Kaka, J.C. Imlan, A.A. Abubakar, K.D. Adeyemi, A.Q. Sazili, Bleeding Efficiency, Microbiological Quality and Oxidative Stability of Meat from Goats Subjected to Slaughter without Stunning in Comparison with Different Methods of Pre-Slaughter Electrical Stunning, PLoS One. 11 (2016) 1–18. https://doi.org/10.1371/journal.pone.0152661.

[93] D. Dave, A.E. Ghaly, Meat Spoilage Mechanisms and Preservation Techniques: A Critical Review, Am. J. Agric. Biol. Sci. 6 (2011) 486–510. https://doi.org/10.3844/ajabssp.2011.486.510.

[94] S. Hameed, L. Xie, Y. Ying, Conventional and emerging detection techniques for pathogenic bacteria in food science: A review, Trends Food Sci. Technol. 81 (2018) 61–73. https://doi.org/10.1016/j.tifs.2018.05.020.

[95] L. Petruzzi, M.R. Corbo, M. Sinigaglia, A. Bevilacqua, Microbial Spoilage of Foods: Fundamentals, in: A. Bevilacqua, M.R. Corbo, M. Sinigaglia (Eds.), Microbiol. Qual. Food, Elsevier, 2017: pp. 1–21. https://doi.org/10.1016/B978-0-08-100502-6.00002-9.

[96] M. Zagorec, M.-C. Champomier-Vergès, Meat Microbiology and Spoilage, in: F. Toldra´ (Ed.), Lawrie´s Meat Sci., 8th ed., Elsevier, 2017: pp. 187–203. https://doi.org/10.1016/B978-0-08-100694-8.00006-6.

[97] G. Comi, Spoilage of Meat and Fish, in: A. Bevilacqua, M.R. Corbo, M. Sinigaglia (Eds.), Microbiol. Qual. Food Foodborne Spoilers, Elsevier Ltd, 2017: pp. 179–210. https://doi.org/10.1016/B978-0-08-100502-6.00011-X.

[98] H.M. Húngaro, M.Y.R. Caturla, C.N. Horita, M.M. Furtado, A.S. Sant'Ana, Blown pack spoilage in vacuum-packaged meat: A review on clostridia as causative agents, sources, detection methods, contributing factors and mitigation strategies, Trends Food Sci. Technol. 52 (2016) 123–138. https://doi.org/10.1016/j.tifs.2016.04.010.

[99] L. Höll, J. Behr, R.F. Vogel, Identification and growth dynamics of meat spoilage microorganisms in modified atmosphere packaged poultry meat by MALDI-TOF MS, Food Microbiol. 60 (2016) 84–91. https://doi.org/10.1016/j.fm.2016.07.003.

[100] M.A. Tørngren, M. Darré, A. Gunvig, A. Bardenshtein, Case studies of packaging and processing solutions to improve meat quality and safety, Meat Sci. 144 (2018) 149–158. https://doi.org/10.1016/j.meatsci.2018.06.018.

[101] I. Guerrero-Legarreta, MEAT AND POULTRY | Spoilage of Cooked Meat and Meat Products, in: C.A. Batt, M. Lou Tortorello (Eds.), Encycl. Food Microbiol., 2nd ed., Elsevier, 2014: pp. 508–513. https://doi.org/10.1016/B978-0-12-384730-0.00196-8.

[102] A. Casaburi, P. Piombino, G.-J. Nychas, F. Villani, D. Ercolini, Bacterial populations and the volatilome associated to meat spoilage, Food Microbiol. 45 (2015) 83–102. https://doi.org/10.1016/j.fm.2014.02.002.

[103] V. Pothakos, F. Devlieghere, F. Villani, J. Björkroth, D. Ercolini, Lactic acid bacteria and their controversial role in fresh meat spoilage, Meat Sci. 109 (2015) 66–74. https://doi.org/10.1016/j.meatsci.2015.04.014.

[104] L.-C. Fengou, E. Spyrelli, A. Lianou, P. Tsakanikas, E.Z. Panagou, G.-J.E. Nychas, Estimation of Minced Pork Microbiological Spoilage through Fourier Transform Infrared and Visible Spectroscopy and Multispectral Vision Technology, Foods. 8 (2019) 238. https://doi.org/10.3390/foods8070238.

[105] S. Jaafreh, R. Breuch, K. Günther, J. Kreyenschmidt, P. Kaul, Rapid Poultry Spoilage Evaluation Using Portable Fiber-Optic Raman Spectrometer, Food Anal. Methods. 11 (2018) 2320–2328. https://doi.org/10.1007/s12161-018-1223-0.

[106] U. ur Rahman, A. Sahar, I. Pasha, S. ur Rahman, A. Ishaq, Assessing the capability of Fourier transform infrared spectroscopy in tandem with chemometric analysis for predicting poultry meat spoilage, PeerJ. 6 (2018) e5376. https://doi.org/10.7717/peerj.5376.

[107] J.-H. Cheng, D.-W. Sun, Rapid and non-invasive detection of fish microbial spoilage by visible and near infrared hyperspectral imaging and multivariate analysis, LWT - Food Sci. Technol. 62 (2015) 1060–1068. https://doi.org/10.1016/j.lwt.2015.01.021.

[108] F. Han, X. Huang, E. Teye, H. Gu, Quantitative Analysis of Fish Microbiological Quality Using Electronic Tongue Coupled with Nonlinear Pattern Recognition Algorithms, J. Food Saf. 35 (2015) 336–344. https://doi.org/10.1111/jfs.12180.

[109] H.M. Húngaro, W.E.L. Peña, N.B.M. Silva, R.V. Carvalho, V.O. Alvarenga, A.S. Sant'Ana, Food Microbiology, in: N.K. Van Alfen (Ed.), Encycl. Agric. Food Syst., Elsevier, 2014: pp. 213–231. https://doi.org/10.1016/B978-0-444-52512-3.00059-0.

[110] M. Hilgarth, S. Fuertes-Pèrez, M. Ehrmann, R.F. Vogel, An adapted isolation procedure reveals Photobacterium spp. as common spoilers on modified atmosphere packaged meats, Lett. Appl. Microbiol. 66 (2018) 262–267. https://doi.org/10.1111/lam.12860.

[111] N.K. Abd El-Aziz, Y.H. Tartor, A.A.E.-A. Gharib, A.M. Ammar, Propidium Monoazide Quantitative Real-Time Polymerase Chain Reaction for Enumeration of Some Viable but Nonculturable Foodborne Bacteria in Meat and Meat Products, Foodborne Pathog. Dis. 15 (2018) 226–234. https://doi.org/10.1089/fpd.2017.2356.

[112] M. Luciani, M. Schirone, O. Portanti, P. Visciano, G. Armillotta, R. Tofalo, G. Suzzi, L. Sonsini, T. Di Febo, Development of a rapid method for the detection of Yersinia enterocolitica serotype O:8 from food, Food Microbiol. 73 (2018) 85–92. https://doi.org/10.1016/j.fm.2018.01.009.

[113] P. Lasch, M. Drevinek, H. Nattermann, R. Grunow, M. Stämmler, R. Dieckmann, T. Schwecke, D. Naumann, Characterization of Yersinia Using MALDI-TOF Mass Spectrometry and Chemometrics, Anal. Chem. 82 (2010) 8464–8475. https://doi.org/10.1021/ac101036s.

[114] F.T. Tabit, Advantages and limitations of potential methods for the analysis of bacteria in milk: a review, J. Food Sci. Technol. 53 (2016) 42–49. https://doi.org/10.1007/s13197-015-1993-y.

[115] H.J. He, D.W. Sun, Microbial evaluation of raw and processed food products by Visible/Infrared, Raman and Fluorescence spectroscopy, Trends Food Sci. Technol. 46 (2015) 199–210. https://doi.org/10.1016/j.tifs.2015.10.004.

[116] L. Zhu, J. He, X. Cao, K. Huang, Y. Luo, W. Xu, Development of a double-antibody sandwich ELISA for rapid detection of Bacillus Cereus in food, Sci. Rep. 6 (2016) 16092. https://doi.org/10.1038/srep16092.

[117] S. Keleştemur, E. Avci, M. Çulha, Raman and Surface-Enhanced Raman Scattering for Biofilm Characterization, Chemosensors. 6 (2018) 5. https://doi.org/10.3390/chemosensors6010005.

[118] N. AlMasoud, Y. Xu, D.I. Ellis, P. Rooney, J.F. Turton, R. Goodacre, Rapid discrimination of Enterococcus faecium strains using phenotypic analytical techniques, Anal. Methods. 8 (2016) 7603–7613. https://doi.org/10.1039/C6AY02326F.

[119] J. Guicheteau, L. Argue, D. Emge, A. Hyre, M. Jacobson, S. Christesen, Bacillus Spore Classification via Surface-Enhanced Raman Spectroscopy and Principal Component Analysis, Appl. Spectrosc. 62 (2008) 267–272. https://doi.org/10.1366/000370208783759623.

[120] D.S. Read, A.S. Whiteley, Chemical fixation methods for Raman spectroscopy-based analysis of bacteria, J. Microbiol. Methods. 109 (2015) 79–83. https://doi.org/10.1016/j.mimet.2014.12.008.

[121] M.T. Alula, S. Krishnan, N.R. Hendricks, L. Karamchand, J.M. Blackburn, Identification and quantitation of pathogenic bacteria via in-situ formation of silver nanoparticles on cell walls, and their detection via SERS, Microchim. Acta. 184 (2017) 219–227. https://doi.org/10.1007/s00604-016-2013-2.

[122] Z. Pilát, S. Bernatová, J. Ježek, J. Kirchhoff, A. Tannert, U. Neugebauer, O. Samek, P. Zemánek, Microfluidic Cultivation and Laser Tweezers Raman Spectroscopy of E. coli under Antibiotic Stress, Sensors. 18 (2018) 1623. https://doi.org/10.3390/s18051623.

[123] S.B. Rodriguez, M.A. Thornton, R.J. Thornton, Raman Spectroscopy and Chemometrics for Identification and Strain Discrimination of the Wine Spoilage Yeasts Saccharomyces cerevisiae, Zygosaccharomyces bailii, and Brettanomyces bruxellensis, Appl. Environ. Microbiol. 79 (2013) 6264–6270. https://doi.org/10.1128/aem.01886-13.

[124] W.H. Su, D.W. Sun, Fourier Transform Infrared and Raman and Hyperspectral

Imaging Techniques for Quality Determinations of Powdery Foods: A Review, Compr. Rev. Food Sci. Food Saf. 17 (2018) 104–122. https://doi.org/10.1111/1541-4337.12314.

[125] K.H. Liland, A. Kohler, N.K. Afseth, Model-based pre-processing in Raman spectroscopy of biological samples, J. Raman Spectrosc. 47 (2016) 643–650. https://doi.org/10.1002/jrs.4886.

[126] P. Lasch, Spectral pre-processing for biomedical vibrational spectroscopy and microspectroscopic imaging, Chemom. Intell. Lab. Syst. 117 (2012) 100–114. https://doi.org/10.1016/j.chemolab.2012.03.011.

[127] T. Bocklitz, A. Walter, K. Hartmann, P. Rösch, J. Popp, How to pre-process Raman spectra for reliable and stable models?, Anal. Chim. Acta. 704 (2011) 47–56. https://doi.org/10.1016/j.aca.2011.06.043.

[128] P. Chen, A. Shen, X. Zhou, J. Hu, Bio-Raman spectroscopy: a potential clinical analytical method assisting in disease diagnosis, Anal. Methods. 3 (2011) 1257. https://doi.org/10.1039/c1ay05039g.

[129] K.A. Esmonde-White, M. Cuellar, C. Uerpmann, B. Lenain, I.R. Lewis, Raman spectroscopy as a process analytical technology for pharmaceutical manufacturing and bioprocessing, Anal. Bioanal. Chem. 409 (2017) 637–649. https://doi.org/10.1007/s00216-016-9824-1.

[130] J.-L. Damez, S. Clerjon, Meat quality assessment using biophysical methods related to meat structure, Meat Sci. 80 (2008) 132–149. https://doi.org/10.1016/j.meatsci.2008.05.039.

[131] M. Otto, What is Chemometrics?, in: Chemometrics, 3rd ed., Wiley-VCH Verlag GmbH & Co. KGaA, Weinheim, Germany, 2016: pp. 1–13. https://doi.org/10.1002/9783527699377.ch1.

[132] K. Héberger, Chemoinformatics—multivariate mathematical–statistical methods for data evaluation, in: K. Vékey, A. Telekes, A. Vertes (Eds.), Med. Appl. Mass Spectrom., Elsevier, 2008: pp. 141–169. https://doi.org/10.1016/B978-044451980-1.50009-4.

[133] M. Davy, An Introduction to Statistical Signal Processing and Spectrum Estimation, in: A. Klapuri, M. Davy (Eds.), Signal Process. Methods Music Transcr., Springer US, Boston, MA, n.d.: pp. 21–64. https://doi.org/10.1007/0-387-32845-9_2.

[134] L. Saucier, Microbial spoilage, quality and safety within the context of meat sustainability, Meat Sci. 120 (2016) 78–84. https://doi.org/10.1016/j.meatsci.2016.04.027.

[135] S. Rossaint, J. Kreyenschmidt, Intelligent label – a new way to support food waste reduction, Proc. Inst. Civ. Eng. - Waste Resour. Manag. 168 (2015) 63–71. https://doi.org/10.1680/warm.13.00035.

[136] F. Mohareb, M. Iriondo, A.I. Doulgeraki, A. Van Hoek, H. Aarts, M. Cauchi, G.-J.E. Nychas, Identification of meat spoilage gene biomarkers in Pseudomonas putida using gene profiling, Food Control. 57 (2015) 152–160. https://doi.org/10.1016/j.foodcont.2015.04.007.

[137] V. Raab, S. Bruckner, E. Beierle, Y. Kampmann, B. Petersen, J. Kreyenschmidt, Generic model for the prediction of remaining shelf life in support of cold chain management in pork and poultry supply chains, J. Chain Netw. Sci. 8 (2008) 59–73. https://doi.org/10.3920/jcns2008.x089.

[138] G.J.E. Nychas, P.N. Skandamis, C.C. Tassou, K.P. Koutsoumanis, Meat spoilage during distribution, Meat Sci. 78 (2008) 77–89. https://doi.org/10.1016/j.meatsci.2007.06.020.

[139] S. Stöckel, J. Kirchhoff, U. Neugebauer, P. Rösch, J. Popp, The application of Raman spectroscopy for the detection and identification of microorganisms, J. Raman Spectrosc. 47 (2015) 89–109. https://doi.org/10.1002/jrs.4844.

[140] A.G. Yilmaz, H.T. Temiz, E.A. Soykut, K. Halkman, I.H. Boyaci, Rapid Identification of Pseudomonas aeruginosa and Pseudomonas fluorescens Using Raman Spectroscopy, J. Food Saf. 35 (2015) 501–508. https://doi.org/10.1111/jfs.12200.

[141] E. Kastanos, A. Kyriakides, K. Hadjigeorgiou, C. Pitris, A Novel Method for Bacterial UTI Diagnosis Using Raman Spectroscopy, Int. J. Spectrosc. 2012 (2012) 1–13. https://doi.org/10.1155/2012/195317.

[142] M. Santos, E. Gerbino, E. Tymczyszyn, A. Gomez-Zavaglia, Applications of Infrared and Raman Spectroscopies to Probiotic Investigation, Foods. 4 (2015) 283–305. https://doi.org/10.3390/foods4030283.

[143] S. Guo, R. Heinke, S. Stöckel, P. Rösch, T. Bocklitz, J. Popp, Towards an improvement of model transferability for Raman spectroscopy in biological applications, Vib. Spectrosc. 91 (2017) 111–118.

https://doi.org/10.1016/j.vibspec.2016.06.010.

[144] M.K. Grewal, P. Jaiswal, S.N. Jha, Detection of poultry meat specific bacteria using FTIR spectroscopy and chemometrics, J. Food Sci. Technol. 52 (2015) 3859–3869. https://doi.org/10.1007/s13197-014-1457-9.

[145] C. Pomrehn, D. Klein, A. Kolb, P. Kaul, R. Herpers, Supervised classification of monomodal and multimodal hyperspectral data in vibrational microspectroscopy: A comprehensive comparison, Chemom. Intell. Lab. Syst. 184 (2019) 112–122. https://doi.org/10.1016/j.chemolab.2018.11.013.

[146] E. Widjaja, W. Zheng, Z. Huang, Classification of colonic tissues using near-infrared Raman spectroscopy and support vector machines, Int. J. Oncol. 5862 (2008) 653–662. https://doi.org/10.3892/ijo.32.3.653.

[147] M.A. Nanda, K.B. Seminar, D. Nandika, A. Maddu, A comparison study of kernel functions in the support vector machine and its application for termite detection, Inf. 9 (2018). https://doi.org/10.3390/info9010005.

[148] G. Carducci, G. Rizzo, D. Monti, E. Palumbo, M. Morisio, TwitPersonality: Computing personality traits from tweets using word embeddings and supervised learning, Inf. 9 (2018) 1–20. https://doi.org/10.3390/info9050127.

[149] A. Maguire, I. Vega-Carrascal, J. Bryant, L. White, O. Howe, F.M. Lyng, A.D. Meade, Competitive evaluation of data mining algorithms for use in classification of leukocyte subtypes with Raman microspectroscopy, Analyst. 140 (2015) 2473–2481. https://doi.org/10.1039/c4an01887g.

[150] R. Kumar, A. Srivastava, B. Kumari, M. Kumar, Prediction of β-lactamase and its class by Chou's pseudo-amino acid composition and support vector machine, J. Theor. Biol. 365 (2015) 96–103. https://doi.org/10.1016/j.jtbi.2014.10.008.

[151] G. Mountrakis, J. Im, C. Ogole, Support vector machines in remote sensing: A review, ISPRS J. Photogramm. Remote Sens. 66 (2011) 247–259. https://doi.org/10.1016/j.isprsjprs.2010.11.001.

[152] Q. Chen, J. Zhao, C.H. Fang, D. Wang, Feasibility study on identification of green, black and Oolong teas using near-infrared reflectance spectroscopy based on support vector machine (SVM), Spectrochim. Acta - Part A Mol. Biomol. Spectrosc. 66 (2007) 568–574. https://doi.org/10.1016/j.saa.2006.03.038.

[153] A.R.M. Radzol, K.Y. Lee, W. Mansor, Model Selection for PCA-Linear SVM for automated detection of NS1 molecule from Raman spectra of salivary mixture, in: 2015 37th Annu. Int. Conf. IEEE Eng. Med. Biol. Soc., IEEE, 2015: pp. 2824–2827. https://doi.org/10.1109/EMBC.2015.7318979.

[154] F. Pedregosa, G. Varoquaux, A. Gramfort, V. Michel, B. Thirion, O. Grisel, M. Blondel, P. Prettenhofer, R. Weiss, V. Dubourg, J. Vanderplas, A. Passos, D. Cournapeau, Scikit-learn: Machine Learning in Python, J. Mach. Learn. Res. 12 (2011) 2825–2830. https://doi.org/10.1007/s13398-014-0173-7.2.

[155] A.T. Lewis, R. Gaifulina, M. Isabelle, J. Dorney, M.L. Woods, G.R. Lloyd, K. Lau, M. Rodriguez-Justo, C. Kendall, N. Stone, G.M. Thomas, Mirrored stainless steel substrate provides improved signal for Raman spectroscopy of tissue and cells, J. Raman Spectrosc. 48 (2017) 119–125. https://doi.org/10.1002/jrs.4980.

[156] T. Bocklitz, A. Walter, K. Hartmann, P. Rösch, J. Popp, How to pre-process Raman spectra for reliable and stable models?, Anal. Chim. Acta. 704 (2011) 47–56. https://doi.org/10.1016/j.aca.2011.06.043.

[157] N.K. Afseth, V.H. Segtnan, J.P. Wold, Raman Spectra of Biological Samples: A Study of Preprocessing Methods, Appl. Spectrosc. 60 (2006) 1358–1367. https://doi.org/10.1366/000370206779321454.

[158] M. Harz, P. Rösch, K.-D. Peschke, O. Ronneberger, H. Burkhardt, J. Popp, Micro-Raman spectroscopic identification of bacterial cells of the genus Staphylococcus and dependence on their cultivation conditions, Analyst. 130 (2005) 1543. https://doi.org/10.1039/b507715j.

[159] A. Ramoji, K. Galler, U. Glaser, T. Henkel, G. Mayer, J. Dellith, M. Bauer, J. Popp, U. Neugebauer, Characterization of different substrates for Raman spectroscopic imaging of eukaryotic cells, J. Raman Spectrosc. 47 (2016) 773–786. https://doi.org/10.1002/jrs.4899.

[160] I. Romano, A. De Angelis, A. Poli, P. Ragni, L. Lilla, G. Zito, B. Nicolaus, A.C. De Luca, P. Di Donato, Resistance and Raman spectroscopy analysis of Parageobacillus thermantarcticus spores after γ-ray exposure, Extremophiles. 22 (2018) 931–941. https://doi.org/10.1007/s00792-018-1049-0.

[161] Z. Movasaghi, S. Rehman, I.U. Rehman, Raman Spectroscopy of Biological Tissues, Appl. Spectrosc. Rev. 42 (2007) 493–541.

https://doi.org/10.1080/05704920701551530.

[162] M. Chisanga, H. Muhamadali, D.I. Ellis, R. Goodacre, Surface-Enhanced Raman Scattering (SERS) in Microbiology: Illumination and Enhancement of the Microbial World, Appl. Spectrosc. 72 (2018) 987–1000. https://doi.org/10.1177/0003702818764672.

[163] E. Witkowska, D. Korsak, A. Kowalska, A. Janeczek, A. Kamińska, Strain-level typing and identification of bacteria – a novel approach for SERS active plasmonic nanostructures, Anal. Bioanal. Chem. 410 (2018) 5019–5031. https://doi.org/10.1007/s00216-018-1153-0.

[164] E. Witkowska, D. Korsak, A. Kowalska, M. Księżopolska-Gocalska, J. Niedziółka-Jönsson, E. Roźniecka, W. Michałowicz, P. Albrycht, M. Podrażka, R. Hołyst, J. Waluk, A. Kamińska, Surface-enhanced Raman spectroscopy introduced into the International Standard Organization (ISO) regulations as an alternative method for detection and identification of pathogens in the food industry, Anal. Bioanal. Chem. 409 (2017) 1555–1567. https://doi.org/10.1007/s00216-016-0090-z.

[165] T.J. Moritz, D.S. Taylor, C.R. Polage, D.M. Krol, S.M. Lane, J.W. Chan, Effect of Cefazolin Treatment on the Nonresonant Raman Signatures of the Metabolic State of Individual Escherichia coli Cells, Anal. Chem. 82 (2010) 2703–2710. https://doi.org/10.1021/ac902351a.

[166] M.L. Paret, S.K. Sharma, L.M. Green, A.M. Alvarez, Biochemical Characterization of Gram-Positive and Gram-Negative Plant-Associated Bacteria with Micro-Raman Spectroscopy, Appl. Spectrosc. 64 (2010) 433–441. https://doi.org/10.1366/000370210791114293.

[167] N.P. Ivleva, M. Wagner, H. Horn, R. Niessner, C. Haisch, Towards a nondestructive chemical characterization of biofilm matrix by Raman microscopy, Anal. Bioanal. Chem. 393 (2009) 197–206. https://doi.org/10.1007/s00216-008-2470-5.

[168] M. Wagner, N.P. Ivleva, C. Haisch, R. Niessner, H. Horn, Combined use of confocal laser scanning microscopy (CLSM) and Raman microscopy (RM): Investigations on EPS – Matrix, Water Res. 43 (2009) 63–76. https://doi.org/10.1016/j.watres.2008.10.034.

[169] S. He, S. Fang, W. Xie, P. Zhang, Z. Li, D. Zhou, Z. Zhang, J. Guo, C. Du, J. Du, D. Wang, Assessment of physiological responses and growth phases of different

microalgae under environmental changes by Raman spectroscopy with chemometrics, Spectrochim. Acta Part A Mol. Biomol. Spectrosc. 204 (2018) 287–294. https://doi.org/10.1016/j.saa.2018.06.060.

[170] T.M. Callaghan, K.-P. Wilhelm, A review of ageing and an examination of clinical methods in the assessment of ageing skin. Part 2: Clinical perspectives and clinical methods in the evaluation of ageing skin, Int. J. Cosmet. Sci. 30 (2008) 323–332. https://doi.org/10.1111/j.1468-2494.2008.00455.x.

[171] D. Wei, S. Chen, Q. Liu, Review of Fluorescence Suppression Techniques in Raman Spectroscopy, Appl. Spectrosc. Rev. 50 (2015) 387–406. https://doi.org/10.1080/05704928.2014.999936.

[172] J. Zięba-Palus, A. Michalska, Photobleaching as a useful technique in reducing of fluorescence in Raman spectra of blue automobile paint samples, Vib. Spectrosc. 74 (2014) 6–12. https://doi.org/10.1016/j.vibspec.2014.06.007.

[173] Y. Ren, Y. Ji, L. Teng, H. Zhang, Using Raman spectroscopy and chemometrics to identify the growth phase of Lactobacillus casei Zhang during batch culture at the single-cell level, Microb. Cell Fact. 16 (2017) 233. https://doi.org/10.1186/s12934-017-0849-8.

[174] A. Walter, A. März, W. Schumacher, P. Rösch, J. Popp, Towards a fast, high specific and reliable discrimination of bacteria on strain level by means of SERS in a microfluidic device, Lab Chip. 11 (2011) 1013–1021. https://doi.org/10.1039/c0lc00536c.

[175] R. Ullah, S. Khan, S. Javaid, H. Ali, M. Bilal, M. Saleem, Raman spectroscopy combined with a support vector machine for differentiating between feeding male and female infants mother's milk, Biomed. Opt. Express. 9 (2018) 844–851. https://doi.org/10.1364/BOE.9.000844.

[176] Y.-Z. Feng, D.-W. Sun, Near-infrared hyperspectral imaging in tandem with partial least squares regression and genetic algorithm for non-destructive determination and visualization of Pseudomonas loads in chicken fillets, Talanta. 109 (2013) 74–83. https://doi.org/10.1016/j.talanta.2013.01.057.

[177] W. Cheng, J.-H. Cheng, D.-W. Sun, H. Pu, Marbling Analysis for Evaluating Meat Quality: Methods and Techniques, Compr. Rev. Food Sci. Food Saf. 14 (2015) 523–535. https://doi.org/10.1111/1541-4337.12149.

[178] J. Kreyenschmidt, A. Hübner, E. Beierle, L. Chonsch, A. Scherer, B. Petersen, Determination of the shelf life of sliced cooked ham based on the growth of lactic acid bacteria in different steps of the chain, J. Appl. Microbiol. 108 (2010) 510–520. https://doi.org/10.1111/j.1365-2672.2009.04451.x.

[179] A.M. Herrero, Raman spectroscopy a promising technique for quality assessment of meat and fish: A review, Food Chem. 107 (2008) 1642–1651. https://doi.org/10.1016/j.foodchem.2007.10.014.

[180] A. Sahar, T. Boubellouta, É. Dufour, Synchronous front-face fluorescence spectroscopy as a promising tool for the rapid determination of spoilage bacteria on chicken breast fillet, Food Res. Int. 44 (2011) 471–480. https://doi.org/10.1016/j.foodres.2010.09.006.

[181] J. Kreyenschmidt, R. Ibald, Modeling Shelf Life Using Microbial Indicators, in: M.C. Nicoli (Ed.), Shelf Life Assess. Food, 1st ed., Taylor & Francis Group, 2012: pp. 127–168. https://doi.org/10.1201/b11871-7.

[182] P.J. Sarnoski, S.F. O'Keefe, M.L. Jahncke, P. Mallikarjunan, G.J. Flick, Analysis of crab meat volatiles as possible spoilage indicators for blue crab (Callinectes sapidus) meat by gas chromatography–mass spectrometry, Food Chem. 122 (2010) 930–935. https://doi.org/10.1016/j.foodchem.2010.03.069.

[183] D. Mayr, R. Margesin, E. Klingsbichel, E. Hartungen, D. Jenewein, F. Schinner, T.D. Mark, Rapid Detection of Meat Spoilage by Measuring Volatile Organic Compounds by Using Proton Transfer Reaction Mass Spectrometry, Appl. Environ. Microbiol. 69 (2003) 4697–4705. https://doi.org/10.1128/AEM.69.8.4697-4705.2003.

[184] C. Franke, J. Beauchamp, Real-Time Detection of Volatiles Released During Meat Spoilage: a Case Study of Modified Atmosphere-Packaged Chicken Breast Fillets Inoculated with Br. thermosphacta, Food Anal. Methods. 10 (2017) 310–319. https://doi.org/10.1007/s12161-016-0585-4.

[185] S. Abay, R. Irkin, F. Aydin, H.K. Müştak, K.S. Diker, The prevalence of major foodborne pathogens in ready-to-eat chicken meat samples sold in retail markets in Turkey and the molecular characterization of the recovered isolates, LWT - Food Sci. Technol. 81 (2017) 202–209. https://doi.org/10.1016/j.lwt.2017.03.052.

[186] V.S. Kodogiannis, T. Pachidis, E. Kontogianni, An intelligent based decision support system for the detection of meat spoilage, Eng. Appl. Artif. Intell. 34 (2014) 23–36.

https://doi.org/10.1016/j.engappai.2014.05.001.

[187] E.C.Y. Li-Chan, P.R. Griffiths, J.N.M. Chalmers, eds., Applications of vibrational spectroscopy in food science: Volume I: Instrumentation and fundamental applications., 1st ed., Wiley and Sons, Chichester, United kingdom, 2010.

[188] M. Oroian, S. Ropciuc, S. Paduret, Honey Adulteration Detection Using Raman Spectroscopy, Food Anal. Methods. 11 (2018) 959–968. https://doi.org/10.1007/s12161-017-1072-2.

[189] M. Oroian, S. Ropciuc, Botanical authentication of honeys based on Raman spectra, J. Food Meas. Charact. 12 (2018) 545–554. https://doi.org/10.1007/s11694-017-9666-3.

[190] H. Schmidt, K. Sowoidnich, H.-D. Kronfeldt, A Prototype Hand-Held Raman Sensor for the in situ Characterization of Meat Quality, Appl. Spectrosc. 64 (2010) 888–894. https://doi.org/10.1366/000370210792081028.

[191] J.N. Miller, J.C. Miller, Statistics and Chemometrics for Analytical Chemistry, 6th ed., Pearson Education Limited, Harlow, 2010.

[192] M.S. Ammor, A. Argyri, G.-J.E. Nychas, Rapid monitoring of the spoilage of minced beef stored under conventionally and active packaging conditions using Fourier transform infrared spectroscopy in tandem with chemometrics, Meat Sci. 81 (2009) 507–514. https://doi.org/10.1016/j.meatsci.2008.10.015.

[193] O. Papadopoulou, E.Z. Panagou, C.C. Tassou, G.-J.E. Nychas, Contribution of Fourier transform infrared (FTIR) spectroscopy data on the quantitative determination of minced pork meat spoilage, Food Res. Int. 44 (2011) 3264–3271. https://doi.org/10.1016/j.foodres.2011.09.012.

[194] H. Vasconcelos, C. Saraiva, J.M.M.M. de Almeida, Evaluation of the Spoilage of Raw Chicken Breast Fillets Using Fourier Transform Infrared Spectroscopy in Tandem with Chemometrics, Food Bioprocess Technol. 7 (2014) 2330–2341. https://doi.org/10.1007/s11947-014-1277-y.

[195] A. Zając, L. Dymińska, J. Lorenc, J. Hanuza, Fourier Transform Infrared and Raman Spectroscopy Studies of the Time-Dependent Changes in Chicken Meat as a Tool for Recording Spoilage Processes, Food Anal. Methods. 10 (2017) 640–648. https://doi.org/10.1007/s12161-016-0636-x.

[196] J.F. Kelly, T.A. Blake, B.E. Bernacki, T.J. Johnson, Design Considerations for a

Portable Raman Probe Spectrometer for Field Forensics, Int. J. Spectrosc. 2012 (2012) 1–15. https://doi.org/10.1155/2012/938407.

[197] J.B. Cooper, M. Abdelkader, K.L. Wise, Sequentially Shifted Excitation Raman Spectroscopy: Novel Algorithm and Instrumentation for Fluorescence-Free Raman Spectroscopy in Spectral Space, Appl. Spectrosc. 67 (2013) 973–984. https://doi.org/10.1366/12-06852.

[198] T. Rojalin, L. Kurki, T. Laaksonen, T. Viitala, J. Kostamovaara, K.C. Gordon, L. Galvis, S. Wachsmann-Hogiu, C.J. Strachan, M. Yliperttula, Fluorescence-suppressed time-resolved Raman spectroscopy of pharmaceuticals using complementary metal-oxide semiconductor (CMOS) single-photon avalanche diode (SPAD) detector, Anal. Bioanal. Chem. 408 (2016) 761–774. https://doi.org/10.1007/s00216-015-9156-6.

[199] K.I. Hildrum, J.P. Wold, V.H. Segtnan, J.-P. Renou, É. Dufour, New Spectroscopic Techniques for Online Monitoring of Meat Quality, in: L.M.L. Nollet, F. Toldra (Eds.), Adv. Technol. Meat Process., 1st ed., CRC, Taylor & Francis Group, Boca Raton, 2006: pp. 87–130.

[200] H.G. Schulze, R.F.B. Turner, A Fast, Automated, Polynomial-Based Cosmic Ray Spike–Removal Method for the High-Throughput Processing of Raman Spectra, Appl. Spectrosc. 67 (2013) 457–462. https://doi.org/10.1366/12-06839.

[201] O. Ryabchykov, T. Bocklitz, A. Ramoji, U. Neugebauer, M. Foerster, C. Kroegel, M. Bauer, M. Kiehntopf, J. Popp, Automatization of spike correction in Raman spectra of biological samples, Chemom. Intell. Lab. Syst. 155 (2016) 1–6. https://doi.org/10.1016/j.chemolab.2016.03.024.

[202] R.A. Bailey, K.A. Watson, S.F. Bilgili, S. Avendano, The genetic basis of pectoralis major myopathies in modern broiler chicken lines, Poult. Sci. 94 (2015) 2870–2879. https://doi.org/10.3382/ps/pev304.

[203] J.R. Beattie, S.E.J. Bell, C. Borggaard, A.M. Fearon, B.W. Moss, Classification of Adipose Tissue Species using Raman Spectroscopy, Lipids. 42 (2007) 679–685. https://doi.org/10.1007/s11745-007-3059-z.

[204] L.B. Lyndgaard, K.M. Sørensen, F. Berg, S.B. Engelsen, Depth profiling of porcine adipose tissue by Raman spectroscopy, J. Raman Spectrosc. 43 (2012) 482–489. https://doi.org/10.1002/jrs.3067.

[205] A.M. Herrero, Raman Spectroscopy for Monitoring Protein Structure in Muscle Food

Systems, Crit. Rev. Food Sci. Nutr. 48 (2008) 512–523. https://doi.org/10.1080/10408390701537385.

[206] R.J. Beattie, S.J. Bell, L.J. Farmer, B.W. Moss, D. Patterson, Preliminary investigation of the application of Raman spectroscopy to the prediction of the sensory quality of beef silverside, Meat Sci. 66 (2004) 903–913. https://doi.org/10.1016/j.meatsci.2003.08.012.

[207] A. Nawrocka, M. Szymańska-Chargot, A. Miś, A.Z. Wilczewska, K.H. Markiewicz, Dietary Fiber-Induced Changes in the Structure and Thermal Properties of Gluten Proteins Studied by Fourier Transform-Raman Spectroscopy and Thermogravimetry, J. Agric. Food Chem. 64 (2016) 2094–2104. https://doi.org/10.1021/acs.jafc.5b05712.

[208] F.L. Martin, M.J. German, E. Wit, T. Fearn, N. Ragavan, H.M. Pollock, Identifying Variables Responsible for Clustering in Discriminant Analysis of Data from Infrared Microspectroscopy of a Biological Sample, J. Comput. Biol. 14 (2007) 1176–1184. https://doi.org/10.1089/cmb.2007.0057.

[209] M. Li Vigni, C. Durante, M. Cocchi, Exploratory Data Analysis, in: F. Marini (Ed.), Chemom. Food Chem., 1st ed., Elsevier, Amsterdam, 2013: pp. 55–126. https://doi.org/10.1016/B978-0-444-59528-7.00003-X.

[210] M. Sarstedt, E. Mooi, Cluster Analysis, in: M. Sarstedt, E. Mooi (Eds.), A Concise Guid. to Mark. Res., 2nd ed., Springer Berlin Heidelberg, 2014: pp. 273–324. https://doi.org/10.1007/978-3-642-53965-7_9.

[211] B. Abu-Jamous, R. Fa, A.K. Nandi, Integrative Cluster Analysis in Bioinformatics, John Wiley & Sons, Ltd, Chichester, UK, 2015. https://doi.org/10.1002/9781118906545.

[212] K. Sowoidnich, H.-D. Kronfeldt, Fluorescence Rejection by Shifted Excitation Raman Difference Spectroscopy at Multiple Wavelengths for the Investigation of Biological Samples, ISRN Spectrosc. 2012 (2012) 1–11. https://doi.org/10.5402/2012/256326.

[213] J. Engel, J. Gerretzen, E. Szymańska, J.J. Jansen, G. Downey, L. Blanchet, L.M.C. Buydens, Breaking with trends in pre-processing?, TrAC Trends Anal. Chem. 50 (2013) 96–106. https://doi.org/10.1016/j.trac.2013.04.015.

[214] E. Cordero, F. Korinth, C. Stiebing, C. Krafft, I. Schie, J. Popp, Evaluation of Shifted Excitation Raman Difference Spectroscopy and Comparison to Computational Background Correction Methods Applied to Biochemical Raman Spectra, Sensors. 17

(2017) 1724. https://doi.org/10.3390/s17081724.

[215] Z. Li, M. Deen, S. Kumar, P. Selvaganapathy, Raman Spectroscopy for In-Line Water Quality Monitoring—Instrumentation and Potential, Sensors. 14 (2014) 17275–17303. https://doi.org/10.3390/s140917275.

[216] K. Sowoidnich, H.-D. Kronfeldt, Shifted excitation Raman difference spectroscopy at multiple wavelengths for in-situ meat species differentiation, Appl. Phys. B. 108 (2012) 975–982. https://doi.org/10.1007/s00340-012-5160-0.

[217] D. Mafra, N.A. Borges, L.F.M. de F. Cardozo, J.S. Anjos, A.P. Black, C. Moraes, P. Bergman, B. Lindholm, P. Stenvinkel, Red meat intake in chronic kidney disease patients: Two sides of the coin, Nutrition. 46 (2018) 26–32. https://doi.org/10.1016/j.nut.2017.08.015.

[218] M. Careche, A.M. Herrero, A. Rodriguez-Casado, M.L. Del Mazo, P. Carmona, Structural Changes of Hake (Merluccius merluccius L.) Fillets: Effects of Freezing and Frozen Storage, J. Agric. Food Chem. 47 (1999) 952–959. https://doi.org/10.1021/jf9809481.

[219] S. Thawornchinsombut, J.W. Park, G. Meng, E.C.Y. Li-Chan, Raman Spectroscopy Determines Structural Changes Associated with Gelation Properties of Fish Proteins Recovered at Alkaline pH, J. Agric. Food Chem. 54 (2006) 2178–2187. https://doi.org/10.1021/jf0518958.

[220] A.M. Herrero, M.I. Cambero, J.A. Ordóñez, L. de la Hoz, P. Carmona, Raman spectroscopy study of the structural effect of microbial transglutaminase on meat systems and its relationship with textural characteristics, Food Chem. 109 (2008) 25–32. https://doi.org/10.1016/j.foodchem.2007.12.003.

[221] E.D. Strange, R.C. Benedict, J.L. Smith, C.E. Swift, Evaluation of Rapid Tests for Monitoring Alterations in Meat Quality During Storage, J. Food Prot. 40 (1977) 843–847. https://doi.org/10.4315/0362-028X-40.12.843.

[222] W. Zhang, S. Xiao, D.U. Ahn, Protein Oxidation: Basic Principles and Implications for Meat Quality, Crit. Rev. Food Sci. Nutr. 53 (2013) 1191–1201. https://doi.org/10.1080/10408398.2011.577540.

[223] X. Feng, S.H. Moon, H.Y. Lee, D.U. Ahn, Effect of irradiation on the parameters that influence quality characteristics of raw turkey breast meat, Radiat. Phys. Chem. 130 (2017) 40–46. https://doi.org/10.1016/j.radphyschem.2016.07.015.

[224] A. Albrecht, M. Hebel, M. Mittler, C. Hurck, K. Kustwan, B. Heitkönig, D. Bitschinski, J. Kreyenschmidt, Influence of Different Production Systems on the Quality and Shelf Life of Poultry Meat: A Case Study in the German Sector, J. Food Qual. 2019 (2019) 1–11. https://doi.org/10.1155/2019/3718057.

[225] E.K. Silbergeld, J. Graham, L.B. Price, Industrial Food Animal Production, Antimicrobial Resistance, and Human Health, Annu. Rev. Public Health. 29 (2008) 151–169. https://doi.org/10.1146/annurev.publhealth.29.020907.090904.

[226] I. Leinonen, I. Kyriazakis, How can we improve the environmental sustainability of poultry production?, Proc. Nutr. Soc. 75 (2016) 265–273. https://doi.org/10.1017/S0029665116000094.

[227] D.J. Troy, K.S. Ojha, J.P. Kerry, B.K. Tiwari, Sustainable and consumer-friendly emerging technologies for application within the meat industry: An overview, Meat Sci. 120 (2016) 2–9. https://doi.org/10.1016/j.meatsci.2016.04.002.

[228] E. von Borell, J.T. Sørensen, Organic livestock production in Europe: aims, rules and trends with special emphasis on animal health and welfare, Livest. Prod. Sci. 90 (2004) 3–9. https://doi.org/10.1016/j.livprodsci.2004.07.003.

[229] A. Taheri-Garavand, S. Fatahi, M. Omid, Y. Makino, Meat quality evaluation based on computer vision technique: A review, Meat Sci. 156 (2019) 183–195. https://doi.org/10.1016/j.meatsci.2019.06.002.

[230] N. Prieto, R. Roehe, P. Lavín, G. Batten, S. Andrés, Application of near infrared reflectance spectroscopy to predict meat and meat products quality: A review, Meat Sci. 83 (2009) 175–186. https://doi.org/10.1016/j.meatsci.2009.04.016.

[231] T. Yang, B. Zhao, L. He, Raman instruments for food quality evaluation, in: J. Zhong, X. Wang (Eds.), Eval. Technol. Food Qual., Elsevier, 2019: pp. 119–143. https://doi.org/10.1016/B978-0-12-814217-2.00008-1.

[232] A. Beganović, L. Hawthorne, K. Bach, C. Huck, Critical Review on the Utilization of Handheld and Portable Raman Spectrometry in Meat Science, Foods. 8 (2019) 49. https://doi.org/10.3390/foods8020049.

[233] B.G. Logan, D.L. Hopkins, L. Schmidtke, S. Morris, S.M. Fowler, Preliminary investigation into the use of Raman spectroscopy for the verification of Australian grass and grain fed beef, Meat Sci. 160 (2020) 107970. https://doi.org/10.1016/j.meatsci.2019.107970.

[234] P.V. Andersen, J.P. Wold, E. Gjerlaug-Enger, E. Veiseth-Kent, Predicting post-mortem meat quality in porcine longissimus lumborum using Raman, near infrared and fluorescence spectroscopy, Meat Sci. 145 (2018) 94–100. https://doi.org/10.1016/j.meatsci.2018.06.016.

[235] C.C. Santos, J. Zhao, X. Dong, S.M. Lonergan, E. Huff- Lonergan, A. Outhouse, K.B. Carlson, K.J. Prusa, C.A. Fedler, C. Yu, S.D. Shackelford, D.A. King, T.L. Wheeler, Predicting aged pork quality using a portable Raman device, Meat Sci. 145 (2018) 79–85. https://doi.org/10.1016/j.meatsci.2018.05.021.

[236] S.M. Fowler, H. Schmidt, R. van de Ven, D.L. Hopkins, Preliminary investigation of the use of Raman spectroscopy to predict meat and eating quality traits of beef loins, Meat Sci. 138 (2018) 53–58. https://doi.org/10.1016/j.meatsci.2018.01.002.

[237] M. Nache, J. Hinrichs, R. Scheier, H. Schmidt, B. Hitzmann, Prediction of the pH as indicator of porcine meat quality using Raman spectroscopy and metaheuristics, Chemom. Intell. Lab. Syst. 154 (2016) 45–51. https://doi.org/10.1016/j.chemolab.2016.03.011.

[238] V. Sharma, R. Kumar, K. Devgan, P.K. Mishra, A. Ekielski, V. Kumar, V. Kumar, Multivariate analysis for forensic characterization, discrimination, and classification of marker pen inks, Spectrosc. Lett. 51 (2018) 205–215. https://doi.org/10.1080/00387010.2018.1452265.

[239] C. Piña-Torres, P. Lucero-Gómez, S. Nieto, A. Vázquez, L. Bucio, I. Belio, R. Vega, C. Mathe, C. Vieillescazes, An analytical strategy based on Fourier transform infrared spectroscopy, principal component analysis and linear discriminant analysis to suggest the botanical origin of resins from Bursera. Application to archaeological Aztec Samples, J. Cult. Herit. 33 (2018) 48–59. https://doi.org/10.1016/j.culher.2018.02.006.

[240] J.L. Pichardo-Molina, C. Frausto-Reyes, O. Barbosa-García, R. Huerta-Franco, J.L. González-Trujillo, C.A. Ramírez-Alvarado, G. Gutiérrez-Juárez, C. Medina-Gutiérrez, Raman spectroscopy and multivariate analysis of serum samples from breast cancer patients, Lasers Med. Sci. 22 (2007) 229–236. https://doi.org/10.1007/s10103-006-0432-8.

[241] J.G. Cruz-Castillo, S. Ganeshanandam, B.R. MacKay, G.S. Lawes, C.R.O. Lawoko, D.J. Woolley, Applications of Canonical Discriminant Analysis in Horticultural Research, HortScience. 29 (1994) 1115–1119.

https://doi.org/10.21273/HORTSCI.29.10.1115.

[242] A.S. Luna, A.P. da Silva, C.S. da Silva, I.C.A. Lima, J.S. de Gois, Chemometric methods for classification of clonal varieties of green coffee using Raman spectroscopy and direct sample analysis, J. Food Compos. Anal. 76 (2019) 44–50. https://doi.org/10.1016/j.jfca.2018.12.001.

[243] M. Friendly, M. Sigal, Visualizing Tests for Equality of Covariance Matrices, Am. Stat. (2018) 1–12. https://doi.org/10.1080/00031305.2018.1497537.

[244] A. Kassambara, Machine Learning Essentials: Practical Guide in R, 1st ed., STHDA, 2018.

[245] A. Tharwat, Linear vs. quadratic discriminant analysis classifier: a tutorial, Int. J. Appl. Pattern Recognit. 3 (2016) 145. https://doi.org/10.1504/IJAPR.2016.079050.

[246] N.J. Pizzi, R.L. Somorjai, W. Pedrycz, Classifying Biomedical Spectra Using Stochastic Feature Selection and Parallelized Multi-Layer Perceptrons, in: B. Bouchon-Meunier, G. Coletti, R.R. Yager (Eds.), Mod. Inf. Process., Elsevier, 2006: pp. 383–393. https://doi.org/10.1016/B978-044452075-3/50032-7.

[247] T. Strauss, M.J. von Maltitz, Generalising Ward's Method for Use with Manhattan Distances, PLoS One. 12 (2017) e0168288. https://doi.org/10.1371/journal.pone.0168288.

[248] H. Wang, S. Ding, G. Wang, X. Xu, G. Zhou, In situ characterization and analysis of Salmonella biofilm formation under meat processing environments using a combined microscopic and spectroscopic approach, Int. J. Food Microbiol. 167 (2013) 293–302. https://doi.org/10.1016/j.ijfoodmicro.2013.10.005.

[249] C. Xie, J. Mace, M.A. Dinno, Y.Q. Li, W. Tang, R.J. Newton, P.J. Gemperline, Identification of Single Bacterial Cells in Aqueous Solution Using Confocal Laser Tweezers Raman Spectroscopy, Anal. Chem. 77 (2005) 4390–4397. https://doi.org/10.1021/ac0504971.

[250] M. Marounek, A. Pebriansyah, Use of carotenoids in feed mixtures for poultry: a review, Agric. Trop. Subtrop. 51 (2018) 107–111. https://doi.org/10.1515/ats-2018-0011.

[251] W.S. DARWISH, Y. IKENAKA, A.E. MORSHDY, K.I. ELDESOKY, S. NAKAYAMA, H. MIZUKAWA, M. ISHIZUKA, β-carotene and retinol contents in

the meat of herbivorous ungulates with a special reference to their public health importance, J. Vet. Med. Sci. 78 (2016) 351–354. https://doi.org/10.1292/jvms.15-0287.

[252] C.E. Scott, A.L. Eldridge, Comparison of carotenoid content in fresh, frozen and canned corn, J. Food Compos. Anal. 18 (2005) 551–559. https://doi.org/10.1016/j.jfca.2004.04.001.

[253] R. Ahmed, W. Wang, A.W. Zia, C. Lau, Collagen formation observed from healing calvarial defects with principal component analysis of Raman scattering, Analyst. 143 (2018) 4614–4622. https://doi.org/10.1039/C8AN01021H.

[254] D. Berrar, Cross-Validation, in: Encycl. Bioinforma. Comput. Biol., Elsevier, 2019: pp. 542–545. https://doi.org/10.1016/B978-0-12-809633-8.20349-X.

[255] Z. He, Phosphorylation site prediction, in: Data Min. Bioinforma. Appl., Elsevier, 2015: pp. 29–37. https://doi.org/10.1016/B978-0-08-100100-4.00004-1.

[256] R. Matignon, Neural Network Modeling Using SAS Enterprise Miner, AuthorHouse, 2005.

[257] N.J. Salkind, ed., Encyclopedia of Research Design, Volume 1, SAGE, 2010.

[258] A. Rygula, K. Majzner, K.M. Marzec, A. Kaczor, M. Pilarczyk, M. Baranska, Raman spectroscopy of proteins: a review, J. Raman Spectrosc. 44 (2013) 1061–1076. https://doi.org/10.1002/jrs.4335.

[259] I.H. Boyaci, H.T. Temiz, H.E. Geniş, E. Acar Soykut, N.N. Yazgan, B. Güven, R.S. Uysal, A.G. Bozkurt, K. İlaslan, O. Torun, F.C. Dudak Şeker, Dispersive and FT-Raman spectroscopic methods in food analysis, RSC Adv. 5 (2015) 56606–56624. https://doi.org/10.1039/C4RA12463D.

[260] K. Maquelin, C. Kirschner, L.-P. Choo-Smith, N. van den Braak, H.P. Endtz, D. Naumann, G.. Puppels, Identification of medically relevant microorganisms by vibrational spectroscopy, J. Microbiol. Methods. 51 (2002) 255–271. https://doi.org/10.1016/S0167-7012(02)00127-6.

[261] Y. Liu, H. Zhou, Z. Hu, G. Yu, D. Yang, J. Zhao, Label and label-free based surface-enhanced Raman scattering for pathogen bacteria detection: A review, Biosens. Bioelectron. 94 (2017) 131–140. https://doi.org/10.1016/j.bios.2017.02.032.

[262] S. Wang, B. Gu, J. Li, C. Wang, H. Kang, L. Shao, L. Hu, R. Xiao, Label-free

identification carbapenem-resistant Escherichia coli based on surface-enhanced resonance Raman scattering†, RSC Adv. 8 (2018) 4761–4765. https://doi.org/10.1039/c7ra13063e.

[263] X. Chen, M. Tang, Y. Liu, J. Huang, Z. Liu, H. Tian, Y. Zheng, M.L. de la Chapelle, Y. Zhang, W. Fu, Surface-enhanced Raman scattering method for the identification of methicillin-resistant Staphylococcus aureus using positively charged silver nanoparticles, Microchim. Acta. 186 (2019) 102. https://doi.org/10.1007/s00604-018-3150-6.

[264] K. Liu, S. Jin, Z. Song, L. Jiang, L. Ma, Z. Zhang, Label-free surface-enhanced Raman spectroscopy of serum based on multivariate statistical analysis for the diagnosis and staging of lung adenocarcinoma, Vib. Spectrosc. 100 (2019) 177–184. https://doi.org/10.1016/j.vibspec.2018.12.007.

[265] C. Wei, M. Li, X. Zhao, Surface-enhanced raman scattering (SERS) with silver nano substrates synthesized by microwave for rapid detection of foodborne pathogens, Front. Microbiol. 9 (2018) 1–9. https://doi.org/10.3389/fmicb.2018.02857.

[266] T. Horinouchi, T. Ichimura, C. Furusawa, T.M. Watanabe, A. Germond, H. Fujita, Raman spectral signature reflects transcriptomic features of antibiotic resistance in Escherichia coli, Commun. Biol. 1 (2018). https://doi.org/10.1038/s42003-018-0093-8.

[267] O. Samek, K. Mlynariková, S. Bernatová, J. Ježek, V. Krzyžánek, M. Šiler, P. Zemánek, F. Růžička, V. Holá, M. Mahelová, Candida parapsilosis Biofilm Identification by Raman Spectroscopy, Int. J. Mol. Sci. 15 (2014) 23924–23935. https://doi.org/10.3390/ijms151223924.

8 List of Publications

8.1 Publications Covered in this Thesis:

8.1.1 Peer Reviewed Publications:

S. Jaafreh, O. Valler, J. Kreyenschmidt, K. Günther, P. Kaul, In vitro discrimination and classification of Microbial Flora of Poultry using two dispersive Raman spectrometers (microscope and Portable Fiber-Optic systems) in tandem with chemometric analysis, *Talanta*. 202 (2019) 411–425. doi:10.1016/j.talanta.2019.04.082.

S. Jaafreh, R. Breuch, K. Günther, J. Kreyenschmidt, P. Kaul, Rapid Poultry Spoilage Evaluation Using Portable Fiber-Optic Raman Spectrometer, *Food Anal. Methods*. 11 (2018) 2320–2328. doi:10.1007/s12161-018-1223-0.

8.1.2 Publication in Preparation:

S. Jaafreh, M. Hebel, J. Kreyenschmidt, K. Günther, P. Kaul, Investigation of the Influence of Different Production Systems on the Quality and Shelf Life of Poultry Meat Using a Portable Fiber-Optic Raman Spectrometer, *In preparation*.

8.2 Other Peer Reviewed Publications:

H.M. Abdel-Halim, S. Jaafreh, Effects of the Vibrational and Rotational Energy on Reaction Cross-Section in a Classical Trajectory Study of Atom-Diatomic Molecule Collisions, *Zeitschrift Für Naturforsch. A.* 63 (2008) 721 – 734. doi:10.1515/zna-2008-10-1116.

H.M. Abdel-Halim, S. Jaafreh, Reaction Rate Constants from Classical Trajectories of Atom-Diatomic Molecule Collisions, *Zeitschrift Für Naturforsch. A*. 63 (2008) 159 – 169. doi:10.1515/zna-2008-3-408.

9 Acknowledgments

Ph.D as a life goal cannot succeed without the support of outstanding and supportive people. This Ph.D could not have been possible without the support of my supervisor, Prof. Dr. Peter Kaul. I am and will be always grateful for the opportunity he gave me and the guidance he provided with his knowledge, experience and patience during my doctoral thesis. He was ready to help 24/7 a week. Prof. Dr. Peter Kaul: I appreciate your careful supervision and motivation, especially during the times of hardship and hopelessness. Thank you for the encouragement that guided me through these difficult years and for letting me grow as a research scientist. Your advice on research as well as on my career is invaluable.

I would also like to express my appreciation to Prof. Dr. Klaus Günther for agreeing to supervise me, for his guidance and help throughout my Ph.D. I would also like to thank Prof. Dr. Matthias Wüst for accepting to be my second supervisor and for his help and his comments. Moreover, I am thankful to Prof. Dr. Helmut Baltruschat and Prof. Dr. Judith Kreyenschmidt for their willingness to review my thesis and be part of the examination committee.

Also, special thanks go to my colleagues at the ISF and IDT Groups. Their scientific discussions and constructive comments made it possible to accomplish this task and more importantly helped in building the attitude of systematic scientific investigations and scientific writings in me. I am also grateful to the Hochschule Bonn-Rhein-Sieg (HBRS) staff for their unfailing support and assistance. What a great place to work in!

A special acknowledgement goes to all down at HBRS (Graduate Institute) and Erasmus Mundus (Avempace II) for helping and providing the funding during my work.

And, special credit go to my family for their endless love, support and understanding, in particular I credit my sister Cezar who has always believed in me, no matter what and she was there for me in times of joy and sorrow equally.

And finally, many thanks to my friends: Shatha AbuShanab, Abla Alzagameem, Siva Pulikallu, Maysoon Saleh, Fidaa Al-Masri, Asma Naas, Hussein Koschar, Cherien Nadim, Ann-Marie Lukas, Basma El Khaldi-Hansen, Ruba Al-Qaruoty, Sahar Jebarah, Enas Nabeh Mahmoud and Lamis Omar for their support at all times. Thanks for all your encouragement. Thank you all for being with me in this journey!

10 Declaration

I hereby declare that the work presented in the current thesis is my own work except where explicitly stated otherwise in the text or in the bibliography. The current thesis has not been submitted as a whole or in a part for obtaining the doctoral degree to any other university except the University of Bonn.

Bonn, 12.08.2020

Sawsan Jaafreh